Direct Fitting of Analytical Potential Functions to Diatomic Molecular Spectroscopic Data

by

Jenning Y. Seto

A thesis
presented to the University of Waterloo
in fulfilment of the
thesis requirement for the degree of
Master of Science
in
Chemistry

Waterloo, Ontario, Canada, 2000

I hereby declare that I am the sole author of this thesis.

This is a true copy of the thesis, including any required final revisions, as accepted by my examiners.

I understand that my thesis may be made electronically available to the public.

Abstract

The standard practice of spectroscopic data reduction is generally to fit data to level energy expansions in terms of the vibrational and rotational quantum numbers. However, the utility of such expressions is limited because they extrapolate poorly and they need very large sets of parameters, many of which have no independent physical significance. One method of addressing these problems is to fit the spectroscopic data directly to analytical potential energy functions incorporating the natural physical behaviour of the molecule in question. Although there have been a number of successful applications of this approach, there are still certain problems associated with the types of potential forms being used. This thesis will explore some of these problems and determine how effective the potential forms being used are for a number of specific cases.

Acknowledgements

I would like to thank quite a number of people.

In order of appearance, the people who were a part of this group during my stay here: Greg Clark, Ken Crowell, Hasan Sabzyan, Brad Bart, Hwa Wei, Geoff Kraemer, Doug Weir, Yiye Huang, and Jeff Irwin.

Two of the three stooges (who were very good at giving me reasons to procrastinate): Dustin Dickens and Randall Skelton.

Also a big thank you to those in the basement who acquired the spectroscopic data which I used for my analyses: Zulfikar Morbi, Gang Li, Tsuyoshi Hirao, and Treana Parekunnel.

I'd also like to thank everyone I've actually met while I was at the University of Waterloo, they've all been a great help.

Of course, I would like to thank the professors that made me realize just how little I knew (and hopefully remedied that deficiency): Peter Bernath, Carey Bissonnette, Fred McCourt, and my supervisor Robert Le Roy.

Funding for this whole affair have come from both NSERC and the University of Waterloo.

Contents

List of Tables

List of Figures

List of Abbreviations

BOB	Born-Oppenheimer Breakdown
DPF	Direct Potential Fit
EMO	Expanded Morse Oscillator
GMO	Generalized Morse Oscillator
IPA	Inverted Perturbation Analysis/Approach
MLJ	Modified Lennard-Jones
MMO	Modified Morse Oscillator
OT	Ogilvie-Tipping
RKR	Rydberg-Klein-Rees
SCE	Self-Constraining Expansion
SMO	Simple Morse Oscillator
SPF	Simons-Parr-Finlan
WKB	Wentzel-Kramers-Brillouin

Chapter 1

Introduction

Early in the nineteenth century, Joseph Fraunhofer, a Bavarian astronomer, split the light from the sun into a continuous spectrum of colours and discovered that the spectrum was littered with a number of sharp dark lines. These dark lines were later determined to be caused by the absorption of light by hydrogen and other atoms in the atmosphere of the sun. This observation not only shed some new light on the composition of the sun, but also led to the birth of the field of spectroscopy.

Webster [1] defines spectroscopy as being "physics that deals with the theory and interpretation of interactions between matter and radiation". Although this definition is concise and accurate, it does not explain the true potential of this field of study. Most of the matter in this universe is made up of atoms and molecules. Because spectroscopy analyzes the light emitted or absorbed by an object, it allows us to "see" these molecules and study them even if they are too few, too far away, or too difficult to observe by any other technique.

Spectroscopy has been used to study the compositions of the stars, planets, and other objects in space. It can be used to study environments too inhospitable or inaccessible for standard methods; for example an explosion that produces short-lived compounds, or

the fiery inferno in the middle of a blast furnace. Rare and fragile objects, like expensive paintings and priceless antiques, can be studied spectroscopically without destroying them. Furthermore, trace amounts of toxins can be found in the air, soil, or water using spectroscopic methods. The number of uses is endless; from giant stars to tiny atoms, spectroscopy has given scientists a tool with which to examine the universe around us in a literally different light.

One of the main tasks in spectroscopy is to compress the huge volume of data that is produced when analyzing a molecule and to ascertain some of the molecule's characteristics. To do this, one must realize that the absorption or emission lines in the spectra collected correspond to transitions between pairs of energy states in the molecule. Knowledge of the distribution of the energy levels can then be used to generate molecular constants from which a potential energy function (PEF) can be obtained (see Figure 1.1). The PEF governs how the atoms in the molecule interact with each other, and it can be used to predict many of the properties of that molecule. Examples of some important molecular properties would include the bond lengths, force constants, and dissociation energies.

Traditionally these PEFs are generated from molecular constants, but ideally one would like to determine the PEFs directly from the spectroscopic data (Figure 1.1). Such a procedure is referred to as "Direct Potential Fitting" (DPF). The benefits of DPF are discussed in the next chapter.

The overall objective of the present project was to develop a flexible and robust computer program `DSPotFit` (Diatomic Singlet Potential Fit) for using DPF of diatomic molecular spectral data to determine potential energy curves for the molecular states of interest [2], and when appropriate, also to determine the associated Born-Oppenheimer breakdown correction terms [3, 4]. Currently, only a few programs actually use the DPF method, most of which are proprietary and limited by the types of functions or number

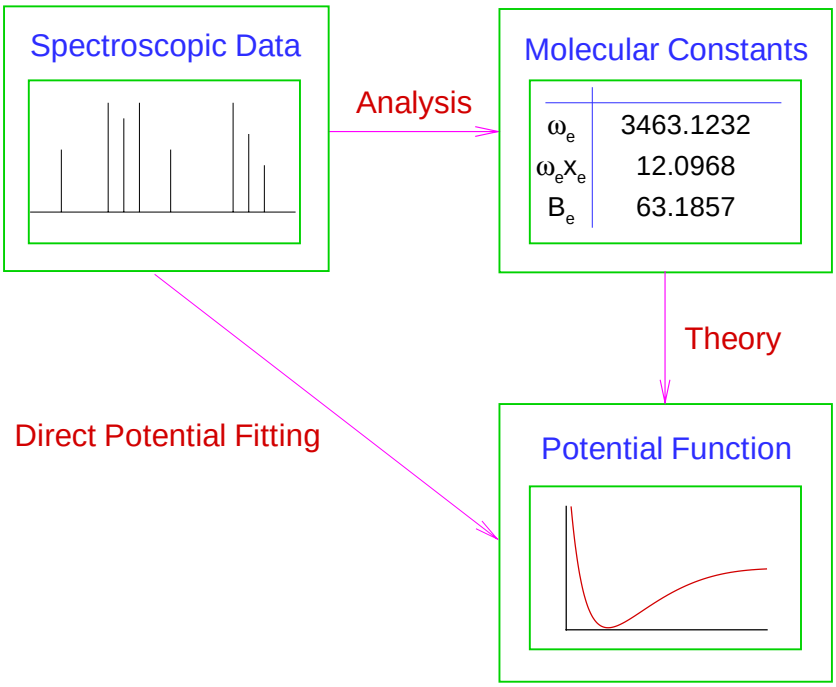

Figure 1.1: A Flowchart for the Data Reduction Procedure.

of electronic states that can be used in the analysis.

There were a number of tasks that needed to be completed before the development and testing of `DSPotFit` was complete. In the initial phase, attention was focused on the problem of fitting analytic potential energy functions of various forms to vibrational-rotational data from multiple electronic states and multiple isotopomers of a given species. This program has already been successfully applied to a number of molecules, including GeO [5], the coinage hydrides [6], and the rubidium dimer [7]. Another factor that needed to be considered was the reliability of the potential functions beyond the range of the experimental data. The potential functions being considered were studied to look for any

unphysical behaviour occurring in the extrapolation region, and if found, to determine whether ensuing problems could be corrected or minimized. Finally, an investigation was made to determine the effectiveness of these potential forms for fitting to potentials, such as shelf or double minimum type potentials, that do not have the "standard" shape.

This thesis has been divided into a number of chapters. In Chapter 2, some historical background is given with regard to spectroscopic data reduction and the evolution of direct potential fitting. It also includes some background theory on Born-Oppenheimer breakdown (BOB) and the methodology behind DPF. Chapters 3 to 5 describe the experimental aspects of this work, including illustrative results obtained using `DSPotFit`. Chapter 3 examines the effects of extrapolation into the short range (inner wall) region, focusing on the multi-state, multi-isotopomeric data from the coinage hydrides as test cases. Chapter 4 looks into the long-range (potential tail) extrapolation problem using a very large data set for the rubidium dimer. Chapter 5 presents a short discussion of the feasibility and current progress in the area of fitting analytical potential functions to non-standard potential forms, with the double minimum potential of the $C\,^1\Sigma^+$ state of LiH as a specific example. The final chapter summarizes and discusses the results obtained in this thesis.

Chapter 2

Background

2.1 Spectroscopic Data Reduction

Modern spectroscopy can produce vast amounts of high resolution data for almost any chosen molecule. Such data have traditionally been used to determine sets of molecular constants, from which extrapolated data predictions and fundamental molecular properties have then been calculated. For a given transition i of a diatomic molecule, the energy $h\nu_i$ can be expressed as the difference in level energies

$$h\nu_i \;=\; E_{v',J'} - E_{v'',J''} \;, \tag{2.1}$$

where the energies of the upper ($E_{v',J'}$) and lower ($E_{v'',J''}$) diatomic states can be decomposed so that

$$E_{v,J} \;=\; G_v + F_v(J) \;, \tag{2.2}$$

with G_v and $F_v(J)$ being the vibrational and rotational contribution to the energy of vibrational level v. $F_v(J)$ can be further expanded in terms of the rotational quantum

number J

$$\begin{aligned} F_v(J) &= \sum_{m=1} K_m(v)[J(J+1)]^m \\ &= B_v[J(J+1)] - D_v[J(J+1)]^2 + H_v[J(J+1)]^3 + \cdots , \end{aligned} \tag{2.3}$$

in which the $\{K_m(v)\}$ (B_v, D_v, H_v, etc.) are the rotational constants for the vibrational level v.

Another, more compact, way to represent $E_{v,J}$ is to use a double expansion in terms of the vibrational (v) and rotational (J) quantum numbers, such as

$$E_{v,J} = \sum_{l=0} \sum_{m=0} Y_{l,m} \left(v + \frac{1}{2}\right)^l [J(J+1)]^m , \tag{2.4}$$

with the $Y_{l,m}$ known as Dunham $Y_{l,m}$ constants. The $m = 0, 1$ contributions to this general term-value expression are the energies (G_v) and inertial rotational constants (B_v) for each vibrational level,

$$\begin{aligned} G_v &= \sum_{l=1} Y_{l,0} \left(v + \frac{1}{2}\right)^l \\ &= \omega_e \left(v + \frac{1}{2}\right) - \omega_e x_e \left(v + \frac{1}{2}\right)^2 + \omega_e y_e \left(v + \frac{1}{2}\right)^3 + \cdots , \end{aligned} \tag{2.5}$$

$$\begin{aligned} B_v &= \sum_{l=0} Y_{l,1} \left(v + \frac{1}{2}\right)^l \\ &= B_e - \alpha_e \left(v + \frac{1}{2}\right) + \gamma_e \left(v + \frac{1}{2}\right)^2 + \cdots , \end{aligned} \tag{2.6}$$

in which ω_e is the equilibrium vibrational frequency, $\{\omega_e x_e,\ \omega_e y_e,\ \cdots\}$ are corrections to ω_e that take into account the anharmonicity of the potential, B_e is the equilibrium rotational constant, and $\{\alpha_e,\ \gamma_e,\ \cdots\}$ take into account the vibrational dependence of the rotational constant.

A more effective method of representing the properties of the molecule and extrapolating to energies beyond the range of data is to use potential energy functions. Conventionally, these potential energy functions can be calculated from the molecular constants (G_v and B_v) using the semi-classical Rydberg-Klein-Rees (RKR) [8, 9, 10] procedure. Unfortunately, several problems plague this traditional approach. The use of molecular constants requires many parameters to reproduce the data accurately, most of which have no independent physical meaning. It also extrapolates poorly beyond the range of the existing data, and it requires an extra step to obtain the potentials from the spectroscopic data. Finally, since the RKR method for determining a potential energy curve from a knowledge of the vibrational quantum number dependence of vibrational energies and initial rotational constants [8, 9, 10] is based on the first-order Wentzel-Kramers-Brillouin (WKB) approximation, the potential so generated does not reflect the data to "quantum mechanical" accuracy; i.e., for highly precise data, transition frequencies calculated from an RKR potential often will not reproduce the experimental observations within the experimental uncertainties.

2.2 Direct Potential Fitting

An inherently better approach to spectroscopic data reduction is to fit the observed transition frequencies directly to eigenvalue differences calculated from analytic potential energy functions. This method was first developed by Le Roy and van Kranendonk [11], who used it to analyse data for H_2-Rg (Rg = rare gas) Van der Waals complexes to obtain the first accurate three-dimensional potential functions for an atom-diatom system. Since that time, this "Direct Potential Fit" (DPF) approach has been the central technique used in almost all quantitative determinations of multi-dimensional potential energy surfaces from spectroscopic data for Van der Waals molecules [12, 13].

The use of this approach for diatomic molecules was first proposed by Kosman and Hinze, who applied it to synthetic data generated from a simple analytic model potential for HgH [14]. The name they used for this (DPF) approach is the "inverted perturbation analysis/approach" (IPA); this name arose from the fact that the sum of the corrections to the potential in each iterative step in the DPF can be viewed as a first-order perturbation correction of the starting potential. Its application in practical diatomic spectroscopic data analysis was pioneered by Vidal and Scheingraber [15] who used it to determine accurate potential energy functions for the $X\,^1\Sigma_g^+$ and $A\,^1\Sigma_u^+$ states of Mg_2. They used an IPA procedure to calculate a radial correction function to a first-order potential (in their case the RKR potential) so that the eigenvalues computed from the new (corrected) potential curve would match the spectroscopic term values within experimental uncertainty. An ingenious alternative approach proposed by Gouedard and Vigue [16] involves the determination of expressions for "effective" G_v and B_v constants (different from the experimental ones), defined so that their employment in the semi-classical RKR inversion procedure yields a potential energy curve whose quantal eigenvalues agree with the experimental data.

Another advance came after Watson developed a method to take account of Born-Oppenheimer Breakdown (BOB) in diatomic molecules [3, 4]. Coxon was able to use Watson's formulation to determine directly atomic-mass-dependent adiabatic corrections to the potential energy curve and non-adiabatic corrections to the centrifugal term in a simultaneous analysis of data for ground-state HCl and DCl [2]. Fits to determine these BOB correction functions have since been used with great success in analyzing small molecules for which BOB is readily apparent, or with data sets from larger molecules in which the experimental precision pushes the bounds of the Born-Oppenheimer approximation.

Coxon continued to improve upon the DPF (or IPA) method when he examined the

possibility of using an analytical potential function, the "Generalized Morse Oscillator" (GMO), to represent a corrected RKR potential [17]. The use of analytical potential forms that take into account the physical nature of the molecule improves the predictive ability of the model and reduces the number of parameters required. It was not long before these analytical functions were fitted directly to the data [18]. There were some problems associated with the GMO type of function, so other functional forms were proposed [19, 20, 5] in attempts to address these problems. However, most of those "better" potential forms have their own limitations, which will be discussed later in this thesis.

The growing trend of describing spectroscopic data sets directly in terms of the underlying potential functions [5, 6, 18, 19, 21, 22] has created a demand for a robust computer program that will fit spectroscopic data directly to *any* chosen analytical potential function. Programs currently in use (e.g., those developed and applied by Coxon and Hajigeorgiou, and by Dulick, Bernath and coworkers) are not readily available, are designed to fit to specific potential forms, and have not yet generally been used in simultaneous fits to determining potentials for more than one electronic state. In spite of the apparent superiority of this approach for spectroscopic data reduction, there appears to be no well documented and robust computer program available for distribution to and use by the general scientific community. One objective of this thesis is to remedy that deficiency.

2.3 Born-Oppenheimer Breakdown

One of the most effective and well-known approximations in quantum mechanics was that developed by Born and Oppenheimer [23] in the early part of this century. Due to the mass difference between the nuclei and electrons, they assumed that the nuclei

in a molecule are effectively stationary compared to electrons. The Born-Oppenheimer approximation allows the separation of the electronic and nuclear components of the Schrödinger equation, which in turn makes it much easier to solve. This is an excellent approximation, especially for heavier molecules, as the slow nuclei are three or more orders of magnitude heavier than the (fast) electrons. However, as the masses of the nuclei decrease, the difference between the velocities of the electrons and nuclei also decreases. Therefore, the Born-Oppenheimer approximation will tend to break down for lighter (small reduced mass) molecules such as LiH. These differences may even be noticed when analyzing data for heavy molecules involving more than one isotopomer.

Atomic-mass-dependent radial potential correction terms can be used to compensate for this Born-Oppenheimer breakdown (BOB). The current, most popular description, as derived by Watson [3, 4], defines the effective centrifugally-distorted potential $V^{\alpha}_{\mathrm{eff},J}(R)$ for isotopomer-α to be

$$V^{\alpha}_{\mathrm{eff},J}(R) \;=\; V^{\alpha}_{\mathrm{ad}}(R) + \frac{\hbar^2}{2\mu R^2}[1 + q^{\alpha}(R)][J(J+1)] \;, \tag{2.7}$$

with

$$V^{\alpha}_{\mathrm{ad}}(R) \;=\; U_{\mathrm{CN}}(R) + \Delta U^{\alpha}_{\mathrm{ad}}(R) \;, \tag{2.8}$$

in which R is the intermolecular distance, μ the reduced mass of the isotopomer, J the rotational quantum number, $U_{\mathrm{CN}}(R)$ the "clamped-nuclei" (or Born-Oppenheimer) potential function, and $\Delta U^{\alpha}_{\mathrm{ad}}(R)$ corrects for adiabatic and non-rotational non-adiabatic BOB terms (i.e., the difference between the isotope-independent "clamped-nuclei" potential and the effective adiabatic potential for each isotopomeric species). The quantity $q^{\alpha}(R)$ is a correction function representing the effect of rotational non-adiabatic BOB

effects. The correction terms are conventionally written as [3]

$$\Delta U_{\rm ad}^{\alpha}(R) \;=\; \frac{1}{M_{\rm A}^{\alpha}}\Delta U_{\rm ad}^{\rm A}(R) + \frac{1}{M_{\rm B}^{\alpha}}\Delta U_{\rm ad}^{\rm B}(R)\;, \tag{2.9}$$

and

$$q^{\alpha}(R) \;=\; \frac{1}{M_{\rm A}^{\alpha}}q^{\rm A}(R) + \frac{1}{M_{\rm B}^{\alpha}}q^{\rm B}(R)\;, \tag{2.10}$$

in which $\Delta U_{\rm ad}^{\rm A,B}(R)$ and $q^{\rm A,B}(R)$ are mass-independent radial functions, and $M_{\rm A}^{\alpha}$ and $M_{\rm B}^{\alpha}$ are the atomic rest masses of atoms A and B for isotopomer-α.

The most commonly employed method for representing the BOB correction terms was introduced by Coxon [2], who used the following expansions for the correction functions:

$$\Delta U_{\rm ad}^{\rm A}(R) \;=\; \sum_l u_l^{\rm A}(R-R_e)^l\;, \quad \Delta U_{\rm ad}^{\rm B}(R) \;=\; \sum_l u_l^{\rm B}(R-R_e)^l\;, \tag{2.11}$$

and

$$q^{\rm A}(R) \;=\; \sum_l q_l^{\rm A}(R-R_e)^l\;, \quad q^{\rm B}(R) \;=\; \sum_l q_l^{\rm B}(R-R_e)^l\;, \tag{2.12}$$

with R_e the equilibrium bond distance, and $u_l^{\rm A}$, $u_l^{\rm B}$, $q_l^{\rm A}$ and $q_l^{\rm B}$ mass-independent parameters for the BOB correction terms.

The polynomial forms of the Coxon correction functions means that at large R these functions always tend to "blow up", causing the potential to be physically unrealistic at long range. Further, the "clamped-nuclei" potential $U_{\rm ad}(R)$ of Eq. (2.8) does not actually define the potential for any particular isotopic species, and so has no true physical meaning. However, by following an approach introduced by Le Roy [24], an improved form of the effective potential for any given isotopomer can be obtained by replacing the reference potential $U_{\rm ad}(R)$ with an effective adiabatic potential $V_{\rm ad}^{\alpha'}(R)$ for the isotopomer α' for which the widest range of data is available. Identifying this species as isotopomer-1

gives

$$V_{\rm ad}^{1}(R) \;=\; U_{\rm ad}(R) + \Delta U_{\rm ad}^{1}(R) \;, \tag{2.13}$$

and the general expression for the non-rotational part of the potential for an arbitrary isotopomer-α may be written as

$$V_{\rm ad}^{\alpha}(R) \;=\; V_{\rm ad}^{1}(R) + \Delta V_{\rm ad}^{\alpha}(R) \;, \tag{2.14}$$

in which the function $\Delta V_{\rm ad}^{\alpha}(R)$ corrects for the difference between the potentials for isotopomer-α and isotopomer-1 ($\Delta V_{\rm ad}^{1}(R) \;\equiv\; 0$). The BOB correction functions ($\Delta V_{\rm ad}^{\alpha}(R)$, $q^{\alpha}(R)$) are now defined to be

$$\Delta V_{\rm ad}^{\alpha}(R) \;=\; \frac{\Delta M_{\rm A}^{\alpha}}{M_{\rm A}^{\alpha}} \Delta V_{\rm ad}^{\rm A}(R) + \frac{\Delta M_{\rm B}^{\alpha}}{M_{\rm B}^{\alpha}} \Delta V_{\rm ad}^{\rm B}(R) \;, \tag{2.15}$$

and

$$q^{\alpha}(R) \;=\; \frac{M_{\rm A}^{1}}{M_{\rm A}^{\alpha}} q^{\rm A}(R) + \frac{M_{\rm B}^{1}}{M_{\rm B}^{\alpha}} q^{\rm B}(R) \;, \tag{2.16}$$

with $\Delta M_{\rm A}^{\alpha} \;=\; M_{\rm A}^{\alpha} - M_{\rm A}^{1}$ and $\Delta M_{\rm B}^{\alpha} \;=\; M_{\rm B}^{\alpha} - M_{\rm B}^{1}$. Here, the BOB correction functions $\Delta V_{\rm ad}^{\rm A,B}(R)$ and $q^{\rm A,B}(R)$ are written as polynomial expansions

$$\Delta V_{\rm ad}^{\rm A}(R) \;=\; \sum_{l} u_{l}^{\rm A} z^{l} \;, \quad \Delta V_{\rm ad}^{\rm B}(R) \;=\; \sum_{l} u_{l}^{\rm B} z^{l} \;, \tag{2.17}$$

and

$$q^{\rm A}(R) \;=\; \sum_{l} q_{l}^{\rm A} z^{l} \;, \quad q^{\rm B}(R) \;=\; \sum_{l} q_{l}^{\rm B} z^{l} \;, \tag{2.18}$$

in terms of the variable $z \;\equiv\; (R - R_e)/(R + R_e)$, which is half of the dimensionless Ogilvie-Tipping parameter $z_{\rm OT}$ ($z \;=\; z_{\rm OT}/2$) [25]. The mass-independent parameters for the adiabatic terms $u_{l}^{\rm A}$ and $u_{l}^{\rm B}$ appearing here have units of energy, while the rotational

non-adiabatic parameters $q_l^{\rm A}$ and $q_l^{\rm B}$ are unitless. One must note that although the values of these parameters will be fixed from one isotopomer to another, they will depend on the choice of the reference isotopomer ($\alpha = 1$).

When working with data for only one isotopomer, it is still possible to determine rotational non-adiabatic BOB correction terms [26], but there is not enough information to generate both sets of parameters $\{q_l^{\rm A}\}$ and $\{q_l^{\rm B}\}$. However, as both sets are effectively equivalent, it does not matter which set of $\{q_l\}$ parameters is used to fit to the data.

Inclusion of these BOB correction terms [2, 3, 4, 17, 18, 27, 28] has improved the ability to fit model potentials to multi-isotopomer data, allowed more compact, accurate and systematic treatment of data for different isotopomers, and has yielded a greater understanding of the essential nature of these interactions.

2.4 Families of Analytic Potential Energy Functions

Four families of analytic potential energy functions are considered in this thesis, all of which may be thought of as being generalizations of the well known "Simple Morse Oscillator" (SMO) function [29]

$$V_{\rm SMO}(R) \;=\; \mathcal{D}_e \left[1 - e^{-\beta_M\,(R-R_e)}\right]^2 \;, \tag{2.19}$$

where $\mathcal{D}_e$ is the potential well depth, β_M is a constant, R is the intermolecular distance, and R_e is the equilibrium distance. While this function has the correct qualitative behaviour for a normal potential energy curve, its small number of free parameters give it limited flexibility, making it unable to reproduce experimental data accurately over a wide range of observed vibrational-rotational levels.

Within the past three decades, attempts have been made to add some flexibility to

the SMO by replacing the constant exponent term β_M with either a quadratic [30] or cubic [31] polynomial in $(R - R_e)$. Although used mainly for chemical kinetics analysis, these forms of the SMO were still quite limited in their use. It was almost a decade ago, when Coxon and Hajigeorgiou [18] showed that the simple step of replacing the constant exponent parameter β_M by a smoothly varying function of R transformed the SMO into a very flexible potential function able to represent experimental data accurately over a wide range of levels. The function they proposed, the "Generalized Morse Oscillator" or GMO, has the form

$$V_{\rm GMO}(R) \;=\; \mathcal{D}_e \left[1 - e^{-\beta_{\rm GMO}(R)\,(R-R_e)}\right]^2 \;, \tag{2.20}$$

with $\beta_{\rm GMO}(R)$ represented as a polynomial expansion in $(R - R_e)$, namely

$$\beta_{\rm GMO}(R) \;=\; \beta_0^{\rm GMO} + \beta_1^{\rm GMO}(R - R_e) + \beta_2^{\rm GMO}(R - R_e)^2 + \cdots \;, \tag{2.21}$$

in which the exponent expansion parameters $\beta_i^{\rm GMO}$ are constants. While it has been successfully applied in fits to experimental data for a variety of cases, a significant deficiency of the GMO function is that it may have pathologically unrealistic behaviour in the limit that $R \to \infty$. This will occur when the coefficient of the highest-order term included in the expansion of Eq. (2.21) is negative, in which case the potential will become singular at large R instead of approaching an asymptote.

One means of avoiding the above problem was introduced by Dulick, Bernath and co-workers [19] , who proposed the "Modified Morse Oscillator" or MMO potential form

$$V_{\rm MMO}(R) \;=\; \mathcal{D}_e \left[1 - e^{-\beta_{\rm MMO}(z)\,z}\right]^2 / \left[1 - e^{-\beta^{\infty}_{\rm MMO}}\right]^2 \;, \tag{2.22}$$

in which

$$\beta_{\rm MMO}(z) \;=\; \beta_0^{\rm MMO} \;+\; \beta_1^{\rm MMO}\; z \;+\; \beta_2^{\rm MMO}\; z^2 \;+\; \cdots \;, \tag{2.23}$$

and

$$\beta_{\rm MMO}^{\infty} \;\equiv\; \beta_{\rm MMO}(R=\infty) \;=\; \beta_{\rm MMO}(z=1) = \sum_{i=0} \beta_i^{\rm MMO} \;. \tag{2.24}$$

This form has also been successfully applied in fits to highly accurate experimental data sets for a number of diatomic systems [19, 21, 22]. The fact that the MMO distance variable z is restricted to the range [-1,1] for $R \in [0,\infty)$ tends to make this function more stable and well behaved at large R. However, the denominator factor $\left[1-e^{-\beta_{\rm MMO}^{\infty}}\right]^2$ required to make the potential asymptote lie at $\mathcal{D}_e$ makes this form somewhat inconvenient to work with. Furthermore, while generally much better behaved than the GMO, this function may have pathological behaviour if $\beta_{\rm MMO}(z)$ changes sign, or becomes very steep, more specifically, when the slope of $\beta_{\rm MMO}(z)$ has a large positive slope for small radial distances $R < R_e$, or large negative slope for $R > R_e$. Such an event may cause the potential to "turn over" or even produce a spurious second minimum.

An alternate stabilizing modification of the GMO, one which does not require the denominator normalization factor of the MMO, is the "Expanded Morse Oscillator" or EMO function developed and applied in this thesis (see also [5, 6]), namely

$$V_{\rm EMO}(R) \;=\; \mathcal{D}_e \left[1-e^{-\beta_{\rm EMO}(z)\,(R-R_e)}\right]^2 \;, \tag{2.25}$$

with z as defined above, and with $\beta_{\rm EMO}(z)$ expanded as

$$\beta_{\rm EMO}(z) \;=\; \beta_0^{\rm EMO} \;+\; \beta_1^{\rm EMO}\; z \;+\; \beta_2^{\rm EMO}\; z^2 \;+\; \cdots \;. \tag{2.26}$$

Since $z \in [-1,1]$, as with the MMO, this function is usually well-behaved so long as

$\beta_{\rm EMO}(z)$ remains positive over the entire range of R and does not decrease too steeply.

The above three forms are all quite flexible, and for appropriate values of the exponent expansion parameters $\{\beta_i^a\}$ (a = GMO, MMO, or EMO) they will be qualitatively well behaved at large R. However, they all suffer from the deficiency that their asymptotic long-range behaviour does not have the simple inverse-power form expected of all molecular interactions [32], i.e.,

$$V(R) \simeq \mathcal{D}_e - C_n/R^n \ . \tag{2.27}$$

To correct for this problem, Hajigeorgiou and Le Roy introduced what they called the "Modified Lennard-Jones oscillator" or MLJ function, which has the form [20]

$$V_{\rm MLJ}(R) = \mathcal{D}_e \left[1 - \left(\frac{R_e}{R}\right)^n e^{-\beta_{\rm MLJ}(z)\, z}\right]^2 \ . \tag{2.28}$$

The exponent function $\beta_{\rm MLJ}(z)$ has the same analytic form as that for the MMO and EMO potentials, namely

$$\beta_{\rm MLJ}(z) = \beta_0^{\rm MLJ} + \beta_1^{\rm MLJ}\ z + \beta_2^{\rm MLJ}\ z^2 + \cdots \ , \tag{2.29}$$

while for $n = 0$, $V_{\rm MLJ}(R)$ collapses to the MMO form if a normalizing denominator factor $\left[1 - \delta_{n,0}\ e^{-\beta^\infty_{\rm MLJ}}\right]^2$, with $\delta_{n,0}$ the familiar Kroneker delta and $\beta^\infty_{\rm MLJ}$ given by

$$\beta^\infty_{\rm MLJ} = \sum_{i=0} \beta_i^{\rm MLJ} = \beta_0^{\rm MLJ} + \beta_1^{\rm MLJ} + \beta_2^{\rm MLJ} + \cdots \ , \tag{2.30}$$

is included in Eq. (2.28). Unlike the MMO, the ($n > 0$) MLJ function does not require a normalizing factor in the denominator because the $(R_e/R)^n$ factor dominates over the finite exponential term at large R, and as $R \to \infty$ it takes on the theoretically predicted

long-range behaviour of Eq. (2.27), with C_n identified by

$$C_n \;=\; 2\mathcal{D}_e\;(R_e)^n\;e^{-\beta^{\infty}_{\mathrm{MLJ}}}\;. \tag{2.31}$$

Since the functional behaviours of $\beta_{\mathrm{MMO}}(z)$ and $\beta_{\mathrm{MLJ}}(z)$ (for $n \neq 0$) are completely different, it is convenient to treat the MMO function as a separate model, rather than as a limiting ($n = 0$) case of the MLJ function. On the one hand, unlike the previous three potential forms, negative $\beta_{\mathrm{MLJ}}(R)$ values do not necessarily indicate that the potential will become pathological. On the other hand, this does not mean that the MLJ potential is immune to unrealistic behaviour, as a rapidly decreasing $\beta_{\mathrm{MLJ}}(R)$ (as a function of $|R - R_e|$) may overcome the counterbalancing effect of the inverse-power term.

2.5 DPF Methodology

Direct fitting of analytical potentials to spectroscopic data is not a new technique; the process by which this is done is well understood and quite developed. The general methodology behind fitting single-minimum potentials to ro-vibrational transitions is the same as that behind any non-linear least-squares procedure, and the flowchart of Fig. 2.1 illustrates the steps required for the overall process.

First, the spectroscopic data to be used, which can be acquired experimentally, from the literature, or from unpublished archive sources, are assigned line positions with their associated experimental uncertainties. Then a potential form that can be fitted to these data must be chosen. Since an iterative non-linear least-squares method is used to fit the chosen potential function to the data, initial trial parameters for each parameter in the model potential must be obtained prior to starting the fit. During the least-squares fitting procedure, the predicted value of each datum and its partial derivatives with re-

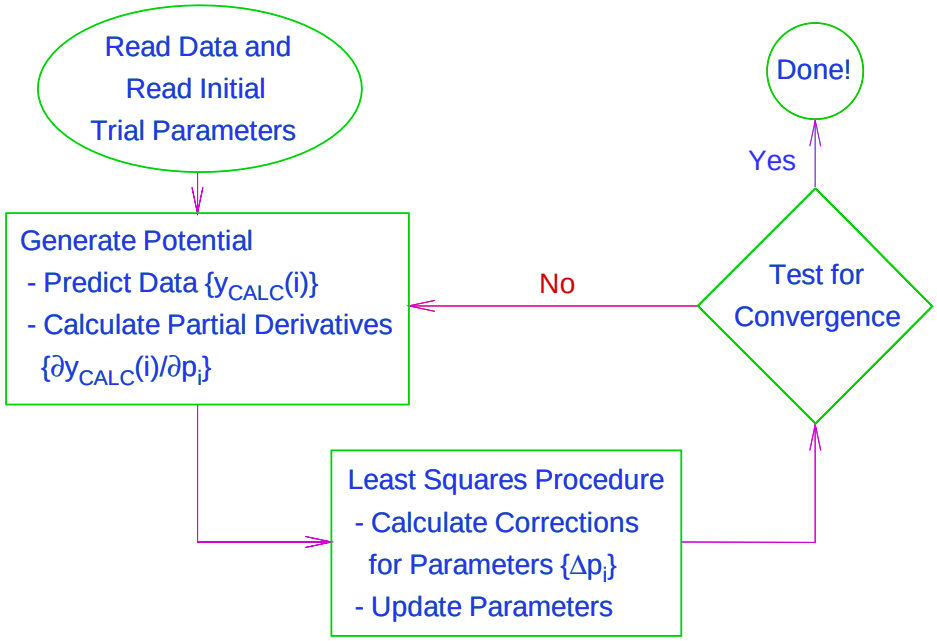

Figure 2.1: A Flowchart for the DPF Procedure.

spect to each potential parameter must be calculated. In each iteration the least-squares procedure generates corrections to the trial parameters, and the whole procedure is repeated iteratively until the changes are less than the "parameter sensitivities", at which point the fit is considered to be converged [33]. To implement this procedure, a computer program capable of handling the various types of data as well as the various potential form(s) being used must be developed. Although the program `DSPotFit` currently can fit only certain generalized Morse-type functions, such as the GMO, MMO, EMO, and MLJ, to spectroscopic transitions, only modest modifications should be required to allow fitting of other potential forms.

One must be careful when choosing the potential form, as there remain some not fully understood limitations to the present application of the DPF method. In particular, it has been found that generalized Morse-type potentials can turn over at very short distances

to yield spurious inner-well minima. This occurred in potential fits to CuH and AgH data, as well as for the published MMO potentials for InF [34] and NaCl [35]. Although such a "turnover" may occur at so high an energy that it can be ignored, this is not always the case, and sometimes a low and thin turnover barrier may occur. Naive use of these potential functions may then lead to poorly calculated properties and expectation values. Some simple methods that we have tested to limit this non-physical behaviour have not been entirely successful, and is one of the problems that will be described below.

The least-squares fitting method requires the calculation of the predicted transition frequencies $\{\nu_i\}$ and their partial derivatives with respect to the potential parameters $\{p_k\}$. Since the observables are differences between the energy levels of the upper and lower states, what is needed are the energy eigenvalues for the upper and lower states, as well as their partial derivatives with respect to the potential parameters, namely

$$h\nu_i \;=\; E_{v',J'} - E_{v'',J''} \quad \text{and} \quad \frac{\partial h\nu_i}{\partial p_k} \;=\; \frac{\partial E_{v',J'}}{\partial p_k} - \frac{\partial E_{v'',J''}}{\partial p_k} \;. \tag{2.32}$$

This is computationally tedious, but with the considerable advances in cheap computational power, this problem is relatively minor.

The calculation of the upper- and lower-state energy eigenvalues ($E_{v,J}$) needed in Eq. (2.32) can be performed by solving the one-dimensional radial Schrödinger equation

$$-\frac{\hbar^2}{2\mu}\,\frac{d^2\Psi_{v,J}(R)}{d^2R} \;+\; V_{\mathrm{eff},J}(R)\Psi_{v,J}(R) \;=\; E_{v,J}\Psi_{v,J}(R) \tag{2.33}$$

numerically, with $V_{\mathrm{eff},J}(R)$ defined in Eq. (2.7). In the `DSPotFit` program package, this is done by a subroutine (`SCHRQ`) [36] based on the Cooley-Cashion-Zare Schrödinger solver SCHR [37, 38, 39, 40, 41], which calculates the closest vibrational level to a given trial energy for the potential. Necessary input to this subroutine includes a good trial energy

for each level required by the fitting procedure.

Determination of the energy levels are done by the Automatic Level Finder (`ALF`) subroutine which is a level-search package developed to calculate systematically all vibrational levels in a potential. These vibrational energies are then combined with the first seven rotational constants (B_v, $-D_v$, H_v, L_v, M_v, N_v, and O_v) calculated by the subroutine `CDJOEL` to calculate good trial energies for any given ro-vibrational level in the potential. The subroutine `ALF` has also been adapted for the systematic generation of good trial energies for a sample "shelf"-state potential [42], as well as for a potential with a double-minimum well [43].

The derivatives of the eigenvalues $\{E_{v,J}\}$ with respect to potential parameters $\{p_k\}$ required in Eq. (2.32) may be calculated readily from the eigenfunctions obtained as part of the eigenvalue calculation using the Hellmann-Feynman theorem [44, 45]

$$\frac{\partial E_{v,J}}{\partial p_k} = \left\langle \Psi_{v,J} \left| \frac{\partial V_{\mathrm{eff},J}}{\partial p_k} \right| \Psi_{v,J} \right\rangle . \tag{2.34}$$

As the wavefunctions for the desired states ($\Psi_{v,J}$) have already been generated during the solution of the Schrödinger equation (Eq. 2.33), and as the partial derivatives ($\partial V_{\mathrm{eff},J}/\partial p_k$) can be calculated analytically, these expectation values can be obtained very easily. A listing of these partial derivatives for various potential forms can be found in Appendix B.

Since the observable line positions or level energy spacings are not linear functions of the parameters defining the potential energy curve(s), the least-squares fits to the experimental data are non-linear. As in any non-linear least-squares problem, the initial hurdle encountered is that of determining realistic initial trial values of the parameters to be optimized by the automated iterative fitting procedure. Once a potential form has been chosen, the determination of adequate initial trial parameters is a straightforward analytical procedure. In particular, comparing the partial derivatives of the model potential

at its minimum (R_e) with those of the analogous Dunham potential,

$$V_{\rm Dun}(R) \;=\; a_0\xi^2\left(1 + a_1\xi + a_2\xi^2 + \cdots\right) \;, \tag{2.35}$$

where $\xi = (R - R_e)/R_e$, one can determine explicit equations for the set of potential parameters $\{p_k\}$ in terms of the Dunham parameters $\{a_i\}$. Because Dunham has already determined equations relating his potential parameters to the conventional $\{Y_{lm}\}$ molecular constants of Eq. (2.4) [46, 47], it is a simple task to find equations to relate some of the low-order spectroscopic constants to the parameters of the desired potential form (see Appendix A). The method used in `DSPotFit` is to generate trial values for $\mathcal{D}_e$, R_e, and the first three exponent parameters (β_0, β_1, and β_2) from the the low order molecular constants ($\mathcal{D}_e$, B_e, α_e, ω_e, and $\omega_e x_e$). These constants can be taken from the literature [48], or obtained from parameter fits to the spectroscopic data. A more detailed discussion of this point can be found in Appendix A. In theory, trial values for higher-order exponent parameters (β_3, β_4, etc.) can also be generated, but the calculations become increasingly tedious and difficult to perform. As the potential defined by the first few leading parameters is in general fairly good, it is much more convenient to determine these higher-order parameters from the fit itself by using a "bootstrapping" method. This method requires the initial value of the yet-to-be-determined parameter to be set to zero, and then freed while the other parameters remain fixed at their previously determined values. The latter are then released one or more at a time and refitted, until all of the parameters have been freed. This cycle repeats until a "good" fit is reached.

In all of the fits reported herein, the observed transition energies were weighted by the inverse square of their uncertainties, and the quality of fit is indicated by the value

of dimensionless standard error

$$\overline{\sigma}_f \quad = \quad \left\{ \frac{1}{N-M} \sum_{i=1}^{N} \left[\frac{y_{\rm calc}(i) - y_{\rm obs}(i)}{u(i)} \right]^2 \right\}^{1/2} \tag{2.36}$$

where each of the N experimental data $y_{\rm obs}(i)$ has an uncertainty of $u(i)$, and $y_{\rm calc}(i)$ is the value of datum–i predicted by the M–parameter model being fitted. All parameter uncertainties quoted here are 95% confidence limit uncertainties, and the atomic masses used were taken from the 1993 mass table [49]. Thus, a fit is considered "good" when the differences between the calculated and observed transitions are on average within the uncertainty of the observations, i.e. $\overline{\sigma}_f \approx 1$.

Chapter 3

The Inner Wall Extrapolation Problem: The Coinage Hydrides

Despite the advantages of using fully analytical potential functions in the DPF procedure, there is always a possibility that the potential may not extrapolate properly outside the experimental data range. One of the more extreme aberrations can occur at small intermolecular distance where, if the $\beta(R)$ function drops off steeply enough, the inner repulsive potential wall can actually go through a maximum and turn over.

This was found to occur for a number of published potential functions, including those for InF [34], NaCl [35], LiI [50], and CuH [6]. The example of the EMO potentials for the coinage hydrides shown in Figure 3.1 shows that within and quite a distance beyond the range of the experimental data (solid curve segments), all of the potential functions are well behaved. However, the bottom frame of Figure 3.2 shows that well beyond the range of the data, it is quite possible for the potentials to have non-physical behaviour. The top frame in Figure 3.2 shows the behaviour of the $\beta(R)$ functions over the same interval. One can see that the potentials start to misbehave when $\beta(R)$ has a steep dip

and plunges into the negative regime. In both figures, the solid line denotes the part of the potential for which experimental data was available, while the dotted portions of the curve are extrapolations.

Although the potentials reported in these papers are not guaranteed to work beyond the experimental range, it is disconcerting that the function has such a behaviour. Furthermore, it is possible for the turn-over point to be at such a large value of R that the aberration can begin to affect calculations within the well itself.

3.1 Data Set Used

The multi-state, multi-isotopomer coinage hydride data for AuH and AuD, AgH and AgD, and CuH and CuD [6] were used to test various techniques to correct for potential turn-over. For the copper hydride system the new infrared data at the core of the present analysis consists of the (1,0), (2,1), (3,2) and (4,3) bands of ^{63}CuH and the (1,0), (2,1) (3,2) bands of ^{65}CuH, ^{63}CuD and ^{63}CuD [51]. For strong un-blended lines the associated measurement uncertainty was estimated to be 0.001 cm^{-1}. In an effort to characterize the X–state of this system optimally, the present analysis also incorporated the pure rotational measurements for the $v = 0$ levels of all four isotopomers [52, 53, 54], as well as the (0,0), (0,1) and (1,0) bands of the electronic A–X systems of ^{63}CuD and ^{65}CuD reported by Fernando *et al.* [55]. The uncertainties used to define the weights used for these published data were 0.000003 [52, 53] and 0.0000005 cm^{-1} [54] for the pure rotational transitions, and 0.004 cm^{-1} for the electronic transitions [55]. While more extensive A–X data have been reported by Ringström [56], they are of much lower accuracy, and so were not used here.

For the silver hydride system the present analysis was based solely on new infrared data [51]. It consists of the (1,0), (2,1) and (3,2) bands of the four isotopomers ^{107}AgH,

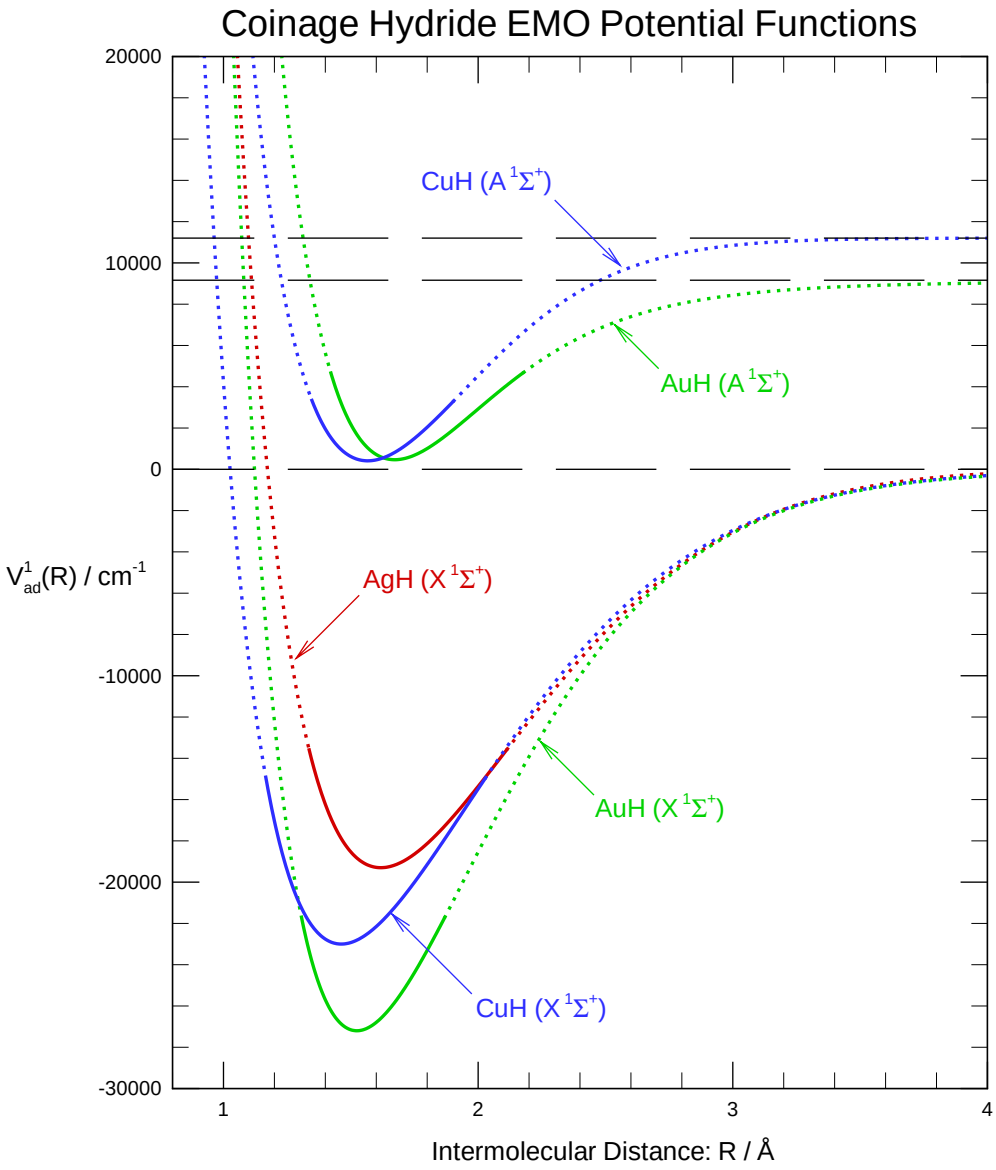

Figure 3.1: Coinage Hydride EMO Effective Adiabatic Potential Functions

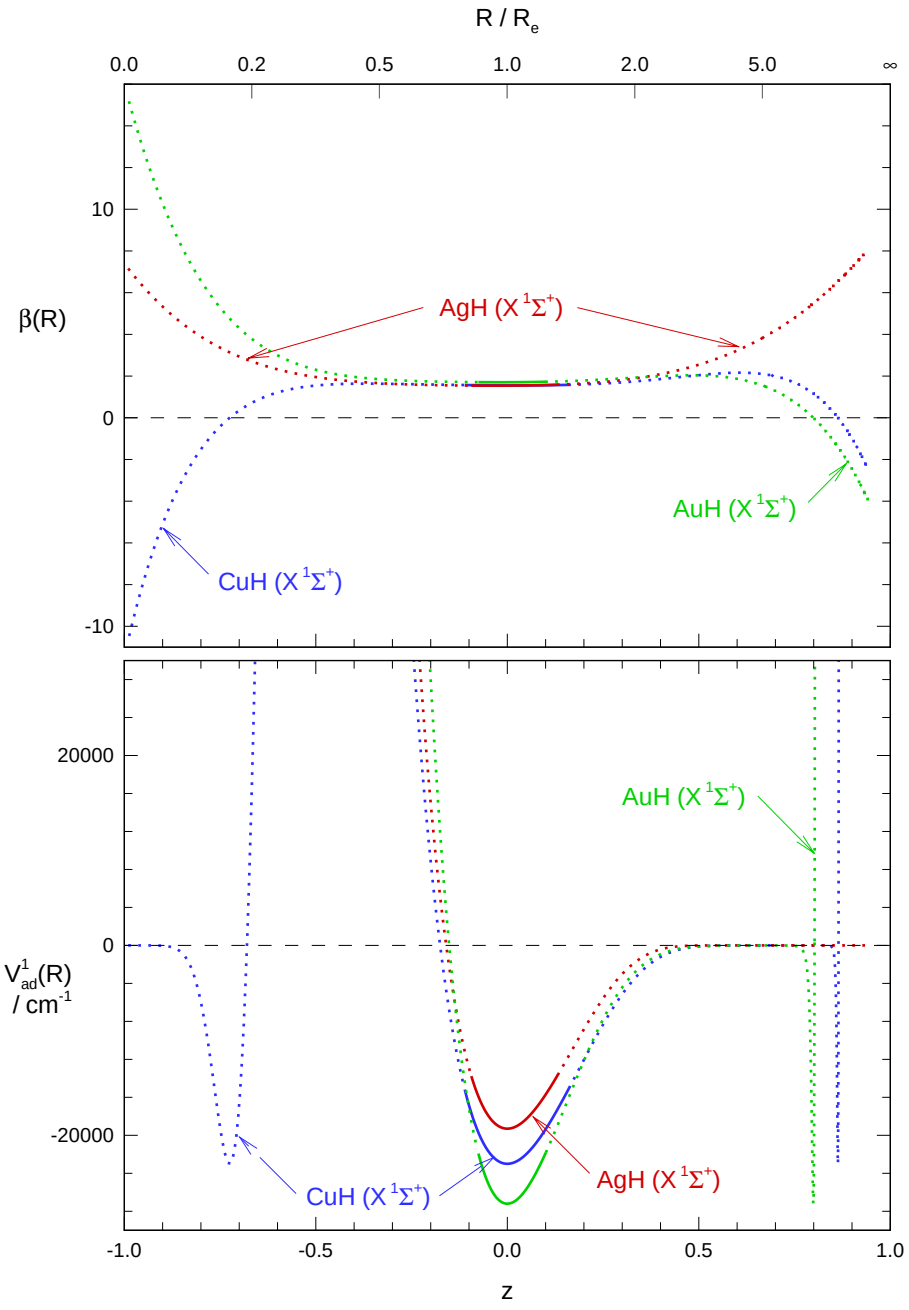

Figure 3.2: Coinage Hydride EMO Potential and $\beta(R)$ Functions

^{109}AgH, ^{107}AgD and ^{109}AgD; the average uncertainty for strong un-blended lines was taken as 0.001 cm^{-1}.

For the gold hydride system the new infrared data consist of the (1,0) and (2,1) bands of ^{197}AuH and the (1,0), (2,0) and (3,2) bands of ^{197}AuD; for these measurements the uncertainty associated with strong un-blended lines was again estimated to be 0.001 cm^{-1} [51]. New high resolution optical measurements of the (0,0), (1,0), (2,0), (0,1), (1,1), (2,1) and (1,2) bands of the A(0^+)–X($^1\Sigma^+$) system of ^{197}AuH reported by Fellows *et al.* [57], with estimated uncertainties of 0.003 cm^{-1}, were also included in this analysis.

As the data range only spanned a fraction of the potential well, it was unlikely that accurate values of the dissociation energies could be calculated from these fits. Therefore, all of the fits to the coinage hydride data had fixed dissociation energies: $\mathcal{D}_e$(AgH) = 19300 cm^{-1}, $\mathcal{D}_e$(AuH) = 23000 cm^{-1}, and $\mathcal{D}_e$(CuH) = 27200 cm^{-1} taken from the literature [48]. Unless otherwise stated, the numerical calculations were performed over a radial range $0.500 \leq R \leq 5.000$ Å with a mesh size of 0.0005 Å.

3.2 Constraints on $\beta(R)$ at $R = 0$

Our main goal was to develop some sort of "simple" constraint to prevent the potential function from turning over. One of the simplest constraints was to fix the $\beta(R)$ function to a positive value at $R = 0$ ($z = 1$) using what we call a "power-series constraint", in hopes that the function would stay in the positive regime. This would reduce the possibility of $\beta(R)$ having a large positive slope, which would in turn reduce the chances of the potential form misbehaving.

The power-series constraint can be implemented for the EMO by adding an extra

term to the $\beta(R)$ function, i.e.

$$\beta(R) \;=\; \sum_{i=0}^{n} \beta_i z^i + \beta_a z^a \;, \tag{3.1}$$

and setting this constraining parameter β_a to be

$$\beta_a \;=\; (-1)^a \left[\beta_{\rm va} - \sum_{i=0}^{n} (-1)^i \beta_i \right] \;, \tag{3.2}$$

in which $\beta_{\rm va}$ is the value to which $\beta(R)$ is to be constrained at $R = 0$.

The example shown in Figure 3.3 uses the EMO potential for the ground state of AgH. The BOB correction terms are ignored in this analysis in order to reduce the complexity of the calculations. For the sake of comparison, all constrained potentials were fitted with six unconstrained exponent parameters, with $a = 6$ and β_6 being the constraining parameter. The fits were performed by optimizing all of the potential parameters (except for $\mathcal{D}_e$) and changing the constraining parameter β_a with each iteration of the non-linear least-squares fit so that $\beta_{\rm va}$ always remains fixed. The overall quality of fit to the data for the three potentials was essentially the same. All other aspects of the fit are the same as those for the published AgH ground state potential [6]. The bottom frame of Figure 3.3 shows the potential functions obtained using various values for $\beta_{\rm va}$, including the unconstrained (free) fit. The top frame shows the behaviour of the $\beta(R)$ functions for all four potentials. As with the previous figure, the solid line is the portion of the potential corresponding to the available experimental data, while the dotted line is extrapolation.

It can readily be seen that even with a moderately strong constraint, such as fixing $\beta_{\rm va} = 25$, a spurious inner minima still occurs due to the steepness of $\beta(R)$ near the small dip. To remove this behaviour completely, a very strong constraint, such as setting $\beta_{\rm va} = 50$, is required, even though from the top segment of Figure 3.3 the function itself

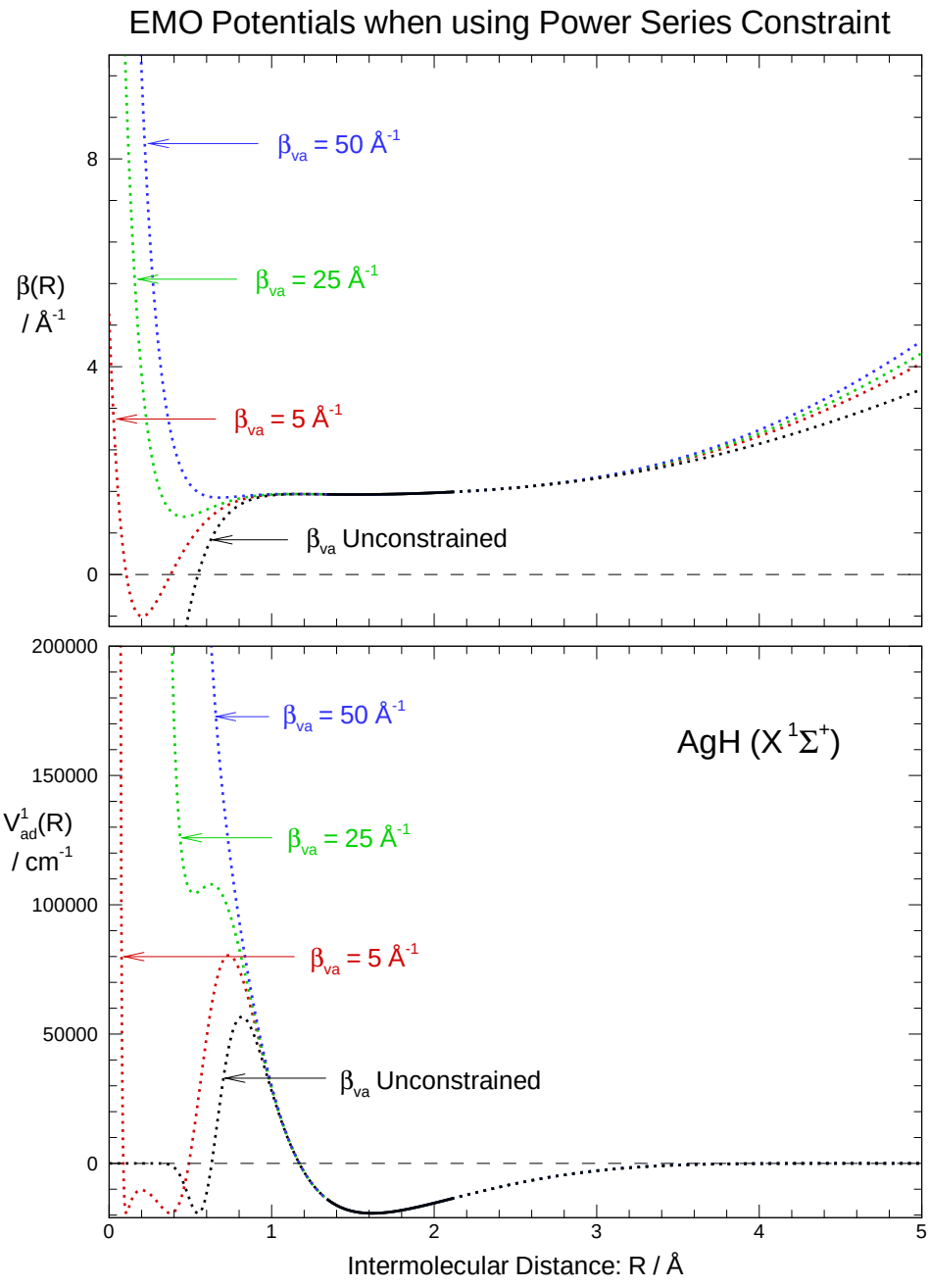

Figure 3.3: AgH EMO Potentials with Power Series Constraint

would seem to approach a smaller limit ($\beta_{\rm va} \approx 1.6$). Thus, the use of this constraint may require un-physically large constraining values which, due to the magnitude of the constraint, affects the rest of the potential, thus making the representation slightly less effective.

Another possible type of power-series constraint is to fix the slope of $\beta(R)$ at $R = 0$. Using the same method as above, an extra term is added to the exponent function

$$\beta(R) \;=\; \sum_{i=0}^{n} \beta_i z^i + \beta_b z^b \tag{3.3}$$

where the constraining parameter (β_b) is set to be

$$\beta_b \;=\; \frac{(-1)^b}{-b}\left[\beta_{\rm sl}\frac{R_e}{2} + \sum_{i=1}^{n} i(-1)^i \beta_i\right] \tag{3.4}$$

so that $\left.\frac{\partial\beta(R)}{\partial R}\right|_{R=0}$ is fixed to the chosen value of $\beta_{\rm sl}$ (namely $\beta_{\rm sl} = 0$). As, the test results were not very encouraging, this method was abandoned.

A combination of the two constraints (i.e. fixing both $\beta(R = 0)$ and $\left.\frac{\partial\beta(R)}{\partial R}\right|_{R=0}$) was also considered, and rejected, since the complexity of the procedure tended to compromise the idea of imposing a simple constraint of the β function. Although it is difficult to believe that this third method would prove more effective than the previous two attempts, this does not mean that the double constraint will necessarily fail. However, detailed tests would be required and this appeared to be an unfruitful approach to the problem.

A detailed presentation of the calculus associated with the imposition of these constraints, including the partial derivatives needed in the non-linear least-squares fitting procedure, can be found in Appendix C.

3.3 The SPF Function

A second possible approach to the problem of pathological behaviour at small-R was to use an exponent expansion parameter that was guaranteed to approach infinity as the intermolecular distance R approached zero. Since the power series in z reached a finite value at $R = 0$, it was assumed that by forcing $\beta(R)$ to positive infinity, the potential could be forced to behave properly.

Efforts in this area were based on replacing the power series in z of Eqs. (2.23), (2.26), and (2.29) by a power series in the Simon-Parr-Finlan (SPF) expansion variable [58, 59] $x \equiv (R - R_e)/R$, and expanding $\beta^{\rm SPF}(x)$ as

$$\beta^{\rm SPF}(x) = \beta_0^{\rm SPF} + \beta_1^{\rm SPF} x + \beta_2^{\rm SPF} x^2 + \cdots . \tag{3.5}$$

The partial derivatives required for calculating trial parameters for this case ($\beta_0^{\rm SPF}$, $\beta_1^{\rm SPF}$, and $\beta_2^{\rm SPF}$) from low-order spectroscopic constants can be found in Appendix A, while the partial derivatives of the potential with respect to its parameters required for the least-squares fitting routine can be found in Appendix B. In both cases, the expansion parameter z can be replaced by the SPF parameter x.

Initial testing showed that some molecules for which the expansion in powers of z had unphysical behaviour were represented well without any anomalies by the EMO using the SPF expansion. This case can be seen with the CuH molecule in Figure 3.4. Unfortunately, further studies showed that some molecules that did behave with the z expansion may misbehave with the x expansion. This can be seen in Figure 3.5 with the AuH example.

Further comparisons of the $\beta(R)$ functions showed that when problems arose, the SPF expansion in powers of x tended to diverge both earlier and more rapidly than the z expansion (see Figures 3.4 and 3.5). This would also tend to cause the potential to turn

over more quickly (at larger R) and at a lower energy. These properties suggest that the SPF expansion will be less dependable than the z expansion.

In both Figures 3.4 and 3.5, the bottom frame shows the potential functions using the three different types of expansion for the exponent function. The top frame in each figure shows the exponent functions for each of the three potentials. In both figures, the solid curve denotes the expansion in terms of the SPF parameter x, the dashed curve represents the expansion in terms of the z parameter, while the dotted curve represents the expansion of the Self-Constraining Expansion (SCE) function described below. As the z power series expansion and the SCE lie on top of each other, they are indistinguishable in the plots.

The fits to the experimental data using all three forms for the ground-state CuH potential used seven exponent parameters, one Cu- and five H-centered adiabatic correction terms, and one Cu- and two H-centered rotational non-adiabatic correction terms. Both of these fits were over the mesh range $0.500 \leq R \leq 9.999$ Å with a mesh size of 0.00075 Å.

The z expansion and SCE ground state AgH potentials were fitted with six exponent parameters, three H-centered adiabatic correction terms, and two H-centered rotational non-adiabatic correction terms, while the SPF potential has seven exponent parameters, four H-centered adiabatic correction terms, and one Ag-centered rotational non-adiabatic correction terms. The SPF expansion was unable to represent the AgH data accurately when only six exponent parameters were utilized.

3.4 The SCE Function

As all of the attempts with the power-series constraint used high-order β_i in the $\beta(R)$ expansion as the constraining term, it was possible that these higher-order terms did not have enough weight in the intermediate extrapolation region where the potential tended

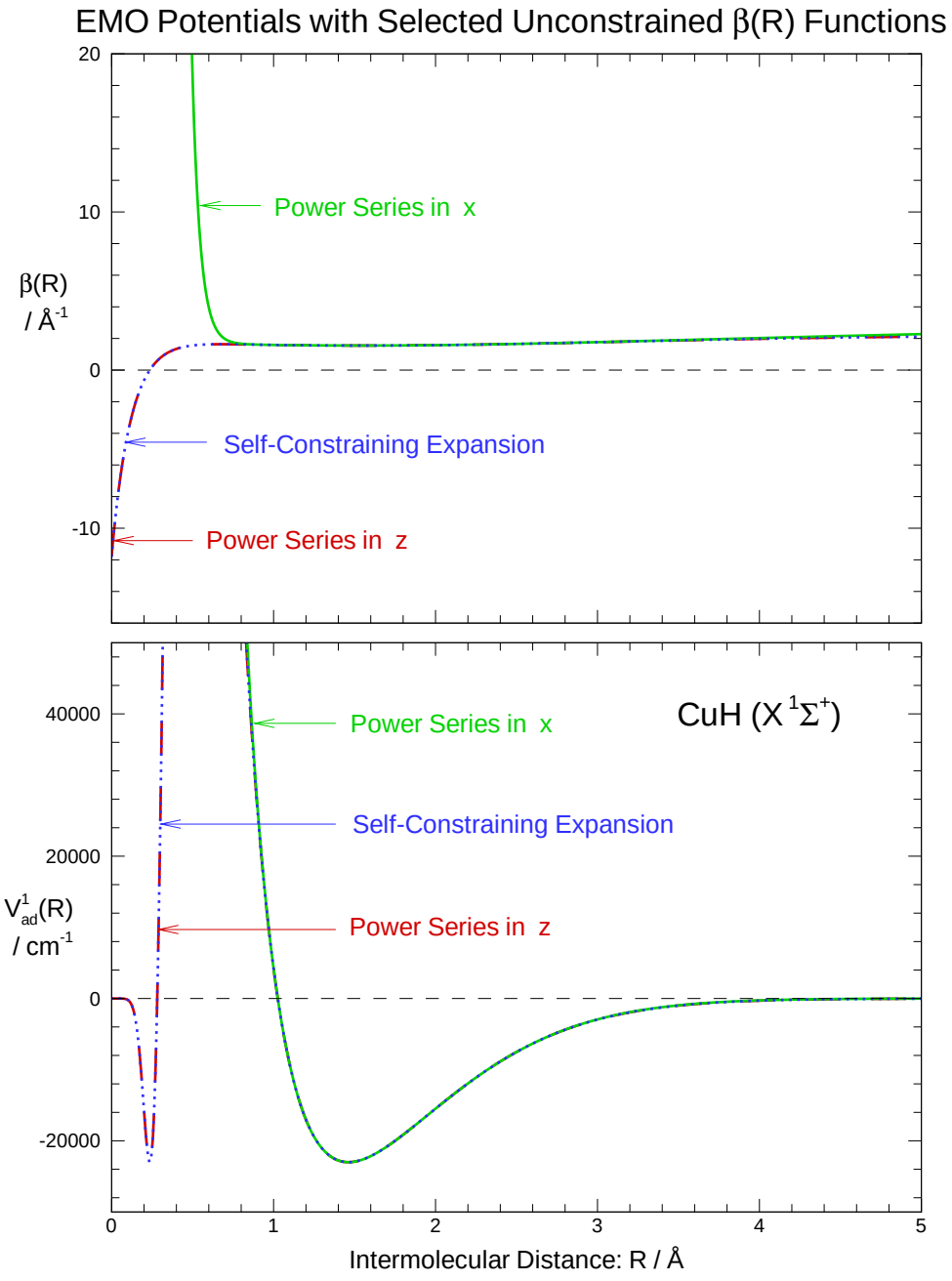

Figure 3.4: Comparing EMO $\beta(R)$ Expansion Parameters for CuH

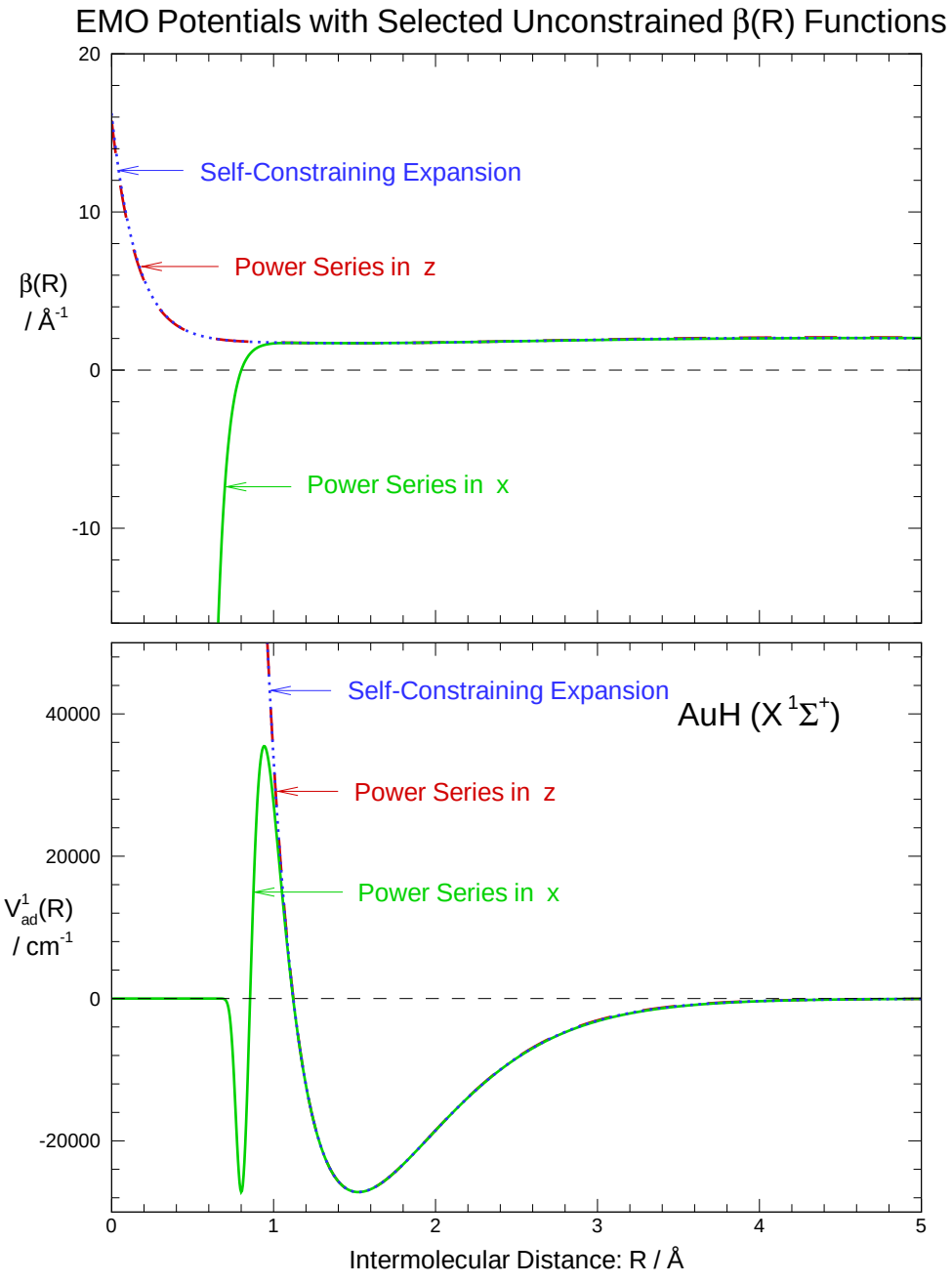

Figure 3.5: Comparing EMO $\beta(R)$ Expansion Parameters for AuH

to behave absurdly. The possibility of using a low-order β_i as a constraining term was considered.

An approach using this method is to employ a type of function in the exponent which does not use a "tacked on" constraint, but has parameters that inherently can be used to constrain the function itself. One such function, dubbed the Self-Constraining Expansion (SCE) function, was tested below.

The SCE function has the form

$$\beta^{\mathrm{SCE}}(R) \;=\; \beta_a + a(R)\left[(-1)^n\beta_a + \beta_b + \sum_{i=1}\beta_i\,[b(R)]^i\right]\;, \tag{3.6}$$

with $a(R)$ and $b(R)$ functions of the intermolecular separation R, and β_a, β_b, and n constants. The functions $a(R)$ and $b(R)$ and the parameter n are chosen in such a way that β_a and/or β_b can be used as constraining terms. For the case of the coinage hydrides, a short-range ($R = 0$) constraint is desired, or more specifically, to require that $\beta^{\mathrm{SCE}}(R = 0) = -\beta_b$: this can be achieved by setting $n = 0$, and

$$a(R) \;=\; \frac{R - R_e}{R + R_e}\;, \quad b(R) \;=\; \frac{R}{R + R_e}\;, \tag{3.7}$$

so that $a(R = 0) = -1$ and $b(R = 0) = 0$. The partial derivatives of the SCE function with respect to the potential parameters required for non-linear least-squares fitting can be found in Appendix D.

The SCE potentials for both AuH and CuH were fitted with the same numbers of potential parameters and over the same radial mesh as their z expansion counterparts (see above). As can be seen by the plots for CuH and AgH in Figures 3.4 and 3.5, the potential and the $\beta(R)$ functions are practically identical for both the z expansion and the unconstrained SCE when the same numbers of potential parameters are used. This

suggests that the unconstrained SCE and the z expansion are essentially identical in functionality.

When testing the constraint capabilities of the SCE, it was found that only a small ($\beta_b = -5$) constraint was required to correct for the unphysical behaviour for CuH (Figure 3.6). However, when testing was carried out for a known "strong" constraint system, such as the AgH potential excluding the Born-Oppenheimer correction terms (Figure 3.7), the SCE was not able to correct the turnover with small values for the constraint. In fact, beyond a constraint of $\beta_b = -10$, the fits did not converge. Therefore, it seems that the SCE also does not provide a robust means for correcting this potential turnover problem.

3.5 Occam's Razor Solution

In the end, it was decided to go with the simplest type of constraint, where the $\beta(R)$ function is fixed at a constant value for $R \leq R_x$, with R_x the point for which the potential begins to behave abnormally. Specifically, this distance is chosen to be the point at which the second partial derivative of the potential becomes zero, so that

$$\left.\frac{\partial^2 V_{\mathrm{ad}}(R)}{\partial R^2}\right|_{R=R_x} = 0 \, . \tag{3.8}$$

Ideally, it would be better to choose a point for fixing $\beta(R)$ *before* the potential misbehaves strongly. This may be achieved by noting that at distances slightly less than R_e, the condition

$$\frac{\partial^2 V_{\mathrm{ad}}(R)}{\partial R^2} \geq 0 \tag{3.9}$$

is satisfied and $V_{\mathrm{ad}}(R)$ is likely to pass through a maximum before crossing zero at R_x, in which case, it is likely that the third derivative will cross zero before the second derivative.

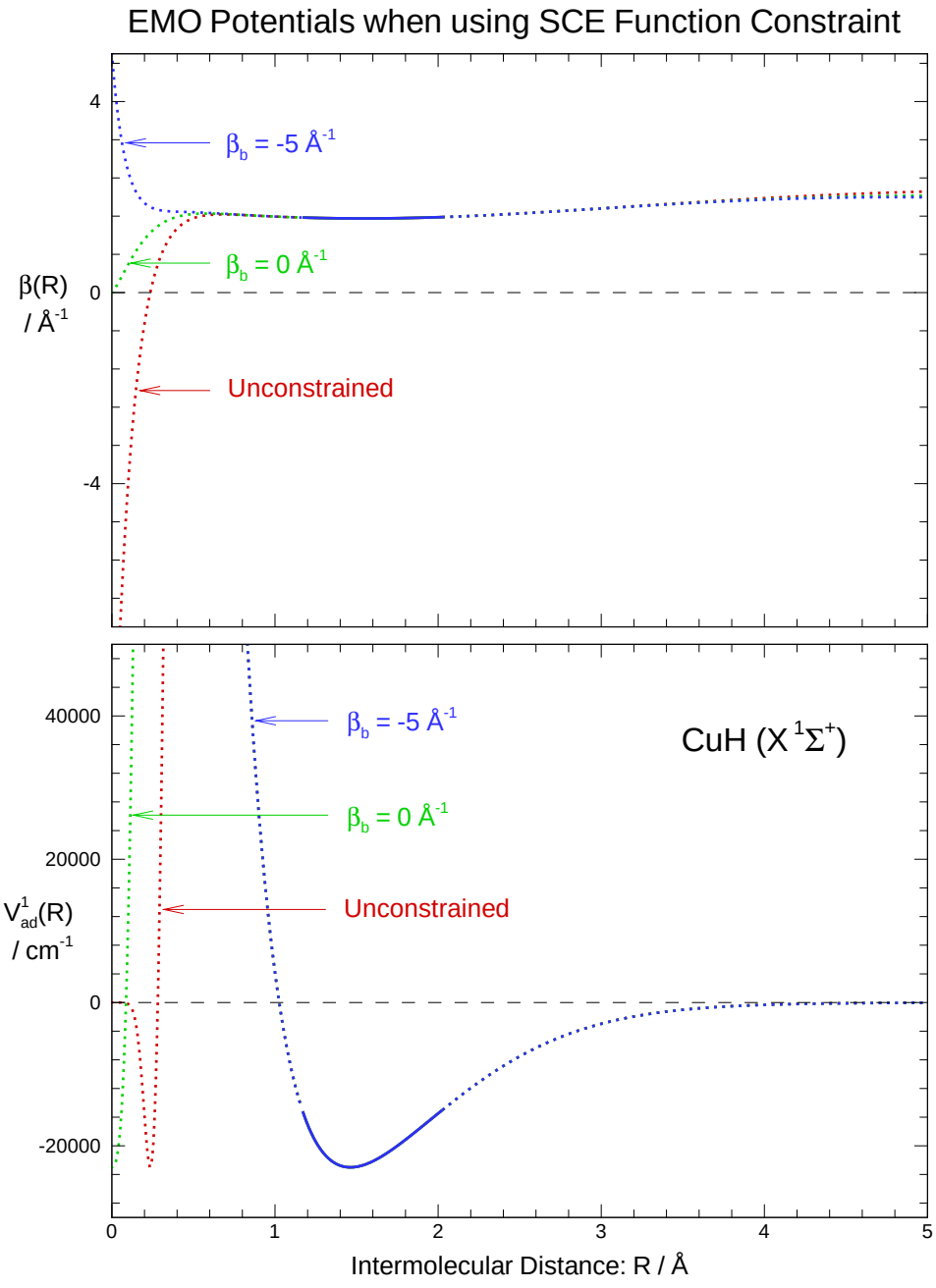

Figure 3.6: CuH EMO Potentials with Self-Constraining Expansion Function Constraint

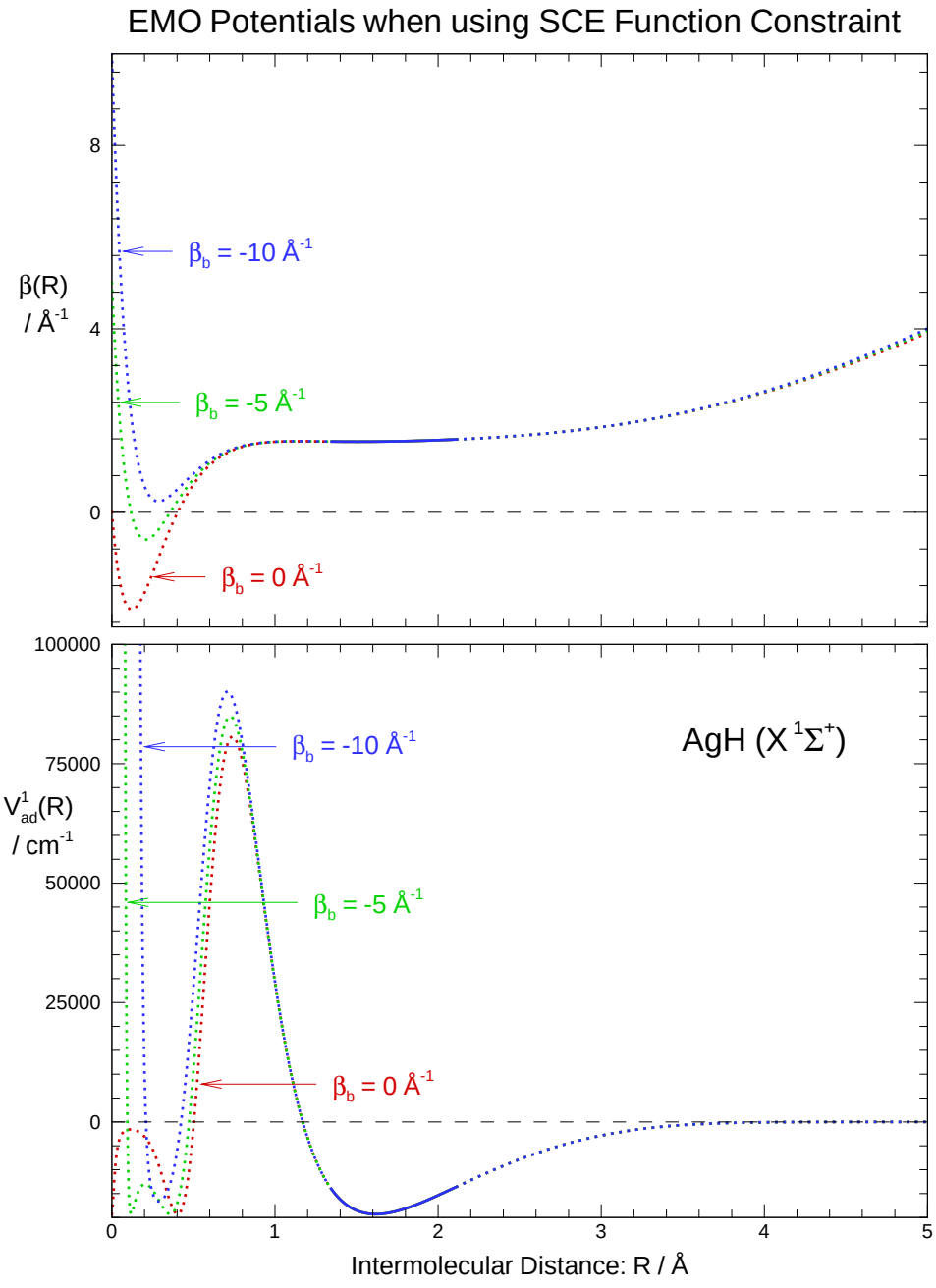

Figure 3.7: AgH EMO Potentials with Self-Constraining Expansion Function Constraint

Therefore the constraint can be set to be

$$\beta(R < R_x) \;=\; R_x \;, \tag{3.10}$$

with

$$\left.\frac{\partial^2 V_{\rm ad}(R)}{\partial R^2}\right|_{R=R_a} \;=\; 0 \quad \text{and} \quad \left.\frac{\partial^3 V_{\rm ad}(R)}{\partial R^3}\right|_{R=R_b} \;=\; 0 \;, \tag{3.11}$$

with $R_x = R_a$ or R_b, whichever is larger.

For the present case, although it is off-scale in the plot in the bottom half of Figure 3.8, the CuH ground state potential has an inner wall inflection point at $R = 0.609$ Å, and turns over at $R = 0.475$ Å. This turnover is far enough away from the potential well region ($R > 1.026$ Å) that by fixing the β function at $R_x = 0.7285$ Å (where $V(R) = 100391$ cm^{-1}) as denoted by the dashed line in the top frame of Figure 3.8, there are no effects of this correction on the bound-state properties of the molecule. The solid line denotes the experimentally defined region of the potential function (bottom frame) and $\beta(R)$ function (top frame). The dotted line is the unconstrained extrapolation, while the dashed line is the constraint of the function. As the corrected portion of the potential continues to grow exponentially, that part of the potential function cannot be seen in the bottom plot.

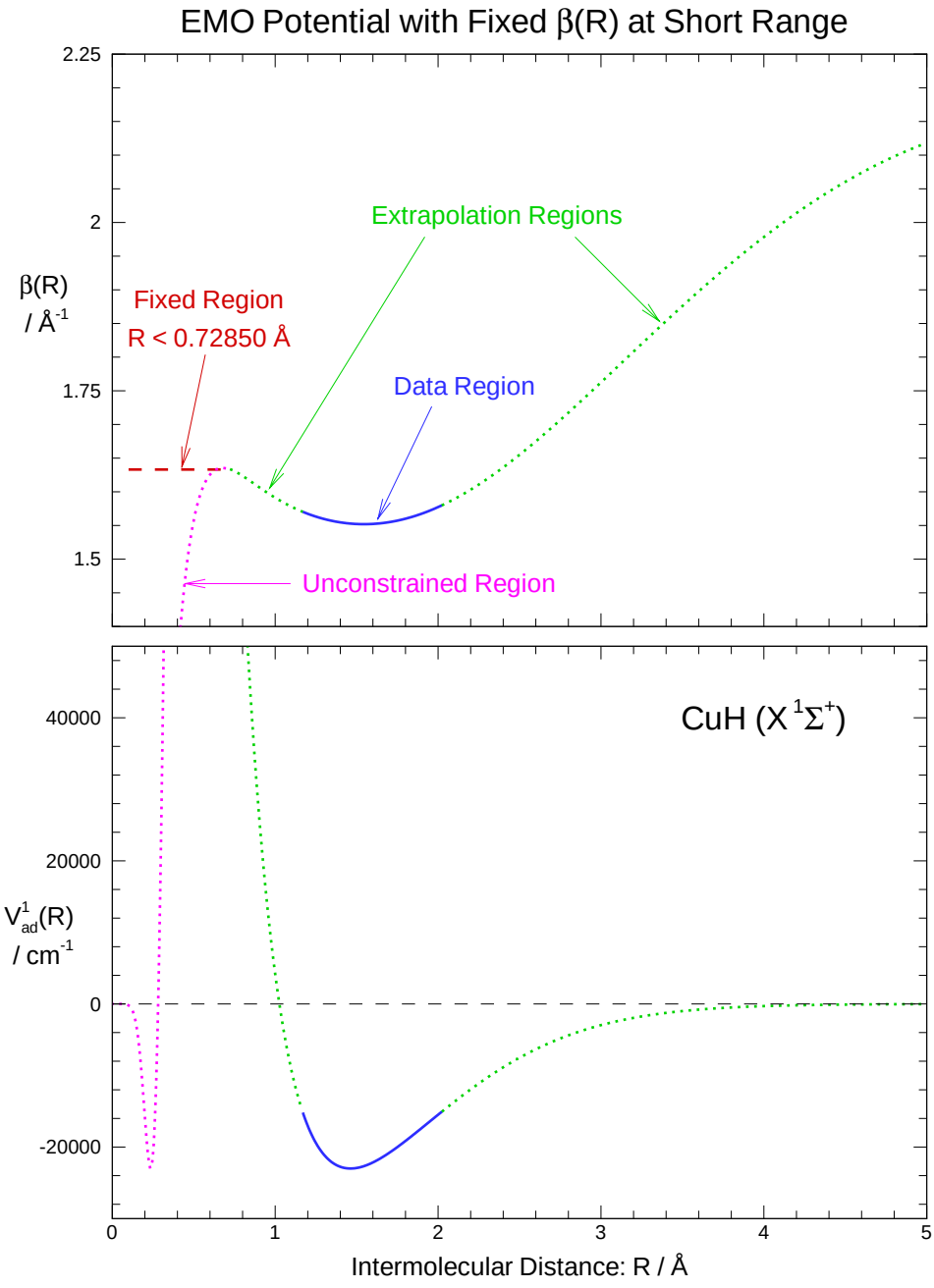

Figure 3.8: CuH EMO Potential with Fixed $\beta(R)$ Short Range Constraint

Chapter 4

Potential Tail Extrapolation Problem: The Rubidium Dimer

Despite the perceived shortcomings of efforts to develop short-range fixup methodologies, it can be hoped that long-range methods would be more fruitful. Unfortunately, the coinage hydride data were inadequate for testing long-range constraints, as they spanned only a small fraction of the well. A more appropriate data set for this purpose is that for the rubidium dimer, which has data up to the $v = 113$ level for the ground electronic state (see Fig. 4.1), which is less than seven wavenumbers[1] from dissociation. Thus, this molecule provides an ideal candidate for testing the long-range tail extrapolation problem.

4.1 Data Set Used

The data set consisted of 12148 transitions from 424 fluorescence series, with each transition having an experimental uncertainty of 0.001 cm^{-1}. The majority of the lines (7005)

[1] In this report, the wavenumber is referred as the reciprocal centimeter (cm^{-1}) as opposed to the SI definition of m^{-1}.

belonged to the primary isotopomer ^{85}Rb^{85}Rb, while the remaining transitions belong to the lesser abundant species.

As Rb_2 is a heavy molecule, no BOB terms were expected to be found. This was confirmed during the analysis of this molecule when both the Dunham and DPF approaches were unable to determine any BOB terms. Thus, the correction functions can be ignored and equations 2.33 and 2.14 simplify to become

$$\left\{ -\frac{\hbar^2}{2\mu}\frac{d^2}{dR^2} + V_{\rm ad}^{\alpha}(R) + \frac{\hbar^2\, J(J+1)}{2\mu\, R^2} - E_{v,J} \right\} \psi_{v,J}(R) \;=\; 0 \;, \tag{4.1}$$

with

$$V_{\rm ad}^{\alpha}(R) \;=\; V_{\rm ad}^{1}(R) \;=\; V_{\rm ad}(R) \;. \tag{4.2}$$

The adiabatic potential $V_{\rm ad}(R)$ was represented by the MLJ potential of Eq. (2.28) with $n = 6$, which theory shows to be the (inverse) power of R for the limiting long-range interaction potential between two S-state atoms [32].

The top frame of Figure 4.1 shows the potential function for Rb_2, with the solid curve representing the part of the potential over which experimental data were available, and the dotted line representing the extrapolation regions. The experimental values [60] for both v_D and $\mathcal{D}_e$ are also listed in the top half of the figure. The numerical integration of Eq. (2.33) was performed on the interval 2.6 Å $\geq R \geq$ 42.0 Å with a grid spacing of 0.001 Å. This sufficed to ensure that the eigenvalues used in the fits were converged to better than 0.0002 cm^{-1} for all of the observed levels. The results have been listed in Table 4.1.

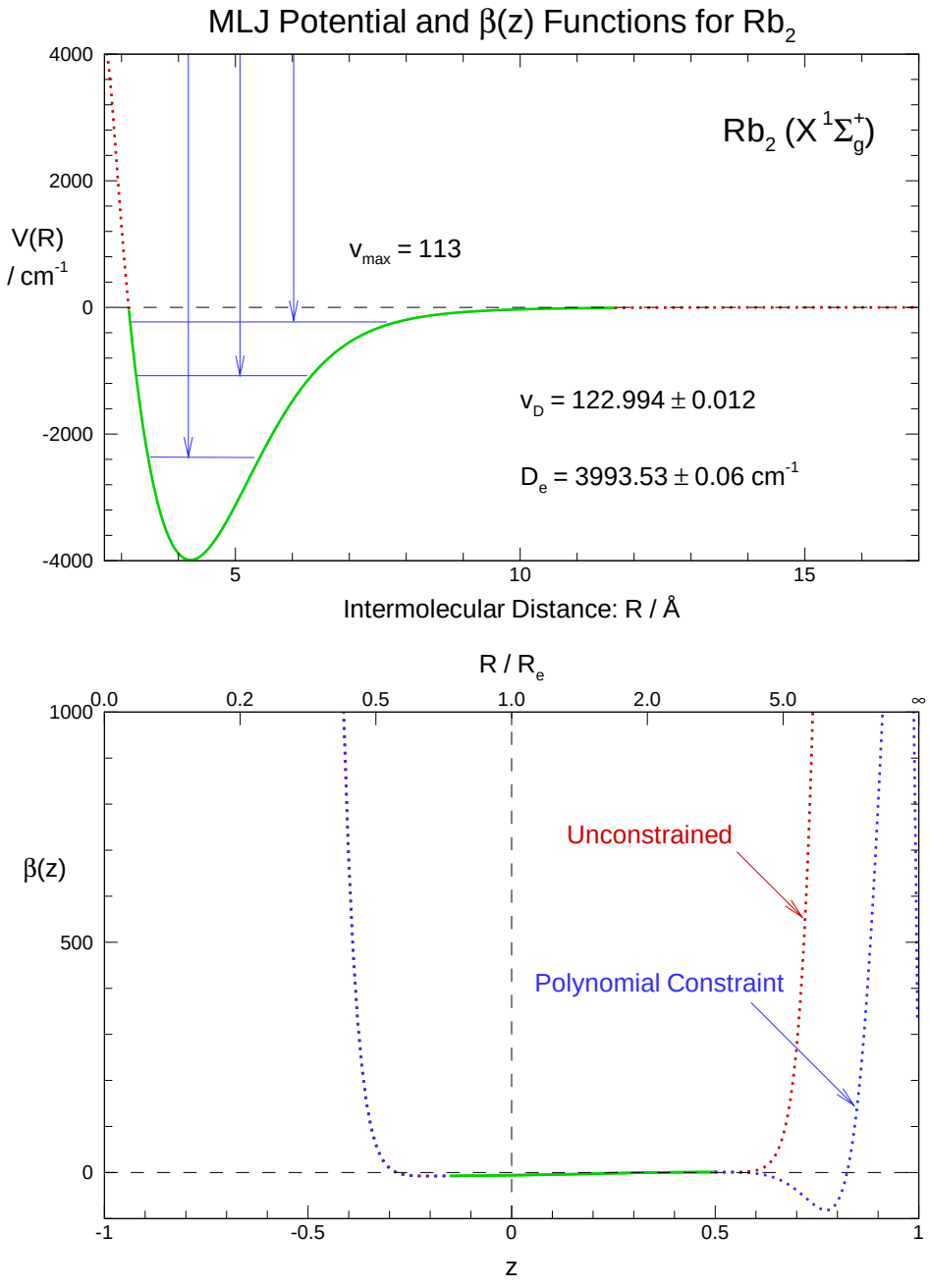

Figure 4.1: The Rubidium Potential and $\beta(R)$ Functions

Table 4.1: MLJ Potential parameters for the $X\,^1\Sigma_g^+$ state of Rb_2 obtained from fitting all observed transition frequencies to eigenvalue differences calculated by solving Eq. (2.33); the numbers in parentheses are the 95% confidence limit uncertainties.

Parameter	$^{85}Rb_2$	
$\mathcal{D}_e$ / cm^{-1}	3993.53[a]	(6×10^{-2})
R_e / Å	4.2099508416	(7.0×10^{-6})
β_0	−5.890526488	(1.4×10^{-5})
β_1	12.12372665	(8.8×10^{-4})
β_2	14.37445982	(3.0×10^{-3})
β_3	32.3419933	(1.6×10^{-1})
β_4	73.470280	(4.8×10^{-1})
β_5	−401.605957	(1.4×10^{1})
β_6	1624.54246	(7.1×10^{1})
β_7	−9574.37042	(4.7×10^{2})
β_8	−72517.6770	(4.2×10^{3})
β_9	443483.7237	(6.1×10^{3})
β_{10}	308764.064	(7.1×10^{4})
β_{11}	−6885490.153	(3.6×10^{5})
β_{12}	19007880.758	(7.8×10^{5})
β_{13}	−22258300.69	(8.5×10^{5})
β_{14}	9904884.41	(3.8×10^{5})
C_6 / cm^{-1} Å^6	1.35	$\times 10^{-191290}$
v_D	118.639	
No. of data	12148	
No. parameters	440	
$\bar{\sigma}_f$	1.153	

[a] Value taken from Ref. [60].

As the highest observed levels are only a few wavenumbers from dissociation, it was hoped that the $\mathcal{D}_e$ could be freed for an accurate determination of the dissociation energy. Unfortunately, the converged fits with $\mathcal{D}_e$ free seemed to differ from current theoretical estimates by several wavenumbers, even taking uncertainties into account. Further, the potential predicted the vibrational level at dissociation (v_D) poorly, even when $\mathcal{D}_e$ was fixed to the best experimental value [60]. Something needed to be done to improve the extrapolation behaviour of this potential function.

4.2 Power Series Constraint

The fact that the MLJ potential was unable to predict the dissociation energy and v_D accurately, despite the range of the data, was a little disconcerting. Closer inspection of the exponent of the MLJ potential function revealed that $\beta(R)$ tended to grow very quickly beyond the range of the data. A large $\beta(R)$ at these long ranges would cause the potential function to approach dissociation quickly, thereby causing the fit to underestimate both v_D and $\mathcal{D}_e$.

One attempt to alleviate this problem was to fix the $\beta(R)$ function using a power-series constraint to require the potential to approach the theoretical C_n value predicted by long-range theory via

$$\beta(R) \;=\; \sum_{j=0}^{a-1} \beta_j z^j + \beta_a z^a \;, \tag{4.3}$$

with β_a constrained by

$$\beta_a \;=\; \beta_\infty - \sum_{j=0}^{a-1} \beta_j \;=\; \ln\left(\frac{2\mathcal{D}_e\,(R_e)^n}{C_n}\right) - \sum_{j=0}^{a-1} \beta_j \;. \tag{4.4}$$

More details regarding these calculations, including the partial derivatives required for the non-linear least-squares fitting procedure, can be found in Appendix C. The power-

series-constrained results are seen in Table 4.2.

Table 4.2: Power-series constrained potential parameters for the $X\,^1\Sigma_g^+$ state of Rb_2 obtained on fitting all observed transition frequencies to eigenvalue differences calculated by solving Eq. (2.33); the numbers in parentheses are the 95% confidence limit uncertainties.

Parameter	$^{85}Rb_2$	
$\mathcal{D}_e$ / cm^{-1}	3993.53[a]	(6×10^{-2})
R_e / Å	4.2099564922	(7.3×10^{-6})
β_0	−5.890554720	(1.4×10^{-5})
β_1	12.12695573	(9.1×10^{-4})
β_2	14.38792467	(3.3×10^{-3})
β_3	31.6251435	(1.7×10^{-1})
β_4	73.064825	(6.3×10^{-1})
β_5	−328.319085	(1.4×10^{1})
β_6	1449.33205	(8.5×10^{1})
β_7	−12896.89522	(4.3×10^{2})
β_8	−55294.6549	(4.7×10^{3})
β_9	480675.1287	(1.0×10^{4})
β_{10}	−164619.343	(6.8×10^{4})
β_{11}	−5831320.614	(4.3×10^{5})
β_{12}	19907393.848	(1.2×10^{6})
β_{13}	−29655760.73	(1.7×10^{6})
β_{14}	21438436.00	(1.3×10^{6})
β_{15}	−6107859.060	
β_∞ / Å^{-1}	0.7346	
C_6 / cm^{-1} Å^6	2.1331[b] $\times 10^7$	
v_D	119.248	
No. of data	12148	
No. parameters	440	
$\bar{\sigma}_f$	1.197	

[a] Value taken from Ref. [60].
[b] Value taken from Ref. [61].

Although the constraint was successful at forcing $\beta(R)$ to reach the theoretical limit, the occurrence of a minimum in the function caused the potential function to misbehave in the extrapolation region. Further, as was reported by Hajigeorgiou and Le Roy [20], the function in the intermediate ranges had an implausible maximum which, if $\beta(R)$ didn't have a minimum, would still lead to a poor prediction for v_D. This effect can be seen on the plot of the $\beta(R)$ in the bottom frame of Figure 4.1.

Note that the radial range has been compressed so that the the entire domain of the intermolecular distance ($0 < R < \infty$) is shown over the interval $-1 < z < 1$. Various values of R/R_e have been added on the top axis of the plot for comparison. As with the top frame, the solid line is the experimentally-defined portion of the function, while the dotted line gives the extrapolated region.

4.3 Switching Function

While somewhat inelegant, one solution to this problem is to follow Hajigeorgiou and Le Roy, and introduce a switching function [20] that gradually "switches" $\beta(R)$ from the function determined by the spectroscopic data to the theoretical long-range limit. The switching function has the form

$$\beta_{\rm sw}(R) \;=\; f_{\rm sw}(R)\,[\beta_{\rm MLJ}(R) - \beta_\infty] + \beta_\infty \;, \tag{4.5}$$

in which

$$f_{\rm sw}(R) \;=\; \frac{1}{e^{\alpha_s(R-R_s)}+1} \;, \tag{4.6}$$

and the parameters α_s and R_s are manually chosen to ensure that $\beta_{\rm sw}(R)$ "looks" smooth. The partial derivatives required for the non-linear least-squares fits can be found in Appendix B.

As R_s effectively determines the distance at which the switching function "turns on", this parameter was chosen 1 Å beyond $R_{\max}$ for the highest observed vibrational level ($v = 113$), so that the switching function would not interfere significantly with the $\beta_{\rm sw}(R)$ function in the data range, yet would have sufficient strength to force the function to attain the proper long range limit without any spurious behaviour.

The strength or abruptness of the switchover is determined by the α_s parameter, which was chosen to have the smallest value at which $\beta_{\rm sw}(R)$ was considered "physical", so that the change from the data range to the theoretical limit did not occur abruptly, yet also did not have an undesired maximum. The fits were performed by fixing the two switching-function parameters and then optimizing all of the remaining potential parameters (excluding $\mathcal{D}_e$) to fit to the entire Rb_2 data set. A comparison of the constrained $\beta_{\rm sw}(R)$ functions obtained for various switching-function parameters can be seen in Fig. 4.2. The top half of the figure shows the behaviour of the $\beta_{\rm sw}(R)$ function in the extrapolation region for various values of α_s with R_s fixed at 13.7 Å. The bottom frame compares the use of various values of R_s when α_s is fixed at 1.30 Å^{-1}. This approach seemed the most fruitful, and the results from the recommended final fit are summarized in Table 4.3.

It is also possible to allow the fit to determine values of α_s and R_s, rather than fixing them to preselected values. This idea is, however, not very useful because these parameters do not have any true physical meaning. Moreover, as their effects occur outside the experimental data range, their proper determination and interpretation can be somewhat dubious.

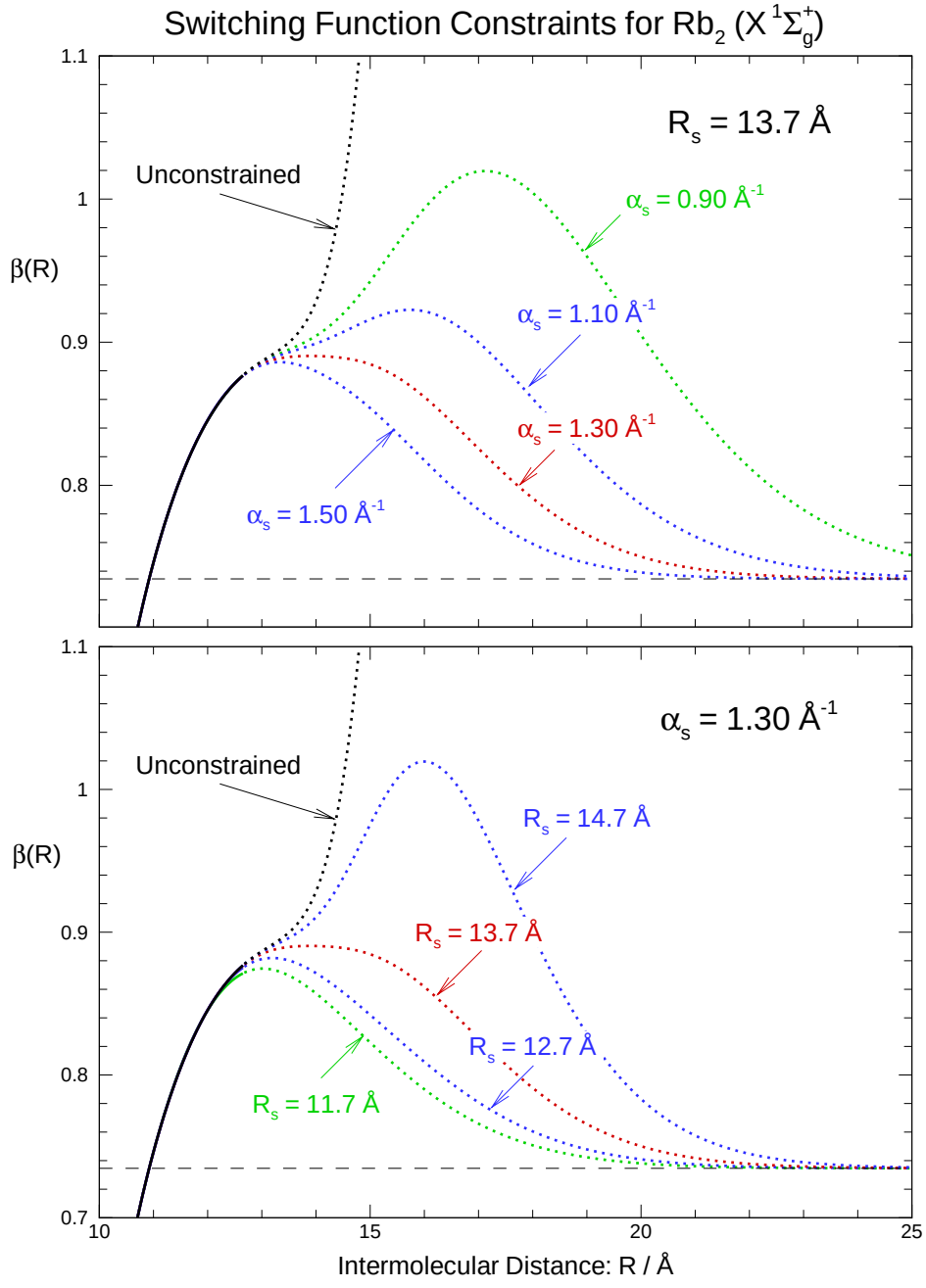

Figure 4.2: Comparing Various Switching Function Constraints for Rb_2

Table 4.3: Switching-function-constrained potential parameters for the $X\,^1\Sigma_g^+$ state of Rb_2 obtained upon fitting all observed transition frequencies to eigenvalue differences calculated by solving Eq. (2.33); the numbers in parentheses are the 95% confidence limit uncertainties in the last significant digits shown.

Parameter	$^{85}Rb_2$	
$\mathcal{D}_e$ / cm^{-1}	3993.53 (6)[a]	
R_e / Å	4.20995150 (700)	
β_0	−5.8905568 (140)	
β_1	1.2123473 (880)	$\times 10^1$
β_2	1.437410 (300)	$\times 10^1$
β_3	3.23360 (1600)	$\times 10^1$
β_4	7.327 (49)	$\times 10^1$
β_5	−4.014 (140)	$\times 10^2$
β_6	1.64 (7)	$\times 10^3$
β_7	−9.63 (47)	$\times 10^3$
β_8	−7.308 (430)	$\times 10^4$
β_9	4.472277 (63000)	$\times 10^5$
β_{10}	3.1 (7)	$\times 10^5$
β_{11}	−6.9587687 (3600000)	$\times 10^6$
β_{12}	1.9270 (800)	$\times 10^7$
β_{13}	−2.2651856 (880000)	$\times 10^7$
β_{14}	1.013 (39)	$\times 10^7$
β_∞ / Å^{-1}	0.7346	
C_6 / cm^{-1} Å^6	2.1331[b]	$\times 10^7$
α_s / Å^{-1}	1.3	
R_s / Å	13.7	
v_D	123.238	
No. of data	12148	
No. parameters	440	
$\bar{\sigma}_f$	1.156	

[a] Value taken from Ref. [60].
[b] Value taken from Ref. [61].

Chapter 5

Double Minimum Potentials: The $C\,^1\Sigma^+$ State of LiH

The final aspect of this thesis examines the ability of the DPF method to fit to spectroscopic data corresponding to non-standard potential shapes. For most diatomic molecules, the ground state potential well has the characteristic single-minimum shape seen in segment a) of Fig. 5.1. However, peculiarities in the intermolecular forces or avoided crossings between different diabatic states can produce a wide range of relatively exotic adiabatic potential shapes. Examples would include a potential "shelf", such as that found for the $4\,^1\Sigma_g^+$ state of Na_2 [42], the double-minimum potential for the $E, F\,^1\Sigma_g^+$ state of H_2, and the non-centrifugal (rotationless) potential barriers found for alkali dimer ions [62] in some excited states. These behaviours are shown in segments b), c), and d) of Fig. 5.1, respectively.

This chapter examines the ability of the MLJ potential to fit to the double-minimum potential of the $C\,^1\Sigma^+$ state of LiH. The particular shape of the C-state potential is due to the avoided crossing of at least four different diabatic potentials of the same symmetry

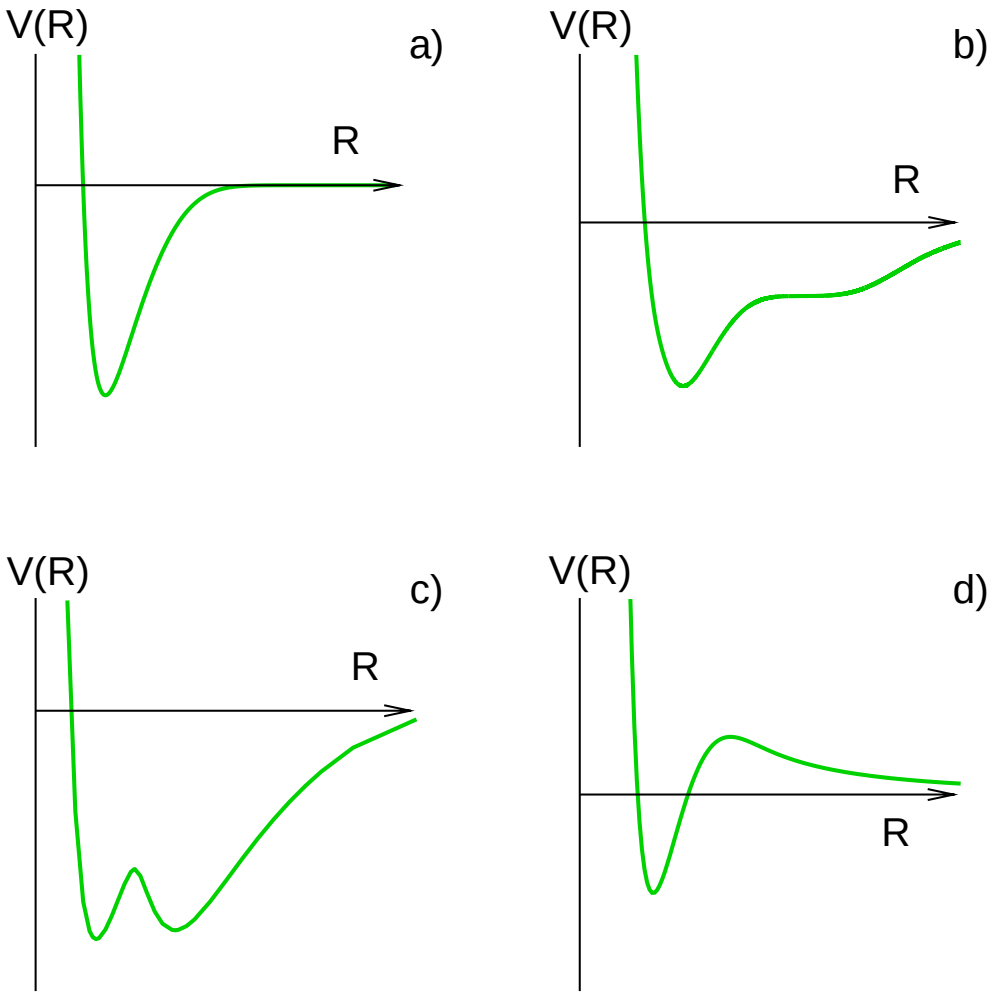

Figure 5.1: Sample potential energy curves for: a) a single-minimum well, b) a potential "shelf", c) a double-minimum well, and d) a rotationless potential barrier.

(see Fig. 5.2). This leads to the small inner well high up on the repulsive wall of the C-state potential seen in Fig. 5.3.

5.1 Data Set Used

The data set consisted of 754 transitions from the C-state with an average experimental uncertainty of 0.05 cm^{-1} [64]. Of these transitions, 734 belonged to the primary isotopomer $^7Li\,^1H$, while the remainder (20 lines) were from the $^6Li\,^1H$ isotopomer. Although the data for the dominant isotopomer spanned most of the well ($2 \leq v \leq 43$), the rotational range was small ($J < 12$). In order to simplify this study and to focus on the double-minimum C-state, the data were modified by using the known X-state constants [65] to calculate X-state term values to allow the representation of the $C - X$ transition data using one common lower-state energy level for all transitions.

5.2 Results

Aspects of the preliminary analysis of this system are summarized in Table 5.1, and some features of the results are shown in Figures 5.4 and 5.5. In Table 5.1, $^{\#}\beta_i$ is the number of exponent parameters used, $^{\#}fixed$ is the number of exponent parameters that were fixed in the fit, and $^{\#}BOB$ is the number of BOB correction parameters used. Numerical integration was performed over the range $R_{\min} < R < R_{\max}$ with a grid spacing ΔR, $v_{\max}$ is the highest vibrational level included in the fit, $G_{v_{\max}}$ is the energy of level $v = v_{\max}$ relative to the dissociation limit of the ground-state potential well, $No.data$ is the number of data in the truncated set, and $\bar{\sigma}_f$ is the dimensionless standard error. The results from the fits can be seen in Table 5.2.

Some of the β_i parameters were fixed, as the fitting procedure did not converge when all of the parameters were set free. The values were calculated by a method similar to

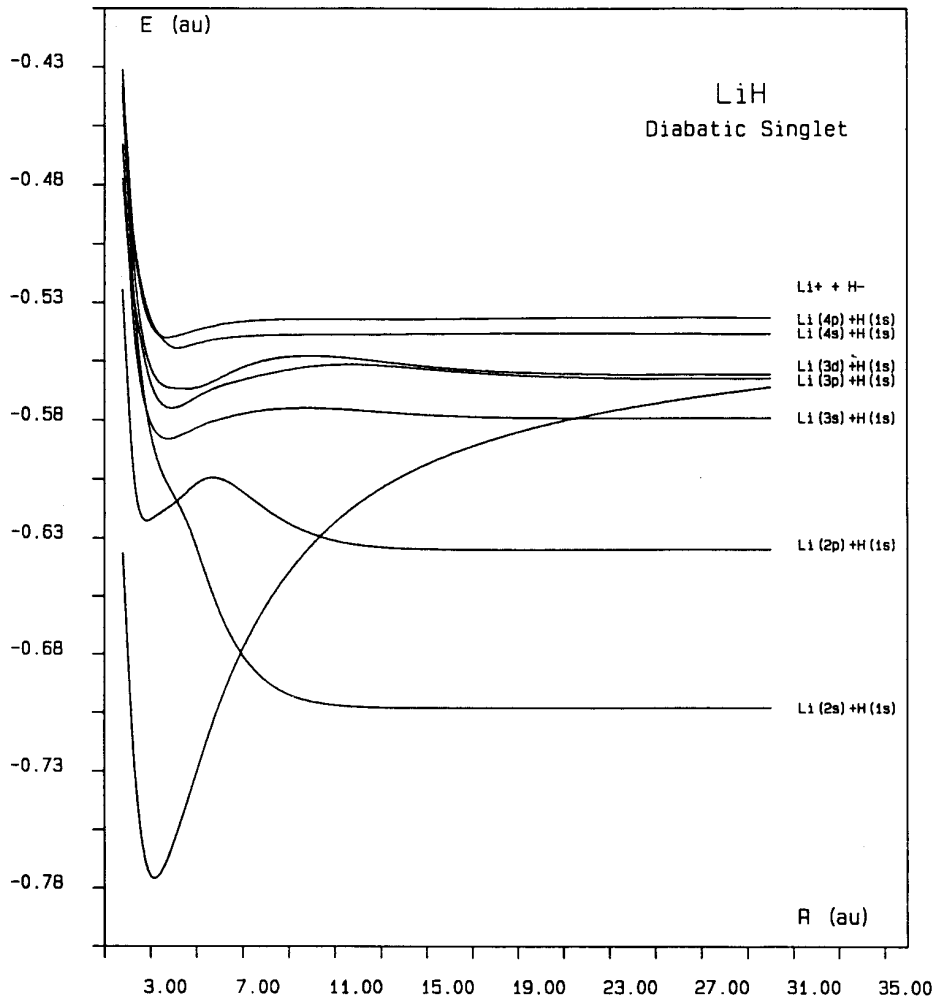

Figure 5.2: *Ab initio* Diabatic Potentials of LiH [63]

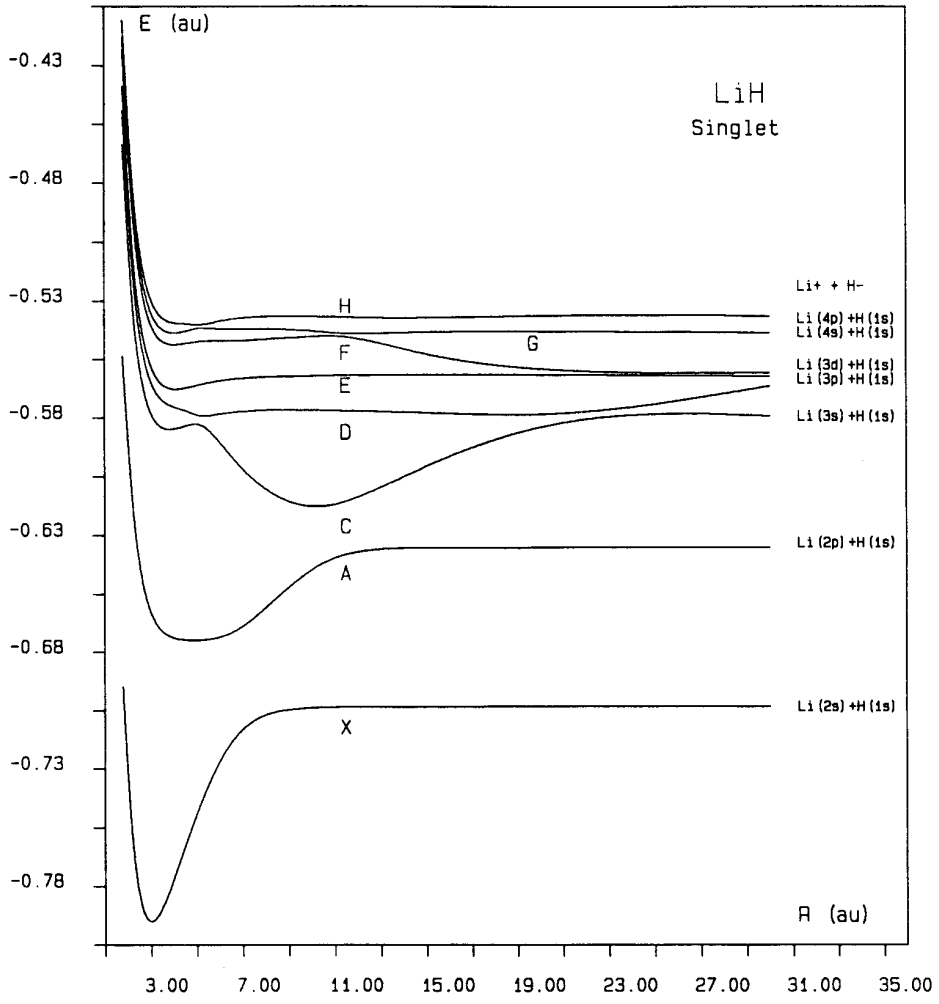

Figure 5.3: *Ab initio* Adiabatic Potentials of LiH [63]

Table 5.1: DPF details for LiH.

	No. of Parameters								*No.*	
Fit	$^{\#}\beta_i$	$^{\#}fixed$	$^{\#}BOB$	$R_{\min}$	$R_{\max}$	ΔR	$v_{\max}$	$G_{v_{\max}}/\mathrm{cm}^{-1}$	*data*	$\bar{\sigma}_f$
0	13	2	1	1.700	16.6000	0.0005	32	25979.63	548	1.008
1	14	0	1	0.600	16.5995	0.0005	36	26427.02	628	2.506
2	17	6	3	0.600	16.5997	0.0003	37	26559.34	648	2.635
3	20	9	2	0.600	16.5997	0.0003	41	26983.93	720	10.69

the "bootstrapping" method of section 2.5. The parameter in question is allowed to go free while the remaining parameters are fixed to pre-determined values. The latter are released one or several at a time until the fit does not converge. This method would eventually lead to the best fit with the least number of fixed parameters.

The potentials and $\beta(R)$ functions generated from each of these fits can be seen in Fig. 5.4, with a close-up look at the inner well being presented in Fig. 5.5. As usual, the solid lines on the "Fit" curves denote the range of the experimental data used to determine those potentials, while the dotted lines give the extrapolated regions. The "extended RKR potential" is the hybrid "CLJ-RKR-CLJ" potential proposed in Ref. [64] whose inner wall and inner well are represented by a shifted *ab initio* potential, the main well (up to $v = 32$) by an RKR potential, by another scaled *ab initio* potential from the top of the RKR potential out to 15.87 Å, and finally by a long-range inverse-power potential for distances beyond 15.87 Å. The "extended RKR potential" $\beta(R)$ plot was determined by equating the "CLJ-RKR-CLJ" potential with the MLJ potential and solving for $\beta(R)$. These plots were included in the figures to compare with the potentials generated from our fits.

The ability of the potentials obtained from the various fits to reproduce the input data on which they are based is shown in Table 5.3, which lists the relative root mean

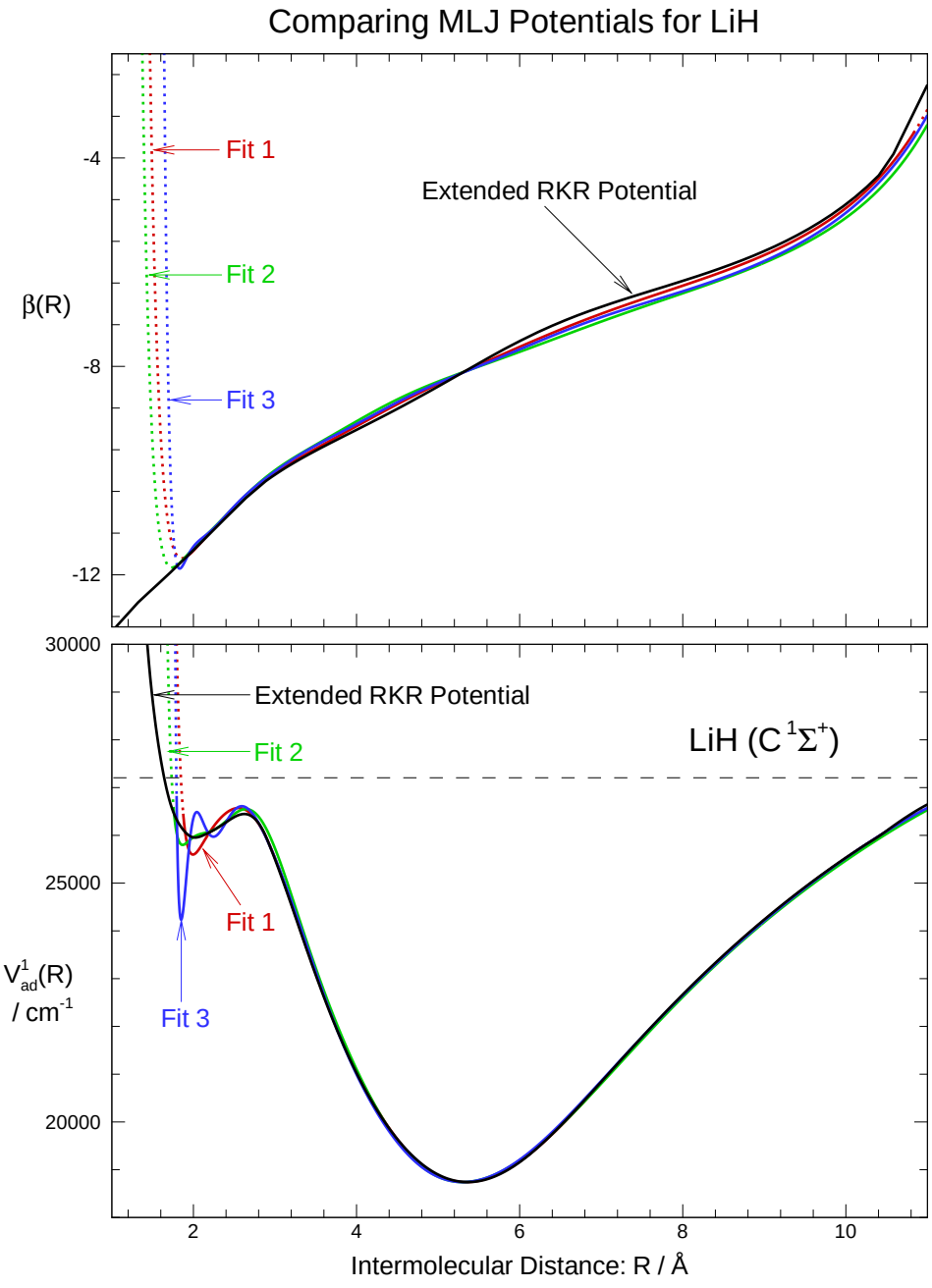

Figure 5.4: A Comparison of MLJ Potentials for the $C\,^1\Sigma^+$ State of LiH

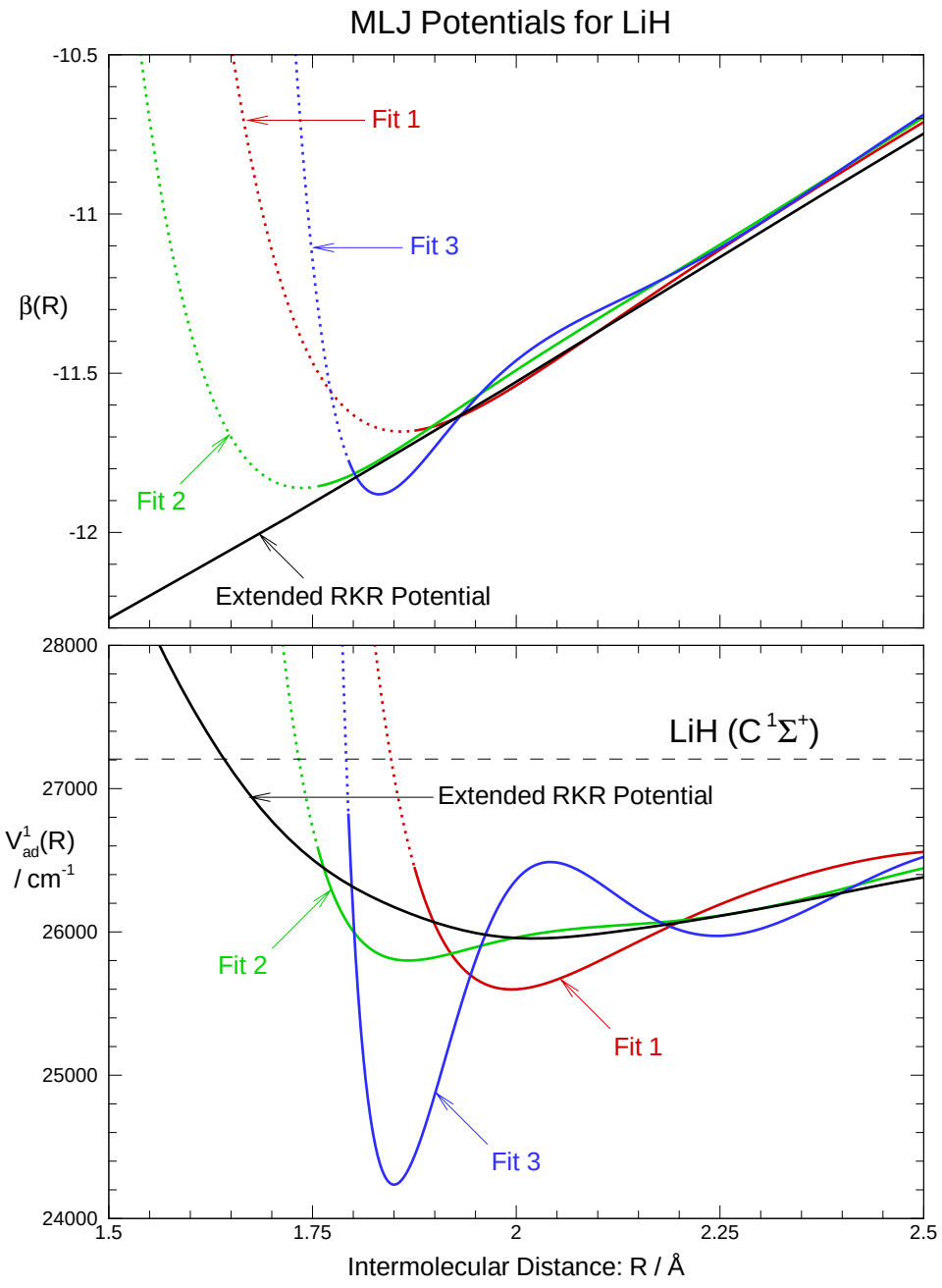

Figure 5.5: A Closer Examination of the Inner Potential Well of LiH ($C\,^1\Sigma^+$)

square residuals (RMSR),

$$\text{RMSR} \;=\; \overline{\sigma}_f \left(\frac{N-M}{N}\right)^{1/2} = \left\{ \frac{1}{N} \sum_{i=1}^{N} \left[\frac{y_{\text{calc}}(i) - y_{\text{obs}}(i)}{u(i)} \right]^2 \right\}^{1/2} , \qquad (5.1)$$

for the several data associated with each observed vibrational level. All of the parameters in equation Eq. (5.1) are the same as for Eq. (2.36), except that N is now the number of data in the specific band considered. It is clear that most of the fitting discrepancies comes from the vibrational levels at or above the $v = 34$ inner well level. However, as the average experimental uncertainty is only 0.05 cm^{-1}, the absolute differences between the calculated transition energies and the experimental values are still less than one wavenumber.

Notice that as the fits use more and more data, approaching the top of the data set, the inner well becomes more and more convoluted and the quality of fit ($\overline{\sigma}_f$) becomes poorer. This may be because as more levels are added to the fitted data set, more exponent parameters are required to fit to these data. Unfortunately, the higher-order parameters become so large that they tend to dominate at the end of the data region, where they have the most effect. Moreover, the changes in these high-order parameters during a fit are very large, and can cause the potential to behave absurdly during a fitting cycle, thereby preventing the fit from converging.

A particular difficulty in determining this potential is the fact that the inner well has only one single bound vibrational level ($v = 34$). As there are only a few rotational levels with dominant wavefunction amplitude in that well, it makes it difficult to characterize the shape of the well fully. This problem is compounded by the fact that the location of this inner minimum is so high up the repulsive potential wall that the top of the barrier lies near the dissociation limit of the main well. Thus, any changes when fitting to the long-range part of the potential can have serious effects on fitting to the secondary well.

From Table 5.2 and Figures 5.4 and 5.5 above, it can be seen that the fits have had reasonable success at reproducing the data up to, and slightly beyond the energy of the one inner-well-based level ($v = 34$). Fit $^{\#}1$ was moderately successful at determining the inner well level and two of the vibrational levels above it. Further, the shape of the inner well for Fit $^{\#}1$ seems plausible, although it still differs from the shape of the inner well of the extended RKR potential.

Despite the lackluster results shown above, the evidence suggests that the MLJ potential is capable of "seeing" the second minimum and getting the proper general shape for that well. This suggests that further study in this area may be worthwhile for determining how effective this method is to fitting to data from other types of systems with non-standard potential shapes.

Table 5.2: Potential parameters obtained on fitting all observed transition frequencies to eigenvalue differences calculated by solving Eq. (2.33).

Parameter	Fit 1	Fit 2
Lower State Potential Parameters		
$\mathcal{D}_e$ / cm^{-1}	21000.	21000.
R_e / Å	5.	5.
β_0 / Å^{-1}	1.133928991	1.133928991
C–State Potential Parameters		
T_e / cm^{-1}	27206.12	27206.12
$\mathcal{D}_e$ / cm^{-1}	8465.31[a]	8465.31[a]
R_e / Å	5.3398928271	5.304470 (5900)
β_0 / Å^{-1}	−8.0886577 (5600)	−8.1127995 (42000)
β_1 / Å^{-1}	7.673092 (180000)	6.031640 (110000)
β_2 / Å^{-1}	3.985580 (390000)	1.239678 (140000)
β_3 / Å^{-1}	20.875414 (11000000)	77.318489 (3100000)
β_4 / Å^{-1}	−94.30060 (2400000)	−8.03688 (250000)
β_5 / Å^{-1}	−1178.60147 (27000000)	−2297.10391 (3700000)
β_6 / Å^{-1}	1719.05766 (63000000)	425.68672 (1500000)
β_7 / Å^{-1}	23187.8434 (33000000)	35067.1225 (1600000)
β_8 / Å^{-1}	−3907.7851 (86000000)	3269.6832244
β_9 / Å^{-1}	−184436.5561 (190000000)	−254025.33447
β_{10} / Å^{-1}	−86522.471 (59000000)	−70225.383051
β_{11} / Å^{-1}	634856.641 (41000000)	891595.35141
β_{12} / Å^{-1}	716370.70 (16000000)	296201.83111
β_{13} / Å^{-1}	504.78 (14000000)	−1169140.6207
β_{14} / Å^{-1}	–	1060285.87 (2700000)
β_{15} / Å^{-1}	–	3596847.22 (5200000)
β_{16} / Å^{-1}	–	1946221.1 (970000)
$\tilde{u}_0^{\mathrm{Li}}$ / cm^{-1}	−41.16 (36)	−41.35 (38)
q_1^{H}	–	0.71470 (5700)
q_2^{H}	–	1.5953 (1800)
No. of data	628	648
No. parameters	15	15
$\bar{\sigma}_f$	2.537	2.666

Parameter	Fit 3
Lower State Potential Parameters	
$\mathcal{D}_e$ / cm^{-1}	21000.
R_e / Å	5.
β_0 / Å^{-1}	1.133928991
C–State Potential Parameters	
T_e / cm^{-1}	27206.12
$\mathcal{D}_e$ / cm^{-1}	8465.31[a]
R_e / Å	5.3018736156
β_0 / Å^{-1}	−8.122045 (1100)
β_1 / Å^{-1}	6.727055 (250000)
β_2 / Å^{-1}	3.85290 (32000)
β_3 / Å^{-1}	101.06073 (930000)
β_4 / Å^{-1}	−113.99251 (1100000)
β_5 / Å^{-1}	−5714.4125 (1400000)
β_6 / Å^{-1}	2568.9902 (1700000)
β_7 / Å^{-1}	149080.9601 (9700000)
β_8 / Å^{-1}	−20691.893 (1300000)
β_9 / Å^{-1}	−2092541.116 (2600000)
β_{10} / Å^{-1}	−77952.482 (3900000)
β_{11} / Å^{-1}	16990218.287
β_{12} / Å^{-1}	3856323.1588
β_{13} / Å^{-1}	−74649484.329
β_{14} / Å^{-1}	−29983319.350
β_{15} / Å^{-1}	137737660.26
β_{16} / Å^{-1}	62904080.176
β_{17} / Å^{-1}	24352596.636
β_{18} / Å^{-1}	123166977.38
β_{19} / Å^{-1}	−34777548.978
$\tilde{u}_0^{\mathrm{Li}}$ / cm^{-1}	−40.7 (15)
q_1^{H}	0.0568 (57)
No. of data	720
No. parameters	13
$\bar{\sigma}_f$	10.78

[a] Value taken from Ref. [48].

Table 5.3: RMSRs calculated for each of the vibrational levels for the three fits to the LiH C-state data.

		RMSR			
v'	No. Data	Fit #0	Fit #1	Fit #2	Fit #3
2	16	1.770	2.212	4.604	3.144
3	16	1.185	1.052	1.618	4.331
4	16	0.734	0.974	1.713	2.685
5	16	1.019	1.275	2.110	1.352
6	16	1.180	1.522	2.447	1.199
7	16	0.893	1.178	1.908	0.994
8	16	0.926	1.176	1.965	0.915
9	16	0.744	0.765	1.359	0.751
10	15	0.848	0.809	1.530	1.337
11	16	0.879	1.019	1.908	2.180
12	16	0.978	1.350	2.183	3.433
13	16	0.988	1.097	1.355	3.081
14	15	0.752	0.712	0.651	2.654
15	13	1.109	1.106	1.517	3.418
16	13	1.107	1.181	1.991	3.697
17	19	1.174	1.371	2.396	6.036
18	17	1.320	1.470	2.627	6.566
19	17	0.783	1.009	2.101	5.353
20	15	0.764	0.898	2.612	7.110
21	20	1.248	1.302	2.063	4.670
22	18	0.582	0.729	1.953	5.035
23	20	0.702	1.090	2.344	4.701
24	18	0.883	1.257	1.582	3.624
25	18	1.133	1.642	1.624	3.517
26	18	1.224	1.997	1.189	3.080
27	18	0.923	1.466	1.089	1.919
28	24	0.620	1.705	2.143	2.148
29	18	0.700	1.840	2.789	2.327
30	18	1.299	1.580	2.954	2.283
31	18	1.127	1.373	1.159	2.680
32	20	0.849	1.049	0.825	1.094
33	19	−−	2.860	3.709	2.964
34	19	−−	5.421	4.005	13.414
35	22	−−	6.375	2.094	13.674
36	20	−−	8.338	5.592	13.168
37	20	−−	−−	6.692	10.317
38	20	−−	−−	−−	11.951
39	18	−−	−−	−−	18.018
40	17	−−	−−	−−	21.869
41	17	−−	−−	−−	51.665

Chapter 6

Summary and Discussion

The development of the `DSPotFit` computer program has been long and fruitful. It has been used in a number of analyses and has been a key factor in producing the results mentioned above. Work with the coinage hydrides has shown that there is currently no elegant, global method by which one can address the problem of the potential turn-over. This does not preclude the possibility that the methods that were rejected here can be used elsewhere, or that they can be modified to become more effective. Further study will be needed to develop a "proper" solution to the short range extrapolation problem, but for now, our "Occam's Razor" solution should suffice so long as the potential turn-over does not occur at too low an energy.

The rubidium dimer results have shown that even with vibrational data which spans over 99% of the potential well, predictions of $\mathcal{D}_e$ and v_D calculated from our potential forms may not be reliable. Further, although the power-series constraint is able to force the $\beta(R)$ function to approach the proper asymptotic limit, it is ineffective at making the function behave in the extrapolation region. Therefore, although crude, the use of a switching function is one method by which to constrain the $\beta(R)$ function, and thus the potential energy curve itself, within more likely bounds.

Our limited success with the C-state of lithium hydride has demonstrated that DPF methods can be used to fit to double-minimum-well type potentials. Although we are currently unable to fit to data from the entire potential, the fact that the potential can "see" the small inner well is a good indication that we are on the right track. The difficulties associated with the small size of the well and the location (so near dissociation) may be a factor regarding the poor fit beyond the inner-well vibrational level. A more interesting case would be a double minimum potential where both the inner and outer wells are roughly the same size. Although trial parameters would be difficult to determine, it is believed that `DSPotFit` would still be able to handle such a situation.

One of the problems with the fits to the C-state potential of LiH was the fact that changes in the long-range potential tail region tended to affect the shape of the inner well minimum. One possible way to fit to the proper long- and short-range behaviour correctly is to use a "modified Maitland-Smith" [66] (MMS) potential which would take into account both the $1/R^n$ long-range attraction as well as the $1/R$ short range repulsion behaviours, without adversely affecting the flexibility of the generalized Morse-type functions in the potential well area. This expansion is effectively a slightly modified version of the MLJ function in Eq. (2.28). The long-range power n is changed from a constant in the MLJ into an R-dependent variable:

$$V_{\mathrm{MMS}}(R) \;=\; \mathcal{D}_e \left[1 - \left(\frac{R_e}{R} \right)^{n(R)} e^{-\beta_{\mathrm{MMS}}(z)\, z} \right]^2 \tag{6.1}$$

with

$$\lim_{R \to 0} n(R) \;=\; \frac{1}{2} \quad \text{and} \quad \lim_{R \,\to\, \infty} n(R) \;=\; n \; . \tag{6.2}$$

It is anticipated that this type of analytical potential function will be effective at addressing both the long-range and short-range extrapolation problems.

Although `DSPotFit` has been successfully applied to a number of systems, there are

still a number of improvements that can be made. One such improvement would include fitting to predissociation lifetimes, which would be useful in determining barrier shapes for potentials with rotationless barriers. Another major upgrade would be to allow the program to fit to non-$^1\Sigma$ type electronic systems. Although there is as yet no clear idea with regards to how to treat non-singlet states correctly, it should require only a small modification to allow the program to take account of lambda doubling effects, and thus allow it to treat data from non-Σ states. For a $^2\Sigma^+$ that has spin-doubling, the method proposed by Bernath and Le Roy [67] is to use a radial correction function $\gamma(R)$ in the centrifugal term of the potential function (Eq. 2.7) via

$$\frac{\hbar^2}{2\mu R^2}[J(J+1)] \Rightarrow \begin{cases} \frac{\hbar^2}{2\mu R^2}\left[N(N+1)+\frac{1}{2}\gamma(R)N\right] & e \\ \\ \frac{\hbar^2}{2\mu R^2}\left[N(N+1)-\frac{1}{2}\gamma(R)(N+1)\right] & f \end{cases} \tag{6.3}$$

in which the rotational quantum number J is replaced by N. These are related by the vector difference

$$\vec{N} = \vec{J} - \vec{S}\ , \tag{6.4}$$

where S is the spin angular momentum of the state in question. Thus, instead of fitting to J rotational levels, the fitting is to N rotational levels.

It is hoped that further refinements to `DSPotFit` will continue in the future, and that this program will be used by chemists worldwide. It is our goal to have direct-potential-fitting become a standard routine in spectroscopic analysis.

Appendix A

Determination of Trial Parameters

For all forms of the potentials described in Eqs. (2.20), (2.22), (2.25), (2.28), realistic initial trial values of the quantities $\mathcal{D}_e$ and R_e are normally available from conventional spectroscopic analysis. However, this is not true for the exponent expansion parameters $\{\beta_i^a\}$ (a = GMO, MMO, EMO or MLJ). One object of the present discussion is to provide a simple means of generating realistic initial trial values of at least the first three of these coefficients.

For any case in which a "direct potential fit" to determine a potential energy function directly from the set of experimental transition frequencies would be considered, proper vibration-rotation assignments for a fairly extensive set of data may be expected to be available. In such a case, it would be a straightforward matter to perform an initial conventional "direct parameter fit" of the data to the Dunham energy expansion

$$E(v,J) = \sum_{l=0}\sum_{m=0} Y_{l,m}\left(v+\frac{1}{2}\right)^l \left[J\left(J+1\right)\right]^m \ . \tag{A.1}$$

This would yield values of at least the first few conventional spectroscopic constants, $\omega_e = Y_{1,0}$, $\omega_e x_e = -Y_{2,0}$, $B_e = Y_{0,1} = \hbar^2/2\mu R_e^2$ and $\alpha_e = -Y_{1,1}$. Dunham theory shows

that the coefficients $\{Y_{l,m}\}$ may be expressed explicitly in terms of the coefficients of a power series expansion representation of the potential energy function as

$$V_{\rm Dun}(R) \;=\; V(R) \;=\; a_0\xi^2\left(1 + a_1\xi + a_2\xi^2 + \cdots\right) \;, \tag{A.2}$$

where $\xi \;=\; (R - R_e)/R_e$ [46, 47]. In particular, neglecting terms of order $\frac{1}{2}(B_e/\omega_e)^2$ or smaller, one can write

$$Y_{0,1} \;=\; B_e \;=\; \frac{\hbar^2}{2\mu R_e^2} \;, \tag{A.3}$$

$$Y_{1,0} \;=\; \omega_e \;=\; \sqrt{4B_e a_0} \;, \tag{A.4}$$

$$Y_{1,1} \;=\; -\,\alpha_e \;=\; \frac{6B_e^2}{\omega_e}\,(1 + a_1) \;, \tag{A.5}$$

$$Y_{2,0} \;=\; -\,\omega_e x_e \;=\; \frac{3B_e}{2}\left(a_2 - \frac{5a_1^2}{4}\right) \;. \tag{A.6}$$

A rearrangement of the above equations then yields

$$a_0 \;=\; \frac{\omega_e^2}{4B_e} \;=\; \frac{1}{2}\,\frac{d^2V}{d\xi^2}\bigg|_{\xi=0} \;=\; \frac{R_e^2}{2}\,\frac{d^2V}{dR^2}\bigg|_{R=R_e} \;, \tag{A.7}$$

$$a_1 \;=\; -\left[\frac{\alpha_e\omega_e}{6B_e^2} + 1\right] \;=\; \frac{R_e}{3}\,\frac{d^3V}{dR^3}\bigg|_{R=R_e} \Big/\, \frac{d^2V}{dR^2}\bigg|_{R=R_e} \;, \tag{A.8}$$

$$a_2 \;=\; \frac{5}{4}a_1^2 - \frac{2\omega_e x_e}{3B_e} \;=\; \frac{R_e^2}{12}\,\frac{d^4V}{dR^4}\bigg|_{R=R_e} \Big/\, \frac{d^2V}{dR^2}\bigg|_{R=R_e} \;. \tag{A.9}$$

The problem we now address is that of obtaining explicit expressions for the leading exponent expansion parameters $\{\beta_i^a\}$ in terms of $\mathcal{D}_e$ and the spectroscopic constants B_e, ω_e, α_e, and $\omega_e x_e$. This is done by deriving explicit expressions for the first four derivatives of the four potential models of Section 2.4, evaluated at R_e, and substituting them into Eqs. (A.7)-(A.9), to obtain the required results.

A.1 Expressions for Derivatives of the Model Potential Functions

All four of the model potentials described above may be written using Gruebele's [68] $f(R)$ notation so that

$$V_a(R) = \mathcal{D}_e^a[1 - f_a(R)]^2 \ , \tag{A.10}$$

with a = GMO, MMO, EMO, MLJ, and

$$f_{\rm GMO}(R) = e^{-\beta_{\rm GMO}(R)\,(R-R_e)} \ , \tag{A.11}$$

$$f_{\rm MMO}(R) = e^{-\beta_{\rm MMO}(z)\,z} \ , \tag{A.12}$$

$$f_{\rm EMO}(R) = e^{-\beta_{\rm EMO}(z)\,(R-R_e)} \ , \tag{A.13}$$

$$f_{\rm MLJ}(R) = \left(\frac{R_e}{R}\right)^n e^{-\beta_{\rm MLJ}(z)\,z} \ . \tag{A.14}$$

For the MMO function, $\mathcal{D}_e^a = \mathcal{D}_e^{\rm MMO} = \mathcal{D}_e / \left[1 - e^{-\beta_{\rm MMO}^{\infty}}\right]^2$, while for the other three forms, $\mathcal{D}_e^a \equiv \mathcal{D}_e$. This exception for the MMO case introduces complications which will be discussed in Appendix A.2.3, but they do not affect the results obtained here.

For all four model potentials, it is readily shown that

$$\frac{\partial f_a(R)}{\partial R} = -f_a(R)\alpha_a \ , \tag{A.15}$$

with

$$\alpha_{\rm GMO} = \beta_{\rm GMO} + (R - R_e)\frac{\partial \beta_{\rm GMO}}{\partial R} \ , \tag{A.16}$$

$$\alpha_{\rm MMO} = \frac{2R_e}{(R+R_e)^2}\beta_{\rm MMO} + \left(\frac{R-R_e}{R+R_e}\right)\frac{\partial \beta_{\rm MMO}}{\partial R} \ , \tag{A.17}$$

$$\alpha_{\rm EMO} = \beta_{\rm EMO} + (R - R_e)\frac{\partial \beta_{\rm EMO}}{\partial R} \ , \tag{A.18}$$

$$\alpha_{\rm MLJ} = \frac{n}{R} + \frac{2R_e}{(R+R_e)^2}\beta_{\rm MLJ} + \left(\frac{R-R_e}{R+R_e}\right)\frac{\partial \beta_{\rm MLJ}}{\partial R} \ . \tag{A.19}$$

Use of the quantities $f_a(R)$ and α_a allows the radial derivatives of these four potential models to be expressed in the same form, namely

$$\frac{\partial V_a}{\partial R} = 2\mathcal{D}_e^a f_a(R)[1-f_a(R)]\alpha_a \ , \tag{A.20}$$

$$\frac{\partial^2 V_a}{\partial R^2} = 2\mathcal{D}_e^a f_a(R)[2f_a(R)-1](\alpha_a)^2 + 2\mathcal{D}_e^a f_a(R)[1-f_a(R)]\frac{\partial \alpha_a}{\partial R} \ , \tag{A.21}$$

$$\begin{aligned}\frac{\partial^3 V_a}{\partial R^3} &= 2\mathcal{D}_e^a f_a(R)[1-4f_a(R)](\alpha_a)^3 + 6\mathcal{D}_e^a f_a(R)[2f_a(R)-1]\alpha_a\frac{\partial \alpha_a}{\partial R} \\ &\quad + 2\mathcal{D}_e^a f_a(R)[1-f_a(R)]\frac{\partial^2 \alpha_a}{\partial R^2} \ ,\end{aligned} \tag{A.22}$$

$$\begin{aligned}\frac{\partial^4 V_a}{\partial R^4} &= 2\mathcal{D}_e^a f_a(R)[8f_a(R)-1](\alpha_a)^4 + 12\mathcal{D}_e^a f_a(R)[1-4f_a(R)](\alpha_a)^2\frac{\partial \alpha_a}{\partial R} \\ &\quad + 6\mathcal{D}_e^a f_a(R)[2f_a(R)-1]\left(\frac{\partial \alpha_a}{\partial R}\right)^2 + 8\mathcal{D}_e^a f_a(R)[2f_a(R)-1]\alpha_a\frac{\partial^2 \alpha_a}{\partial R^2} \\ &\quad + 2\mathcal{D}_e^a f_a(R)[1-f_a(R)]\frac{\partial^3 \alpha_a}{\partial R^3} \ ,\end{aligned} \tag{A.23}$$

$$\begin{aligned}\frac{\partial^5 V_a}{\partial R^5} &= 2\mathcal{D}_e^a f_a(R)[1-16f_a(R)](\alpha_a)^5 + 20\mathcal{D}_e^a f_a(R)[8f_a(R)-1](\alpha_a)^3\frac{\partial \alpha_a}{\partial R} \\ &\quad + 30\mathcal{D}_e^a f_a(R)[1-4f_a(R)]\alpha_a\left(\frac{\partial \alpha_a}{\partial R}\right)^2 + 20\mathcal{D}_e^a f_a(R)[1-4f_a(R)](\alpha_a)^2\frac{\partial^2 \alpha_a}{\partial R^2} \\ &\quad + 20\mathcal{D}_e^a f_a(R)[2f_a(R)-1]\frac{\partial \alpha_a}{\partial R}\frac{\partial^2 \alpha_a}{\partial R^2} + 10\mathcal{D}_e^a f_a(R)[2f_a(R)-1]\alpha_a\frac{\partial^3 \alpha_a}{\partial R^3} \\ &\quad + 2\mathcal{D}_e^a f_a(R)[1-f_a(R)]\frac{\partial^4 \alpha_a}{\partial R^4} \ .\end{aligned} \tag{A.24}$$

Moreover, for all four potential forms, $f_a(R=R_e)=1$, and hence at the potential minimum

$$\left.\frac{\partial^2 V_a}{\partial R^2}\right|_{R=R_e} = 2\mathcal{D}_e^a\left(\alpha_a|_{R=R_e}\right)^2 \ , \tag{A.25}$$

$$\left.\frac{\partial^3 V_a}{\partial R^3}\right|_{R=R_e} = -6\mathcal{D}_e^a\left(\alpha_a|_{R=R_e}\right)^3 + 6\mathcal{D}_e^a\left(\alpha_a|_{R=R_e}\right)\left.\frac{\partial \alpha_a}{\partial R}\right|_{R=R_e} \ , \tag{A.26}$$

$$\left.\frac{\partial^4 V_a}{\partial R^4}\right|_{R=R_e} = 14\mathcal{D}_e^a \left(\alpha_a|_{R=R_e}\right)^4 - 36\mathcal{D}_e^a \left(\alpha_a|_{R=R_e}\right)^2 \left.\frac{\partial \alpha_a}{\partial R}\right|_{R=R_e} + 6\mathcal{D}_e^a \left(\left.\frac{\partial \alpha_a}{\partial R}\right|_{R=R_e}\right)^2 + 8\mathcal{D}_e^a \left(\alpha_a|_{R=R_e}\right) \left.\frac{\partial^2 \alpha_a}{\partial R^2}\right|_{R=R_e} , \quad \text{(A.27)}$$

$$\left.\frac{\partial^5 V_a}{\partial R^5}\right|_{R=R_e} = -30\mathcal{D}_e^a \left(\alpha_a|_{R=R_e}\right)^5 + 140\mathcal{D}_e^a \left(\alpha_a|_{R=R_e}\right)^3 \left.\frac{\partial \alpha_a}{\partial R}\right|_{R=R_e} - 90\mathcal{D}_e^a \left(\alpha_a|_{R=R_e}\right) \left(\left.\frac{\partial \alpha_a}{\partial R}\right|_{R=R_e}\right)^2 - 60\mathcal{D}_e^a \left(\alpha_a|_{R=R_e}\right)^2 \left.\frac{\partial^2 \alpha_a}{\partial R^2}\right|_{R=R_e} + 20\mathcal{D}_e^a \left.\frac{\partial \alpha_a}{\partial R}\right|_{R=R_e} \left.\frac{\partial^2 \alpha_a}{\partial R^2}\right|_{R=R_e} + 10\mathcal{D}_e^a \left(\alpha_a|_{R=R_e}\right) \left.\frac{\partial^3 \alpha_a}{\partial R^3}\right|_{R=R_e} \quad \text{(A.28)}$$

Values of the α_a and their radial derivatives, evaluated at $R = R_e$, are tabulated in Appendix A.3.

A.2 Predicting Initial Trial Parameters of the Exponent Expansion Parameters

The Dunham expressions of Eqs. (A.7)-(A.9) show that the radial derivatives of the potential evaluated at R_e are directly related to the familiar spectroscopic constants. Since the derivatives of Eqs. (A.25)-(A.27) depend explicitly on the values of the leading $\{\beta_i^a\}$ coefficients, substituting the former into Eqs. (A.7)-(A.9) yields explicit expressions for the first three β_i^a ($i = 0$, 1 and 2) coefficients in terms of these spectroscopic constants.

In particular, Eqs. (A.7) and (A.25) yield

$$\mathcal{D}_e^a \left[\alpha_a|_{R=R_e}\right]^2 = \frac{a_0}{R_e^2} , \quad \text{(A.29)}$$

from which $\alpha_a|_{R=R_e}$ is obtained as

$$\alpha_a|_{R=R_e} = \frac{1}{R_e}\sqrt{\frac{a_0}{\mathcal{D}_e^a}} \,. \tag{A.30}$$

Similarly, Eqs. (A.8) and (A.26) yield

$$-\mathcal{D}_e^a\left(\alpha_a|_{R=R_e}\right)^3 + \mathcal{D}_e^a\left(\alpha_a|_{R=R_e}\right)\left.\frac{\partial\alpha_a}{\partial R}\right|_{R=R_e} = \frac{a_0}{R_e^3}a_1 \,, \tag{A.31}$$

from which $\left.\frac{\partial\alpha_a}{\partial R}\right|_{R=R_e}$ may be obtained as

$$\left.\frac{\partial\alpha_a}{\partial R}\right|_{R=R_e} = \frac{1}{R_e^2}\sqrt{\frac{a_0}{\mathcal{D}_e^a}}\left[\sqrt{\frac{a_0}{\mathcal{D}_e^a}} + a_1\right] \,. \tag{A.32}$$

Similarly, Eqs. (A.9) and (A.27) yield

$$\begin{aligned} &14\mathcal{D}_e^a\left(\alpha_a|_{R=R_e}\right)^4 - 36\mathcal{D}_e^a\left(\alpha_a|_{R=R_e}\right)^2\left.\frac{\partial\alpha_a}{\partial R}\right|_{R=R_e} \\ &+ 6\mathcal{D}_e^a\left(\left.\frac{\partial\alpha_a}{\partial R}\right|_{R=R_e}\right)^2 + 8\mathcal{D}_e^a\left(\alpha_a|_{R=R_e}\right)\left.\frac{\partial^2\alpha_a}{\partial R^2}\right|_{R=R_e} = 24\frac{a_0}{R_e^4}a_2 \,, \end{aligned} \tag{A.33}$$

which, when combined with Eqs. (A.30) and (A.32) gives

$$\begin{aligned} \left.\frac{\partial^2\alpha_a}{\partial R^2}\right|_{R=R_e} &= \frac{1}{R_e^3}\sqrt{\frac{a_0}{\mathcal{D}_e^a}}\left[3a_2 - \frac{3}{4}a_1^2 + 3a_1\sqrt{\frac{a_0}{\mathcal{D}_e^a}} + 2\frac{a_0}{\mathcal{D}_e^a}\right] \\ &= \frac{1}{R_e^3}\sqrt{\frac{a_0}{\mathcal{D}_e^a}}\left[3a_1^2 + 3a_1\sqrt{\frac{a_0}{\mathcal{D}_e^a}} + 2\frac{a_0}{\mathcal{D}_e^a} - \frac{2\omega_e x_e}{B_e}\right] \,. \end{aligned} \tag{A.34}$$

Using the equations found in Appendix A.3, we can now replace the partial derivatives of α_a in Eqs. (A.30), (A.32), and (A.34) with the corresponding functions of β_a for each of the four potentials. The details of these calculations have been left out and only the results shown below.

A.2.1 Generalized Morse Oscillator

For a = GMO, the equations for the first three exponential parameters are

$$\beta_0^{\rm GMO} = \frac{1}{R_e}\sqrt{\frac{a_0}{\mathcal{D}_e}} = \frac{1}{R_e}\sqrt{\frac{\omega_e^2}{4\mathcal{D}_e B_e}} = \frac{\omega_e}{2}/\sqrt{\frac{\hbar^2}{2\mu}\mathcal{D}_e}\ , \tag{A.35}$$

$$\begin{aligned}\beta_1^{\rm GMO} &= \frac{1}{2R_e^2}\sqrt{\frac{a_0}{\mathcal{D}_e}}\left[\sqrt{\frac{a_0}{\mathcal{D}_e}} + a_1\right] \\ &= \frac{1}{2R_e^2}\sqrt{\frac{\omega_e^2}{4\mathcal{D}_e B_e}}\left[\sqrt{\frac{\omega_e^2}{4\mathcal{D}_e B_e}} - \left(\frac{\alpha_e\,\omega_e}{6B_e^2} + 1\right)\right]\ ,\end{aligned} \tag{A.36}$$

$$\begin{aligned}\beta_2^{\rm GMO} &= \frac{1}{6R_e^3}\sqrt{\frac{a_0}{\mathcal{D}_e}}\left[3a_1\left(a_1 + \sqrt{\frac{a_0}{\mathcal{D}_e}}\right) + 2\frac{a_0}{\mathcal{D}_e} - \frac{2\omega_e x_e}{B_e}\right] \\ &= \frac{1}{6R_e^3}\sqrt{\frac{\omega_e^2}{4\mathcal{D}_e B_e}}\left[3\left(\frac{\alpha_e\,\omega_e}{6B_e^2} + 1\right)\left(\frac{\alpha_e\,\omega_e}{6B_e^2} + 1 - \sqrt{\frac{\omega_e^2}{4\mathcal{D}_e B_e}}\right) + \frac{\omega_e^2}{2\mathcal{D}_e B_e} - \frac{2\omega_e x_e}{B_e}\right]\ .\end{aligned} \tag{A.37}$$

As a simple check, we have determined each of these beta parameters for the SMO case. This is done by knowing that for the SMO

$$\mathcal{D}_e = \frac{\omega_e^2}{4\omega_e x_e}\ , \quad \text{and} \quad \alpha_e = 6\frac{B_e}{\omega_e}\left[\sqrt{\omega_e x_e B_e} - B_e\right]\ , \tag{A.38}$$

so that

$$a_1 = -\sqrt{\frac{\omega_e x_e}{B_e}}\ , \quad \text{and} \quad a_2 = \frac{7\omega_e x_e}{12B_e}\ . \tag{A.39}$$

Using these relations and substituting them back into Eqs. (A.35)-(A.37) shows that

$$\beta_0 \equiv \beta_M = \frac{1}{R_e}\sqrt{\frac{\omega_e^2}{4\mathcal{D}_e B_e}} = \frac{\omega_e}{2}/\sqrt{\frac{\hbar^2}{2\mu}\mathcal{D}_e}\ , \tag{A.40}$$

and $\beta_1 = 0 = \beta_2$, which is exactly what is expected for the SMO [29].

A.2.2 Expanded Morse Oscillator

For a = EMO, the equations for the first three exponential parameters are

$$\beta_0^{\rm EMO} = \frac{1}{R_e}\sqrt{\frac{a_0}{\mathcal{D}_e}} = \frac{1}{R_e}\sqrt{\frac{\omega_e^2}{4\mathcal{D}_e B_e}} = \frac{\omega_e}{2}/\sqrt{\frac{\hbar^2}{2\mu}\mathcal{D}_e}\ , \tag{A.41}$$

$$\begin{aligned}\beta_1^{\rm EMO} &= \frac{1}{R_e}\sqrt{\frac{a_0}{\mathcal{D}_e}}\left[\sqrt{\frac{a_0}{\mathcal{D}_e}} + a_1\right] \\ &= \frac{1}{R_e}\sqrt{\frac{\omega_e^2}{4\mathcal{D}_e B_e}}\left[\sqrt{\frac{\omega_e^2}{4\mathcal{D}_e B_e}} - \left(\frac{\alpha_e\,\omega_e}{6B_e^2}+1\right)\right]\ ,\end{aligned} \tag{A.42}$$

$$\begin{aligned}\beta_2^{\rm EMO} &= \frac{1}{R_e}\sqrt{\frac{a_0}{\mathcal{D}_e}}\left[(2a_1+1)\left(a_1+\sqrt{\frac{a_0}{\mathcal{D}_e}}\right)+\frac{4}{3}\left(\frac{a_0}{\mathcal{D}_e}-\frac{\omega_e x_e}{B_e}\right)\right] \\ &= \frac{1}{R_e}\sqrt{\frac{\omega_e^2}{4\mathcal{D}_e B_e}}\left[\left(2\frac{\alpha_e\,\omega_e}{6B_e^2}+1\right)\left(\frac{\alpha_e\,\omega_e}{6B_e^2}+1-\sqrt{\frac{\omega_e^2}{4\mathcal{D}_e B_e}}\right)+\frac{\omega_e^2}{3\mathcal{D}_e B_e}-\frac{4\omega_e x_e}{3B_e}\right]\ .\end{aligned} \tag{A.43}$$

A.2.3 Dulick's Modified Morse Oscillator

For a = MMO, the equations for the first three exponential parameters are:

$$\beta_0^{\rm MMO} = 2\sqrt{\frac{a_0}{\mathcal{D}_e^{\rm MMO}}} = 2\sqrt{\frac{\omega_e^2}{4\mathcal{D}_e^{\rm MMO} B_e}}\ , \tag{A.44}$$

$$\begin{aligned}\beta_1^{\rm MMO} &= 2\sqrt{\frac{a_0}{\mathcal{D}_e^{\rm MMO}}}\left(\sqrt{\frac{a_0}{\mathcal{D}_e^{\rm MMO}}}+a_1+1\right) \\ &= 2\sqrt{\frac{\omega_e^2}{4\mathcal{D}_e^{\rm MMO} B_e}}\left[\sqrt{\frac{\omega_e^2}{4\mathcal{D}_e^{\rm MMO} B_e}}-\frac{\alpha_e\omega_e}{6B_e^2}\right]\ ,\end{aligned} \tag{A.45}$$

$$\begin{aligned}\beta_2^{\rm MMO} &= \sqrt{\frac{a_0}{\mathcal{D}_e^{\rm MMO}}}\left[4\,(a_1+1)\left(a_1+\sqrt{\frac{a_0}{\mathcal{D}_e^{\rm MMO}}}\right)+\frac{8}{3}\left(\frac{a_0}{\mathcal{D}_e^{\rm MMO}}-\frac{\omega_e x_e}{B_e}\right)+2\right] \\ &= \sqrt{\frac{\omega_e^2}{4\mathcal{D}_e^{\rm MMO} B_e}}\left[4\frac{\alpha_e\omega_e}{6B_e^2}\left(\frac{\alpha_e\omega_e}{6B_e^2}+1-\sqrt{\frac{\omega_e^2}{4\mathcal{D}_e^{\rm MMO} B_e}}\right)\right. \\ &\quad \left.+\frac{8}{3}\left(\frac{\omega_e^2}{4\mathcal{D}_e^{\rm MMO} B_e}-\frac{\omega_e x_e}{B_e}\right)+2\right]\ .\end{aligned} \tag{A.46}$$

Since $\mathcal{D}_e^{\rm MMO}$ is defined to include the normalization factor $\left[1-e^{-\beta_\infty}\right]^2$, $\mathcal{D}_e^{\rm MMO}$ is a function of all the exponential parameters. Therefore, the equations above are in fact *not* closed form equations for the first three exponential parameters, and it is not possible to obtain explicit closed form solutions for the $\beta_i^{\rm MMO}$.

Fortunately, this is not a difficult problem to solve as it is a very simple task to calculate the initial trial parameters using an iterative algorithm. In particular, Eqs. (A.44)-(A.46) are evaluated initially with $\beta_i^{\rm MMO} = \infty$ (i.e. $\mathcal{D}_e^{\rm MMO} = \mathcal{D}_e$); the resulting values of $\{\beta_i^{\rm MMO}; i = 0-2\}$ are then used to define an improved estimate of $\mathcal{D}_e^{\rm MMO} = \mathcal{D}_e/\left[1-e^{-\beta_\infty}\right]^2$, and Eqs. (A.44)-(A.46) are used again to generate improved estimates of the $\beta_i^{\rm MMO}$ values. This procedure is then repeated until convergence is achieved. In practice, this seems to require few iterations; typically achieving $< 1\%$ parameter change after five iterations.

A.2.4 Modified Lennard-Jones Oscillator

For a = MLJ, the equations for the first three exponential parameters are

$$\beta_0^{\rm MLJ} = 2\sqrt{\frac{a_0}{\mathcal{D}_e}} - 2n = 2\sqrt{\frac{\omega_e^2}{4\mathcal{D}_e B_e}} - 2n \,, \tag{A.47}$$

$$\beta_1^{\rm MLJ} = 2\sqrt{\frac{a_0}{\mathcal{D}_e}}\left(\sqrt{\frac{a_0}{\mathcal{D}_e}} + a_1 + 1\right) = 2\sqrt{\frac{\omega_e^2}{4\mathcal{D}_e B_e}}\left[\sqrt{\frac{\omega_e^2}{4\mathcal{D}_e B_e}} - \frac{\alpha_e\omega_e}{6B_e^2}\right] \,, \tag{A.48}$$

$$\begin{aligned}\beta_2^{\rm MLJ} &= \sqrt{\frac{a_0}{\mathcal{D}_e}}\left[4\left(a_1+1\right)\left(a_1+\sqrt{\frac{a_0}{\mathcal{D}_e}}\right) + \frac{8}{3}\left(\frac{a_0}{\mathcal{D}_e} - \frac{\omega_e x_e}{B_e}\right) + 2\right] - \frac{2}{3}n \qquad (A.49)\\ &= \sqrt{\frac{\omega_e^2}{4\mathcal{D}_e B_e}}\left[4\frac{\alpha_e\omega_e}{6B_e^2}\left(\frac{\alpha_e\omega_e}{6B_e^2} + 1 - \sqrt{\frac{\omega_e^2}{4\mathcal{D}_e B_e}}\right) + \frac{8}{3}\left(\frac{\omega_e^2}{4\mathcal{D}_e B_e} - \frac{\omega_e x_e}{B_e}\right) + 2\right] - \frac{2}{3}n \,.\end{aligned}$$

A.3 Listing of Partial Derivatives

The partial derivatives of α_a, β_a, and z with respect to the intermolecular distance (R) required for the derivations of Appendix A.2 are listed here.

A.3.1 Derivatives of α_a

For a = GMO or EMO,

$$\alpha_a = \beta_a + (R - R_e)\frac{\partial \beta_a}{\partial R} \Rightarrow \alpha_a|_{R=R_e} = \beta_a|_{R=R_e} , \tag{A.50}$$

$$\frac{\partial \alpha_a}{\partial R} = 2\frac{\partial \beta_a}{\partial R} + (R - R_e)\frac{\partial^2 \beta_a}{\partial R^2} \Rightarrow \left.\frac{\partial \alpha_a}{\partial R}\right|_{R=R_e} = 2 \left.\frac{\partial \beta_a}{\partial R}\right|_{R=R_e} , \tag{A.51}$$

$$\frac{\partial^2 \alpha_a}{\partial R^2} = 3\frac{\partial^2 \beta_a}{\partial R^2} + (R - R_e)\frac{\partial^3 \beta_a}{\partial R^3} \Rightarrow \left.\frac{\partial^2 \alpha_a}{\partial R^2}\right|_{R=R_e} = 3 \left.\frac{\partial^2 \beta_a}{\partial R^2}\right|_{R=R_e} , \tag{A.52}$$

$$\begin{aligned} \frac{\partial^m \alpha_a}{\partial R^m} &= (m+1)\frac{\partial^m \beta_a}{\partial R^m} + (R - R_e)\frac{\partial^{m+1} \beta_a}{\partial R^{m+1}} \\ \Rightarrow \left.\frac{\partial^m \alpha_a}{\partial R^m}\right|_{R=R_e} &= (m+1) \left.\frac{\partial^m \beta_a}{\partial R^m}\right|_{R=R_e} . \end{aligned} \tag{A.53}$$

For a = MMO or MLJ,

$$\begin{aligned} \alpha_a &= \frac{n}{R} + \frac{2R_e}{(R+R_e)^2}\beta_a + \left(\frac{R - R_e}{R + R_e}\right)\frac{\partial \beta_a}{\partial R} \\ \Rightarrow \alpha_a|_{R=R_e} &= \frac{n}{R_e} + \frac{1}{2R_e}\,\beta_a|_{R=R_e} , \end{aligned} \tag{A.54}$$

$$\begin{aligned} \frac{\partial \alpha_a}{\partial R} &= -\frac{n}{R^2} - \frac{4R_e}{(R+R_e)^3}\beta_a + \frac{4R_e}{(R+R_e)^2}\frac{\partial \beta_a}{\partial R} + \left(\frac{R - R_e}{R + R_e}\right)\frac{\partial^2 \beta_a}{\partial R^2} \\ \Rightarrow \left.\frac{\partial \alpha_a}{\partial R}\right|_{R=R_e} &= -\frac{n}{R_e^2} - \frac{1}{2R_e^2}\,\beta_a|_{R=R_e} + \frac{1}{R_e}\left.\frac{\partial \beta_a}{\partial R}\right|_{R=R_e} , \end{aligned} \tag{A.55}$$

$$\begin{aligned}
\frac{\partial^2 \alpha_a}{\partial R^2} &= \frac{2n}{R^3} + \frac{12R_e}{(R+R_e)^4}\beta_a - \frac{12R_e}{(R+R_e)^3}\frac{\partial \beta_a}{\partial R} + \frac{6R_e}{(R+R_e)^2}\frac{\partial^2 \beta_a}{\partial R^2} \\
&\quad + \left(\frac{R-R_e}{R+R_e}\right)\frac{\partial^3 \beta_a}{\partial R^3} \\
\Rightarrow \left.\frac{\partial^2 \alpha_a}{\partial R^2}\right|_{R=R_e} &= \frac{2n}{R_e^3} + \frac{3}{4R_e^3}\,\beta_a|_{R=R_e} - \left.\frac{3}{2R_e^2}\frac{\partial \beta_a}{\partial R}\right|_{R=R_e} + \left.\frac{3}{2R_e}\frac{\partial^2 \beta_a}{\partial R^2}\right|_{R=R_e} \quad ,(A.56)
\end{aligned}$$

$$\begin{aligned}
\frac{\partial^m \alpha_a}{\partial R^m} &= (-1)^m\, m!\, \frac{n}{R^{m+1}} + \sum_{l=0}^{m}(-1)^{m-l}\frac{(m+1)!}{l!}\frac{2R_e}{(R+R_e)^{m+2-l}}\frac{\partial^l \beta_a}{\partial R^l} \\
&\quad + \left(\frac{R-R_e}{R+R_e}\right)\frac{\partial^{m+1} \beta_a}{\partial R^{m+1}} \\
\Rightarrow \left.\frac{\partial^m \alpha_a}{\partial R^m}\right|_{R=R_e} &= (-1)^m\, m!\, \frac{n}{R_e^{m+1}} \\
&\quad + \sum_{l=0}^{m}(-1)^{m-l}\frac{(m+1)!}{l!}(2R_e)^{l-1-m}\left.\frac{\partial^l \beta_a}{\partial R^l}\right|_{R=R_e} . \qquad (A.57)
\end{aligned}$$

Thus, introducing a more general notation to encompass all four cases, namely

$$\alpha = \frac{n}{R} + \frac{\partial}{\partial R}\left[\gamma(R)\beta(R)\right] , \qquad (A.58)$$

where $\gamma(R) = (R - R_e)$ for the GMO and EMO, $\gamma(R) = (R-R_e)/(R+R_e)$ for the MMO and MLJ, and $n = 0$ for the GMO, EMO, and MMO, the m^{th} partial derivative of α with respect to R can be written as

$$\frac{\partial^m \alpha}{\partial R^m} = (-1)^m\, m!\, \frac{n}{R^{m+1}} + \sum_{l=0}^{m+1}\left(\begin{array}{c} m+1 \\ l \end{array}\right)\frac{\partial^{m+1-l}\gamma(R)}{\partial R^{m+1-l}}\frac{\partial^l \beta(R)}{\partial R^l} . \qquad (A.59)$$

A.3.2 Derivatives of β_a

For a = GMO,

$$\beta_{\text{GMO}} = \sum_{l=0}\beta_l^{\text{GMO}}(R-R_e)^l \;\Rightarrow\; \beta_{\text{GMO}}|_{R=R_e} = \beta_0^{\text{GMO}} , \qquad (A.60)$$

$$\frac{\partial \beta_{\rm GMO}}{\partial R} = \sum_{l=1} l \beta_l^{\rm GMO} (R-R_e)^{l-1} \Rightarrow \left.\frac{\partial \beta_{\rm GMO}}{\partial R}\right|_{R=R_e} = \beta_1^{\rm GMO} , \quad \text{(A.61)}$$

$$\frac{\partial^2 \beta_{\rm GMO}}{\partial R^2} = \sum_{l=2} l(l-1) \beta_l^{\rm GMO} (R-R_e)^{l-2}$$
$$\Rightarrow \left.\frac{\partial^2 \beta_{\rm GMO}}{\partial R^2}\right|_{R=R_e} = 2\beta_2^{\rm GMO} , \quad \text{(A.62)}$$

$$\frac{\partial^m \beta_{\rm GMO}}{\partial R^m} = \sum_{l=m} \frac{l!}{(l-m)!} \beta_l^{\rm GMO} (R-R_e)^{l-m}$$
$$\Rightarrow \left.\frac{\partial^m \beta_{\rm GMO}}{\partial R^m}\right|_{R=R_e} = m! \beta_m^{\rm GMO} . \quad \text{(A.63)}$$

For a = MMO, EMO, or MLJ,

$$\beta_a = \sum_{l=0} \beta_l^a z^l = \beta_0^a + \beta_1^a z + \beta_2^a z^2 + \cdots \Rightarrow \beta_a|_{R=R_e} = \beta_0 , \quad \text{(A.64)}$$

$$\frac{\partial \beta_a}{\partial R} = \sum_{l=1} l \beta_l^a \left(\frac{\partial z}{\partial R}\right) z^{l-1} \Rightarrow \left.\frac{\partial \beta_a}{\partial R}\right|_{R=R_e} = \beta_1^a \left.\frac{\partial z}{\partial R}\right|_{R=R_e} , \quad \text{(A.65)}$$

$$\frac{\partial^2 \beta_a}{\partial R^2} = \sum_{l=1} l \beta_l^a \left[\left(\frac{\partial^2 z}{\partial R^2}\right) z^{l-1} + (l-1)\left(\frac{\partial z}{\partial R}\right)^2 z^{l-2}\right]$$
$$\Rightarrow \left.\frac{\partial^2 \beta_a}{\partial R^2}\right|_{R=R_e} = \beta_1^a \left.\frac{\partial^2 z}{\partial R^2}\right|_{R=R_e} + 2\beta_2^a \left.\frac{\partial z}{\partial R}\right|_{R=R_e}^2 , \quad \text{(A.66)}$$

$$\frac{\partial^3 \beta_a}{\partial R^3} = \sum_{l=1} l \beta_l^a \left[\left(\frac{\partial^3 z}{\partial R^3}\right) z^{l-1} + 3(l-1)\left(\frac{\partial^2 z}{\partial R^2}\right)\left(\frac{\partial z}{\partial R}\right) z^{l-2} \right.$$
$$\left. + (l-1)(l-2)\left(\frac{\partial z}{\partial R}\right)^3 z^{l-3}\right]$$
$$\Rightarrow \left.\frac{\partial^3 \beta_a}{\partial R^3}\right|_{R=R_e} = \beta_1^a \left.\frac{\partial^3 z}{\partial R^3}\right|_{R=R_e} + 6\beta_2^a \left.\frac{\partial^2 z}{\partial R^2}\right|_{R=R_e} \left.\frac{\partial z}{\partial R}\right|_{R=R_e} + 6\beta_3^a \left.\frac{\partial z}{\partial R}\right|_{R=R_e}^3 \quad \text{(A.67)}$$

$$\begin{aligned}
\frac{\partial^4\beta_a}{\partial R^4} &= \sum_{l=1} l\beta_l^a \left\{ \left(\frac{\partial^4 z}{\partial R^4}\right) z^{l-1} \right. \\
&\quad + (l-1)\left[4\left(\frac{\partial^3 z}{\partial R^3}\right)\left(\frac{\partial z}{\partial R}\right) + 3\left(\frac{\partial^2 z}{\partial R^2}\right)^2\right] z^{l-2} \\
&\quad + 6(l-1)(l-2)\left(\frac{\partial^2 z}{\partial R^2}\right)\left(\frac{\partial z}{\partial R}\right)^2 z^{l-3} \\
&\quad \left. +(l-1)(l-2)(l-3)\left(\frac{\partial z}{\partial R}\right)^4 z^{l-4}\right\} \\
\Rightarrow \left.\frac{\partial^4\beta_a}{\partial R^4}\right|_{R=R_e} &= \beta_1^a \left.\frac{\partial^4 z}{\partial R^4}\right|_{R=R_e} + 2\beta_2^a \left[4\left.\frac{\partial^3 z}{\partial R^3}\right|_{R=R_e}\left.\frac{\partial z}{\partial R}\right|_{R=R_e} + 3\left.\frac{\partial^2 z}{\partial R^2}\right|^2_{R=R_e}\right] \\
&\quad + 36\beta_3^a \left.\frac{\partial^2 z}{\partial R^2}\right|_{R=R_e}\left.\frac{\partial z}{\partial R}\right|^2_{R=R_e} + 24\beta_4^a \left.\frac{\partial z}{\partial R}\right|^4_{R=R_e} \ , \qquad \text{(A.68)}
\end{aligned}$$

and

$$\begin{aligned}
\frac{\partial^5\beta_a}{\partial R^5} &= \sum_{l=1} l\beta_l^a \left\{ \left(\frac{\partial^5 z}{\partial R^5}\right) z^{l-1} + 5(l-1)\left[\left(\frac{\partial^4 z}{\partial R^4}\right)\left(\frac{\partial z}{\partial R}\right) + 2\left(\frac{\partial^3 z}{\partial R^3}\right)\left(\frac{\partial^2 z}{\partial R^2}\right)\right] z^{l-2} \right. \\
&\quad + 5(l-2)(l-1)\left[2\left(\frac{\partial^3 z}{\partial R^3}\right)\left(\frac{\partial z}{\partial R}\right)^2 + 3\left(\frac{\partial^2 z}{\partial R^2}\right)^2\left(\frac{\partial z}{\partial R}\right)\right] z^{l-3} \\
&\quad + 10(l-3)(l-2)(l-1)\left(\frac{\partial^2 z}{\partial R^2}\right)\left(\frac{\partial z}{\partial R}\right)^3 z^{l-4} \\
&\quad \left. + (l-4)(l-3)(l-2)(l-1)\left(\frac{\partial z}{\partial R}\right)^5 z^{l-5}\right\} \ . \qquad \text{(A.69)}
\end{aligned}$$

There is no known generalized recurrence relation for the derivatives of these β_a parameters.

A.3.3 Derivatives of z

There is a generalized recurrence relation for the partial derivatives of z, obtained via

$$z = \left(\frac{R-R_e}{R+R_e}\right) \Rightarrow z|_{R=R_e} = 0 \ , \qquad \text{(A.70)}$$

$$\frac{\partial z}{\partial R} = \frac{2R_e}{(R+R_e)^2} \Rightarrow \left.\frac{\partial z}{\partial R}\right|_{R=R_e} = \frac{1}{2R_e} , \tag{A.71}$$

$$\frac{\partial^2 z}{\partial R^2} = \frac{-4R_e}{(R+R_e)^3} \Rightarrow \left.\frac{\partial^2 z}{\partial R^2}\right|_{R=R_e} = -\frac{1}{2R_e^2} , \tag{A.72}$$

and

$$\frac{\partial^m z}{\partial R^m} = 2R_e m! \left(\frac{-1}{R+R_e}\right)^{m+1} \Rightarrow \left.\frac{\partial^m z}{\partial R^m}\right|_{R=R_e} = \frac{-m!}{(-2R_e)^m} . \tag{A.73}$$

A.3.4 Derivatives of x

The partial derivatives for the SPF expansion parameter x are given by

$$x = \left(\frac{R-R_e}{R}\right) \Rightarrow x|_{R=R_e} = 0 , \tag{A.74}$$

$$\frac{\partial x}{\partial R} = \frac{R_e}{R^2} \Rightarrow \left.\frac{\partial x}{\partial R}\right|_{R=R_e} = \frac{1}{R_e} , \tag{A.75}$$

$$\frac{\partial^2 x}{\partial R^2} = \frac{-2R_e}{R^3} \Rightarrow \left.\frac{\partial^2 x}{\partial R^2}\right|_{R=R_e} = -\frac{2}{R_e^2} , \tag{A.76}$$

and

$$\frac{\partial^m x}{\partial R^m} = R_e m! \left(\frac{-1}{R}\right)^{m+1} \Rightarrow \left.\frac{\partial^m x}{\partial R^m}\right|_{R=R_e} = \frac{-m!}{(-R_e)^m} . \tag{A.77}$$

Appendix B

Partial Derivatives of Various Model Potential Functions

For the least-squares fitting routine, the partial derivative of each of the observables with respect to each parameter is required. As discussed in Section 2.5, this requires a knowledge of the partial derivatives of the potential with respect to each of its parameters. Thus, using Eqs. (2.7), and (2.14)-(2.18) to define the centrifugally-distorted effective potential for isotopomer-α, the partial derivative of $V^{\alpha}_{\mathrm{eff},J}$ with respect to parameter p_k is

$$\frac{\partial V^{\alpha}_{\mathrm{eff},J}}{\partial p_k} \;=\; \frac{\partial V^{1}_{\mathrm{ad}}}{\partial p_k} + \frac{\partial \Delta V^{\alpha}_{\mathrm{ad}}}{\partial p_k} + \frac{\hbar^2}{2\mu R^2}\left[1 + \frac{\partial q^{\alpha}}{\partial p_k}\right][J(J+1)] \; . \tag{B.1}$$

The functional form of any of the four adiabatic potential functions ($V^{1}_{\mathrm{ad}}(R) = V_a(R)$) considered are

$$V_a(R) \;=\; \mathcal{D}^{a}_{e}[1 - f_a(R)]^2 \; , \tag{B.2}$$

where $\mathcal{D}_e^a = \mathcal{D}_e$ for $a =$ GMO, EMO, MLJ, $\mathcal{D}_e^{\rm MMO} = \mathcal{D}_e / \left(1 - e^{-\beta_\infty^{\rm MMO}}\right)^2$, and

$$f_a(R) = \left(\frac{R_e}{R}\right)^n e^{-\beta_a(R)\gamma_a(R)} , \tag{B.3}$$

in which β_a is a flexible, smoothly-varying function of R and β_i. With the appropriate selection for n, β_a, and γ_a, one can generate any of the GMO, EMO, MMO, or MLJ potentials which are being considered. The first partial derivatives of V_a are thus

$$\frac{\partial V_a}{\partial \mathcal{D}_e} = \frac{\mathcal{D}_e^a}{\mathcal{D}_e}[1 - f_a(R)]^2 , \tag{B.4}$$

$$\frac{\partial V_a}{\partial R_e} = 2\mathcal{D}_e^a f_a(R)\left[1 - f_a(R)\right]\left[-\frac{n}{R_e} + \frac{\partial \gamma_a(R)}{\partial R_e}\beta_a(R) + \gamma_a(R)\frac{\partial \beta_a(R)}{\partial R_e}\right] , \tag{B.5}$$

$$\frac{\partial V_a}{\partial \beta_m} = 2\mathcal{D}_e^a f_a(R)\left[1 - f_a(R)\right]\left[\gamma_a(R)\frac{\partial \beta_a(R)}{\partial \beta_i} - \delta_{n,0}\frac{1 - e^{\beta_a(R)\gamma_a(R)}}{1 - e^{\beta_a^\infty}}\right] , \tag{B.6}$$

while the first partial derivatives for $\Delta V_{\rm ad}^\alpha(R)$ are

$$\frac{\partial \Delta V_{\rm ad}^\alpha}{\partial R_e} = \frac{\Delta M_{\rm A}^\alpha}{M_{\rm A}^\alpha}\left(\sum_l l\ u_l^{\rm A}\ z^{l-1}\right)\frac{\partial z}{\partial R_e} + \frac{\Delta M_{\rm B}^\alpha}{M_{\rm B}^\alpha}\left(\sum_l l\ u_l^{\rm B}\ z^{l-1}\right)\frac{\partial z}{\partial R_e} , \tag{B.7}$$

and

$$\frac{\partial \Delta V_{\rm ad}^\alpha}{\partial u_l^{\rm A}} = \frac{\Delta M_{\rm A}^\alpha}{M_{\rm A}^\alpha} z^l , \quad \frac{\partial \Delta V_{\rm ad}^\alpha}{\partial u_l^{\rm B}} = \frac{\Delta M_{\rm B}^\alpha}{M_{\rm B}^\alpha} z^l . \tag{B.8}$$

The partial derivatives for the centrifugal correction function $q^\alpha(R)$ are

$$\frac{\partial q^\alpha}{\partial R_e} = \frac{M_{\rm A}^1}{M_{\rm A}^\alpha}\left(\sum_l l\ q_l^{\rm A}\ z^{l-1}\right)\frac{\partial z}{\partial R_e} + \frac{M_{\rm B}^1}{M_{\rm B}^\alpha}\left(\sum_l l\ q_l^{\rm B}\ z^{l-1}\right)\frac{\partial z}{\partial R_e} , \tag{B.9}$$

and

$$\frac{\partial q^\alpha}{\partial q_l^{\rm A}} = \frac{M_{\rm A}^1}{M_{\rm A}^\alpha} z^l , \quad \frac{\partial q^\alpha}{\partial q_l^{\rm B}} = \frac{M_{\rm B}^1}{M_{\rm B}^\alpha} z^l . \tag{B.10}$$

The partial derivatives of each function now depend on the type of potential form chosen. These are listed below in sections B.1 through B.6.

B.1 Generalized Morse Oscillator

For the GMO, $n = 0$, $\beta_{\rm GMO}(R) = \sum_{i=0} \beta_i^{\rm GMO}(R - R_e)^i$, and $\gamma_{\rm GMO}(R) = R - R_e$,

$$V_{\rm GMO} = \mathcal{D}_e \left[1 - e^{-\beta_{\rm GMO}(R-R_e)}\right]^2 , \tag{B.11}$$

$$\beta_{\rm GMO} = \beta_0^{\rm GMO} + \beta_1^{\rm GMO}(R - R_e) + \beta_2^{\rm GMO}(R - R_e)^2 + \cdots , \tag{B.12}$$

$$\frac{\partial V_{\rm GMO}}{\partial \mathcal{D}_e} = \left[1 - e^{-\beta_{\rm GMO}(R-R_e)}\right]^2 , \tag{B.13}$$

$$\begin{aligned} \frac{\partial V_{\rm GMO}}{\partial R_e} &= -2\mathcal{D}_e e^{-\beta_{\rm GMO}(R-R_e)} \left[1 - e^{-\beta_{\rm GMO}(R-R_e)}\right] \left[\beta_{\rm GMO} + \sum_{l=1}^{\infty} l\beta_l^{\rm GMO}(R - R_e)^l\right] \\ &= -2\mathcal{D}_e e^{-\beta_{\rm GMO}(R-R_e)} \left[1 - e^{-\beta_{\rm GMO}(R-R_e)}\right] \left[\sum_{l=0}^{\infty}(l+1)\beta_l^{\rm GMO}(R - R_e)^l\right] \end{aligned} \tag{B.14}$$

$$\frac{\partial V_{\rm GMO}}{\partial \beta_m^{\rm GMO}} = 2\mathcal{D}_e e^{-\beta_{\rm GMO}(R-R_e)} \left[1 - e^{-\beta_{\rm GMO}(R-R_e)}\right] (R - R_e)^{m+1} . \tag{B.15}$$

B.2 Expanded Morse Oscillator

For the EMO, $n = 0$, $\beta_{\rm EMO}(R) = \sum_{i=0} \beta_i^{\rm EMO} z^i$, and $\gamma_{\rm EMO}(R) = R - R_e$,

$$V_{\rm EMO} = \mathcal{D}_e \left[1 - e^{-\beta_{\rm EMO}(R-R_e)}\right]^2 , \tag{B.16}$$

$$\beta^{\rm EMO} = \beta_0^{\rm EMO} + \beta_1^{\rm EMO} z + \beta_2^{\rm EMO} z^2 + \cdots , \tag{B.17}$$

$$\frac{\partial V_{\rm EMO}}{\partial \mathcal{D}_e} = \left[1 - e^{-\beta_{\rm EMO}(R-R_e)}\right]^2 , \tag{B.18}$$

$$\frac{\partial V_{\rm EMO}}{\partial R_e} = -2\mathcal{D}_e e^{-\beta_{\rm EMO}(R-R_e)}\left[1-e^{-\beta_{\rm EMO}(R-R_e)}\right]\left[\beta_{\rm EMO}+\frac{2R}{R+R_e}\sum_{l=1}^{\infty} l\,\beta_l^{\rm EMO} z^l\right], \tag{B.19}$$

$$\frac{\partial V_{\rm EMO}}{\partial \beta_m^{\rm EMO}} = 2\mathcal{D}_e e^{-\beta_{\rm EMO}(R-R_e)}\left[1-e^{-\beta_{\rm EMO}(R-R_e)}\right](R-R_e)z^m . \tag{B.20}$$

B.3 Dulick's Modified Morse Oscillator

For the MMO, $n=0$, $\beta_{\rm MMO}(R)=\sum_{i=0}\beta_i^{\rm MMO}z^i$, and $\gamma_{\rm MMO}(R)=z$. However, there is a normalization factor included in the potential; thus

$$V_{\rm MMO} = \mathcal{D}_e\left[\frac{1-e^{-\beta_{\rm MMO}z}}{1-e^{-\beta_\infty^{\rm MMO}}}\right]^2 , \tag{B.21}$$

$$\beta_{\rm MMO} = \beta_0^{\rm MMO}+\beta_1^{\rm MMO}z+\beta_2^{\rm MMO}z^2+\cdots , \tag{B.22}$$

$$\beta_\infty^{\rm MMO} = \beta_{\rm MMO}(R=\infty) = \beta_0^{\rm MMO}+\beta_1^{\rm MMO}+\beta_2^{\rm MMO}+\cdots , \tag{B.23}$$

$$\frac{\partial V_{\rm MMO}}{\partial \mathcal{D}_e} = \left[\frac{1-e^{-\beta_{\rm MMO}z}}{1-e^{-\beta_\infty^{\rm MMO}}}\right]^2 , \tag{B.24}$$

$$\frac{\partial V_{\rm MMO}}{\partial R_e} = -2\mathcal{D}_e e^{-\beta_{\rm MMO}z}\frac{1-e^{-\beta_{\rm MMO}z}}{(1-e^{-\beta_\infty^{\rm MMO}})^2}\left[\frac{2R}{(R+R_e)^2}\sum_{l=0}^{\infty}(l+1)\beta_l^{\rm MMO}z^l\right], \tag{B.25}$$

$$\frac{\partial V_{\rm MMO}}{\partial \beta_m^{\rm MMO}} = 2\mathcal{D}_e e^{-\beta_{\rm MMO}z}\frac{1-e^{-\beta_{\rm MMO}z}}{(1-e^{-\beta_\infty^{\rm MMO}})^2}\left[z^{m+1}-\frac{1-e^{\beta_{\rm MMO}z}}{1-e^{\beta_\infty^{\rm MMO}}}\right] . \tag{B.26}$$

B.4 Modified Lennard-Jones Oscillator

For the MLJ, $n>0$, $\beta_{\rm MLJ}(R)=\sum_{i=0}\beta_i^{\rm MLJ}z^i$, and $\gamma_{\rm MLJ}(R)=z$,

$$V_{\rm MLJ} = \mathcal{D}_e\left[1-\left(\frac{R_e}{R}\right)^n e^{-\beta_{\rm MLJ}z}\right]^2 , \tag{B.27}$$

$$\beta_{\rm MLJ} = \beta_0^{\rm MLJ}+\beta_1^{\rm MLJ}z+\beta_2^{\rm MLJ}z^2+\cdots , \tag{B.28}$$

$$\frac{\partial V_{\rm MLJ}}{\partial \mathcal{D}_e} = \left[1 - \left(\frac{R_e}{R}\right)^n e^{-\beta_{\rm MLJ}\, z}\right]^2 , \tag{B.29}$$

$$\begin{aligned}\frac{\partial V_{\rm MLJ}}{\partial R_e} &= -2\mathcal{D}_e \left(\frac{R_e}{R}\right)^n e^{-\beta_{\rm MLJ}\, z} \left[1 - \left(\frac{R_e}{R}\right)^n e^{-\beta_{\rm MLJ}\, z}\right] \\ &\quad \times \left[\frac{n}{R_e} + \frac{2R}{(R+R_e)^2}\beta_{\rm MLJ} - z\frac{\partial \beta_{\rm MLJ}}{\partial R_e}\right] \\ &= -2\mathcal{D}_e \left(\frac{R_e}{R}\right)^n e^{-\beta_{\rm MLJ}\, z} \left[1 - \left(\frac{R_e}{R}\right)^n e^{-\beta_{\rm MLJ}\, z}\right] \\ &\quad \times \left[\frac{n}{R_e} + \frac{2R}{(R+R_e)^2}\sum_{l=0}^{\infty}(l+1)\beta_l^{\rm MLJ} z^l\right] ,\end{aligned} \tag{B.30}$$

$$\begin{aligned}\frac{\partial V_{\rm MLJ}}{\partial \beta_m^{\rm MLJ}} &= 2\mathcal{D}_e \left(\frac{R_e}{R}\right)^n e^{-\beta_{\rm MLJ}\, z} \left[1 - \left(\frac{R_e}{R}\right)^n e^{-\beta_{\rm MLJ}\, z}\right] \frac{\partial \beta_{\rm MLJ}}{\partial \beta_m^{\rm MLJ}} z \\ &= 2\mathcal{D}_e \left(\frac{R_e}{R}\right)^n e^{-\beta_{\rm MLJ}\, z} \left[1 - \left(\frac{R_e}{R}\right)^n e^{-\beta_{\rm MLJ}\, z}\right] z^{m+1} .\end{aligned} \tag{B.31}$$

B.5 Switching Function Constraint

The switching function has the following form [20],

$$\beta_{\rm sw}(R) = f_{\rm sw}(R)\left[\beta_{\rm MLJ}(R) - \beta_\infty\right] + \beta_\infty , \tag{B.32}$$

where $\beta_\infty = \beta(z=1) = \ln\left[2\mathcal{D}_e (R_e)^n / C_n\right]$,

$$f_{\rm sw}(R) = \frac{1}{e^{\alpha_s (R - R_s)} + 1} , \tag{B.33}$$

and the fixed parameters α_s and R_s are manually chosen so that $\beta(z)$ "looks" smooth and the asymptotic inverse-power constant C_n is assumed to be a known constant. The partial derivatives required for the non-linear least-squares fitting procedure are listed

below:

$$\frac{\partial \beta_{\rm sw}}{\partial \mathcal{D}_e} = (1 - f_{\rm sw})/\mathcal{D}_e \ , \tag{B.34}$$

$$\frac{\partial \beta_{\rm sw}}{\partial R_e} = f_{\rm sw}\frac{\partial \beta_{\rm MLJ}}{\partial R_e} + (1 - f_{\rm sw})\frac{n}{R_e} \ , \tag{B.35}$$

$$\frac{\partial \beta_{\rm sw}}{\partial \beta_m} = f_{\rm sw}\frac{\partial \beta_{\rm MLJ}}{\partial \beta_m^{\rm MLJ}} = f_{\rm sw}\ z^m \ . \tag{B.36}$$

B.6 Other Partial Derivatives

Here are some other important generalized partial derivatives:

$$\frac{\partial z^n}{\partial R_e} = \frac{\partial}{\partial R_e}\left(\frac{R - R_e}{R + R_e}\right)^n = \frac{-2nR}{(R + R_e)^2}\left(\frac{R - R_e}{R + R_e}\right)^{n-1} \ , \tag{B.37}$$

$$\frac{\partial x^n}{\partial R_e} = \frac{\partial}{\partial R_e}\left(\frac{R - R_e}{R}\right)^n = \frac{-n}{R}\left(\frac{R - R_e}{R}\right)^{n-1} \ , \tag{B.38}$$

$$\frac{\partial}{\partial R_e}(R - R_e)^n = -n(R - R_e)^{n-1} \ . \tag{B.39}$$

Appendix C

Power Series Constraints on $\beta(R)$

All four potential forms considered herein (GMO, EMO, MMO, and MLJ) may have a false second minimum at very short internuclear distances ($R < R_e$). This unphysical behaviour occurs when the exponent function $\beta(R)$ drops off so steeply that the inner repulsive potential wall actually turns over.

Two types of constraints, which could be used independently or in conjunction with each other, were considered to fix this problem. The first type of constraint, herein called the constrained value method, is to constrain $\beta(R)$ so that the function is fixed to have a specific (positive) value at $R = 0$. The second approach, dubbed the constrained slope method, constrains the first partial derivative, $\frac{\partial\beta(R)}{\partial R}$, to a fixed value at $R = 0$.

A different problem exists in the large internuclear separation region ($R > R_e$) of the potential. Long-range theory tells us that the potential form

$$V(R) = \mathcal{D}_e - \frac{C_n}{R^n} \tag{C.1}$$

is valid beyond an internuclear distance defined by the Le Roy radius R_{LR} [32], which is

defined as,

$$R_{\mathrm{LR}} \;=\; 2\left(\langle r_{\mathrm{A}}^2\rangle^{\frac{1}{2}} + \langle r_{\mathrm{B}}^2\rangle^{\frac{1}{2}}\right) \;, \tag{C.2}$$

where $\langle r_{\mathrm{X}}^2\rangle$ is the expectation value of the square of the electronic radius of the unfilled valence shell of atom X. The long-range asymptotic limit of the MLJ potential has a similar form,

$$V(R) \;=\; \mathcal{D}_e - 2\mathcal{D}_e\left(\frac{R_e}{R}\right)^n e^{-\beta_\infty} \;, \tag{C.3}$$

with

$$\beta_\infty \;=\; \lim_{R\to\infty}\beta(R) \;=\; \sum_{i=0}^{N}\beta_i \;. \tag{C.4}$$

By equating Eqs. C.1 and C.3, we see that β_∞ is given by

$$\beta_\infty \;=\; \ln\left(\frac{2\mathcal{D}_e R_e^n}{C_n}\right) \;. \tag{C.5}$$

This allows the potential to be constrained at long range to yield a known theoretical C_n.

The simplest method to enforce one of these constraints is to fix one of the parameters in $\beta(R)$ so that the function behaves in the manner required by the constraint. As each constraint requires a separate parameter to be fixed the, imposition of all three constraints requires three separate constraining parameters, so that $\beta(R)$ takes the form

$$\beta(R) \;=\; \sum_{i=0}^{N}\beta_i z^i + \beta_a z^a + \beta_b z^b + \beta_c z^c \;, \tag{C.6}$$

in which β_a constrains the value of $\beta(R)$ at $R = 0$, β_b constrains the slope of $\beta(R)$ at $R = 0$, and β_c constrains β_∞. To allow flexibility with the constraints, we allow a, b, and c to be any integer such that $a,\ b,\ c\ >\ N$, and $a\ \neq\ b\ \neq\ c$.

In terms of the labels

$$\beta(0) \;=\; \beta_{\rm va}\ , \qquad \left.\frac{\partial\beta(R)}{\partial R}\right|_{R=0} \;=\; \beta_{\rm sl}\ , \quad \text{and} \quad \beta(\infty) \;=\; \beta_\infty\ , \tag{C.7}$$

for the three $\beta(R)$ constraints the relevant constraining equations are

$$\beta_{\rm va} \;=\; \sum_{i=0}^{N}(-1)^i\beta_i + (-1)^a\beta_a + (-1)^b\beta_b + (-1)^c\beta_c\ , \tag{C.8}$$

$$\begin{aligned}\beta_{\rm sl} \;&=\; \left.\frac{\partial z}{\partial R}\right|_{R=0}\left[\sum_{i=1}^{N} i(-1)^{i-1}\beta_i + a(-1)^{a-1}\beta_a + b(-1)^{b-1}\beta_b + c(-1)^{c-1}\beta_c\right] \\ &=\; \frac{-2}{R_e}\left[\sum_{i=1}^{N} i(-1)^i\beta_i + a(-1)^a\beta_a + b(-1)^b\beta_b + c(-1)^c\beta_c\right]\ ,\end{aligned} \tag{C.9}$$

and

$$\beta_\infty \;=\; \ln\left(\frac{2\mathcal{D}_e R_e^n}{C_n}\right) \;=\; \sum_{i=0}^{N}\beta_i + \beta_a + \beta_b + \beta_c\ . \tag{C.10}$$

To implement these constraints, we must fix the constraining terms such that

$$\beta_a \;=\; (-1)^a\left[\beta_{\rm va} - \sum_{i=0}^{N}(-1)^i\beta_i - (-1)^b\beta_b - (-1)^c\beta_c\right]\ , \tag{C.11}$$

$$\beta_b \;=\; \frac{(-1)^b}{-b}\left[\beta_{\rm sl}\frac{R_e}{2} + \sum_{i=1}^{N} i(-1)^i\beta_i + a(-1)^a\beta_a + c(-1)^c\beta_c\right]\ , \tag{C.12}$$

and

$$\beta_c \;=\; \ln\left(\frac{2\mathcal{D}_e R_e^n}{C_n}\right) - \sum_{i=0}^{N}\beta_i - \beta_a - \beta_b \;=\; \beta_\infty - \sum_{i=0}^{N}\beta_i - \beta_a - \beta_b\ . \tag{C.13}$$

In this form, β_a, β_b and β_c are all interrelated. To apply these constraints, we must be able to determine the partial derivatives of $\beta(R)$ with respect to the potential parameters ($\mathcal{D}_e$, R_e, and $\{\beta_i\}$), so that we should determine the values for the constraining parameters in terms of the input parameters a, b, c, $\beta_{\rm va}$, $\beta_{\rm sl}$, and C_n.

C.1 Determination of β_a

First, substitute Eq. (C.13) into Eq. (C.11) to obtain

$$\begin{aligned}(-1)^a\beta_a &= \beta_{\rm va} - \sum_{i=0}^{N}(-1)^i\beta_i - (-1)^b\beta_b - (-1)^c\beta_c \\ &= \beta_{\rm va} - \sum_{i=0}^{N}(-1)^i\beta_i - (-1)^b\beta_b - (-1)^c\left(\beta_\infty - \sum_{i=0}^{N}\beta_i - \beta_a - \beta_b\right) ,\end{aligned} \tag{C.14}$$

and

$$\begin{aligned}\beta_a &= -\left[(-1)^c - (-1)^a\right]^{-1}\left\{\beta_{\rm va} - (-1)^b\beta_b - (-1)^c\beta_\infty + (-1)^c\beta_b\right\} \\ &\quad - \left[(-1)^c - (-1)^a\right]^{-1}\left\{-\sum_{i=0}^{N}(-1)^i\beta_i + (-1)^c\sum_{i=0}^{N}\beta_i\right\} \\ &= \left[(-1)^c - (-1)^a\right]^{-1}\left\{-\beta_{\rm va} + \left[(-1)^b - (-1)^c\right]\beta_b + (-1)^c\beta_\infty\right\} \\ &\quad + \left[(-1)^c - (-1)^a\right]^{-1}\left\{\sum_{i=0}^{N}\left[(-1)^i - (-1)^c\right]\beta_i\right\} .\end{aligned} \tag{C.15}$$

Next, substitute Eq. (C.13) into Eq. (C.12) to give

$$\begin{aligned}-b(-1)^b\beta_b &= \beta_{\rm sl}\frac{R_e}{2} + \sum_{i=1}^{N} i(-1)^i\beta_i + a(-1)^a\beta_a + c(-1)^c\beta_c \\ &= \beta_{\rm sl}\frac{R_e}{2} + \sum_{i=1}^{N} i(-1)^i\beta_i + a(-1)^a\beta_a + c(-1)^c\left(\beta_\infty - \sum_{i=0}^{N}\beta_i - \beta_a - \beta_b\right),\end{aligned} \tag{C.16}$$

and

$$\begin{aligned}\beta_b &= -\left[b(-1)^b - c(-1)^c\right]^{-1}\left\{\beta_{\rm sl}\frac{R_e}{2} + a(-1)^a\beta_a + c(-1)^c\beta_\infty - c(-1)^c\beta_a\right\} \\ &\quad - \left[b(-1)^b - c(-1)^c\right]^{-1}\left\{-c(-1)^c\sum_{i=0}^{N}\beta_i + \sum_{i=1}^{N} i(-1)^i\beta_i\right\} \\ &= \left[b(-1)^b - c(-1)^c\right]^{-1}\left\{-\beta_{\rm sl}\frac{R_e}{2} + \left[c(-1)^c - a(-1)^a\right]\beta_a - c(-1)^c\beta_\infty\right\}\end{aligned}$$

$$+\left[b(-1)^b - c(-1)^c\right]^{-1} \sum_{i=0}^{N} \left[c(-1)^c - i(-1)^i\right] \beta_i \ . \tag{C.17}$$

Finally, substitute Eq. (C.17) into Eq. (C.15) to determine β_a explicitly in terms of the desired parameters, namely

$$\begin{aligned}
\beta_a &= [(-1)^c - (-1)^a]^{-1} \left\{ -\beta_{\rm va} + \sum_{i=0}^{N} \left[(-1)^i - (-1)^c\right] \beta_i + (-1)^c \beta_\infty + \frac{(-1)^b - (-1)^c}{b(-1)^b - c(-1)^c} \right. \\
&\qquad \left. \left[-\beta_{\rm sl} \frac{R_e}{2} + \sum_{i=0}^{N} \left[c(-1)^c - i(-1)^i\right] \beta_i + \left[c(-1)^c - a(-1)^a\right] \beta_a - c(-1)^c \beta_\infty \right] \right\} \\
&= -\frac{\left[b(-1)^b - c(-1)^c\right] \beta_{\rm va} + \left[(-1)^b - (-1)^c\right] \beta_{\rm sl} \frac{R_e}{2} - (b-c)(-1)^{b-c} \beta_\infty}{(a-b)(-1)^{a-b} + (b-c)(-1)^{b-c} + (c-a)(-1)^{c-a}} \\
&\qquad - \sum_{i=0}^{N} \frac{\left[(i-b)(-1)^{i-b} + (b-c)(-1)^{b-c} + (c-i)(-1)^{c-i}\right] \beta_i}{(a-b)(-1)^{a-b} + (b-c)(-1)^{b-c} + (c-a)(-1)^{c-a}} \ .
\end{aligned} \tag{C.18}$$

From this generalized equation, one can obtain values for β_a if only one or two of the three constraints were implemented. For example, if $\beta_{\rm sl}$ was left unconstrained (i.e. $\beta_b = 0$), β_a simplifies to become

$$\begin{aligned}
\beta_a &= \frac{-(-1)^b \beta_{\rm va} + (-1)^{b-c} \beta_\infty + \sum_{i=0}^{N} \left[(-1)^{i-b} - (-1)^{b-c}\right] \beta_i}{-(-1)^{a-b} + (-1)^{b-c}} \\
&= \frac{-\beta_{\rm va} + (-1)^c \beta_\infty - \sum_{i=0}^{N} \left[(-1)^c - (-1)^i\right] \beta_i}{(-1)^c - (-1)^a} \ ,
\end{aligned} \tag{C.19}$$

which is equivalent to setting $b \to \infty$ (or $b^{-1} = 0$) in Eq. (C.18). Similarly, if the β_∞ was not constrained (i.e. $\beta_c = 0$), β_a becomes

$$\begin{aligned}
\beta_a &= -\frac{b(-1)^b \beta_{\rm va} + (-1)^b \beta_{\rm sl} \frac{R_e}{2} + \sum_{i=0}^{N} (i-b)(-1)^{i-b} \beta_i}{(a-b)(-1)^{a-b}} \\
&= \frac{(-1)^a}{1 - ab^{-1}} \left[\beta_{\rm va} + b^{-1} \frac{R_e}{2} \beta_{\rm sl} - \sum_{i=0}^{N} (1 - ib^{-1})(-1)^i \beta_i \right] \ ,
\end{aligned} \tag{C.20}$$

which is equivalent to dropping all of the terms that contain the factor $(-1)^c$ from Eq. (C.18). Finally, when both $b \to \infty$ and the terms that contain the factor $(-1)^c$ are ignored, Eq. (C.18) becomes

$$\beta_a \;=\; (-1)^a \left[\beta_{\rm va} - \sum_{i=0}^{N} (-1)^i \beta_i\right] \;, \tag{C.21}$$

which is equivalent to only using the $\beta_{\rm va}$ constraint.

C.2 Determination of β_b

Substitution of Eq. (C.15) into Eq. (C.17) determines β_b explicitly in terms of the desired parameters, namely

$$\begin{aligned}
\beta_b \;=\;& \left[b(-1)^b - c(-1)^c\right]^{-1} \left\{-\beta_{\rm sl}\frac{R_e}{2} + \sum_{i=0}^{N}\left[c(-1)^c - i(-1)^i\right]\beta_i - c(-1)^c\beta_\infty\right\} \\
& + \left[b(-1)^b - c(-1)^c\right]^{-1} \frac{c(-1)^c - a(-1)^a}{(-1)^c - (-1)^a} \\
& \left[-\beta_{\rm va} + \sum_{i=0}^{N}\left[(-1)^i - (-1)^c\right]\beta_i + \left[(-1)^b - (-1)^c\right]\beta_b + (-1)^c\beta_\infty\right] \\
=\;& -\frac{\left[c(-1)^c - a(-1)^a\right]\beta_{\rm va} + \left[(-1)^c - (-1)^a\right]\beta_{\rm sl}\frac{R_e}{2} - (c-a)(-1)^{c-a}\beta_\infty}{(a-b)(-1)^{a-b} + (b-c)(-1)^{b-c} + (c-a)(-1)^{c-a}} \\
& - \sum_{i=0}^{N} \frac{\left[(a-i)(-1)^{a-i} + (i-c)(-1)^{i-c} + (c-a)(-1)^{c-a}\right]\beta_i}{(a-b)(-1)^{a-b} + (b-c)(-1)^{b-c} + (c-a)(-1)^{c-a}} \;.
\end{aligned} \tag{C.22}$$

As with β_a, one can simplify this equation if only one or two of the three constraints are used. For an unconstrained β_a, β_b becomes

$$\begin{aligned}
\beta_b \;=\;& \frac{a(-1)^a\beta_{\rm va} + (-1)^a\beta_{\rm sl}\frac{R_e}{2} + (c-a)(-1)^{c-a}\beta_\infty}{(a-b)(-1)^{a-b} + (c-a)(-1)^{c-a}} \\
& - \sum_{i=0}^{N} \frac{\left[(a-i)(-1)^{a-i} + (c-a)(-1)^{c-a}\right]\beta_i}{(a-b)(-1)^{a-b} + (c-a)(-1)^{c-a}}
\end{aligned}$$

$$= -\frac{\beta_{\rm sl}\frac{R_e}{2} + c(-1)^c\beta_\infty + \sum_{i=0}^{N}\left[i(-1)^i - c(-1)^c\right]\beta_i}{b(-1)^b - c(-1)^c} \ , \qquad \text{(C.23)}$$

which can be derived from Eq. (C.22) by dropping all of the terms that contain the factor $(-1)^a$. If all of the terms in Eq. (C.22) containing the factor $(-1)^c$ were ignored, β_b becomes

$$\begin{aligned}\beta_b &= \frac{a(-1)^a\beta_{\rm va} + (-1)^a\beta_{\rm sl}\frac{R_e}{2} + \sum_{i=0}^{N}(i-a)(-1)^{i-a}\beta_i}{(a-b)(-1)^{a-b}} \\ &= \frac{(-1)^b}{a-b}\left[a\beta_{\rm va} + \beta_{\rm sl}\frac{R_e}{2} + \sum_{i=0}^{N}(i-a)(-1)^i\beta_i\right] \ , \qquad \text{(C.24)}\end{aligned}$$

which is equivalent to having an unconstrained β_∞. Finally, if only the slope was constrained,

$$\beta_b = \frac{(-1)^b}{-b}\left[\beta_{\rm sl}\frac{R_e}{2} + \sum_{i=0}^{N} i(-1)^i\beta_i\right] \ , \qquad \text{(C.25)}$$

which is equal to Eq. (C.22) if all the terms containing either the factor $(-1)^a$ or $(-1)^c$ were dropped.

C.3 Determination of β_c

Now, substitution of Eqs. (C.18) and (C.22) into Eq. (C.13) determines β_c in terms of the desired parameters as

$$\begin{aligned}\beta_c &= \beta_\infty - \sum_{i=0}^{N}\beta_i - \beta_a - \beta_b \\ &= \beta_\infty - \sum_{i=0}^{N}\beta_i + \frac{\left[b(-1)^b - c(-1)^c\right]\beta_{\rm va} + \left[(-1)^b - (-1)^c\right]\beta_{\rm sl}\frac{R_e}{2} - (b-c)(-1)^{b-c}\beta_\infty}{(a-b)(-1)^{a-b} + (b-c)(-1)^{b-c} + (c-a)(-1)^{c-a}} \\ &\quad + \sum_{i=0}^{N}\frac{\left[(i-b)(-1)^{i-b} + (b-c)(-1)^{b-c} + (c-i)(-1)^{c-i}\right]\beta_i}{(a-b)(-1)^{a-b} + (b-c)(-1)^{b-c} + (c-a)(-1)^{c-a}}\end{aligned}$$

$$
\begin{aligned}
&+\frac{[c(-1)^c - a(-1)^a]\,\beta_{\rm va} + [(-1)^c - (-1)^a]\,\beta_{\rm sl}\frac{R_e}{2} - (c-a)(-1)^{c-a}\beta_\infty}{(a-b)(-1)^{a-b}+(b-c)(-1)^{b-c}+(c-a)(-1)^{c-a}} \\
&+\frac{\sum_{i=0}^{N}\left[(a-i)(-1)^{a-i}+(i-c)(-1)^{i-c}+(c-a)(-1)^{c-a}\right]\beta_i}{(a-b)(-1)^{a-b}+(b-c)(-1)^{b-c}+(c-a)(-1)^{c-a}} \\
= \;& \beta_\infty - \frac{\left[a(-1)^a - b(-1)^b\right]\beta_{\rm va} + \left[(-1)^a - (-1)^b\right]\beta_{\rm sl}\frac{R_e}{2}}{(a-b)(-1)^{a-b}+(b-c)(-1)^{b-c}+(c-a)(-1)^{c-a}} \\
&+\frac{\left[(b-c)(-1)^{b-c}+(c-a)(-1)^{c-a}\right]\beta_\infty}{(a-b)(-1)^{a-b}+(b-c)(-1)^{b-c}+(c-a)(-1)^{c-a}} - \sum_{i=0}^{N}\beta_i \\
&+\sum_{i=0}^{N}\frac{\left[(i-b)(-1)^{i-b}+(b-c)(-1)^{b-c}+(a-i)(-1)^{a-i}+(c-a)(-1)^{c-a}\right]\beta_i}{(a-b)(-1)^{a-b}+(b-c)(-1)^{b-c}+(c-a)(-1)^{c-a}} \\
= \;& -\frac{\left[a(-1)^a - b(-1)^b\right]\beta_{\rm va} + \left[(-1)^a - (-1)^b\right]\beta_{\rm sl}\frac{R_e}{2} - (a-b)(-1)^{a-b}\beta_\infty}{(a-b)(-1)^{a-b}+(b-c)(-1)^{b-c}+(c-a)(-1)^{c-a}} \\
&-\sum_{i=0}^{N}\frac{\left[(a-b)(-1)^{a-b}+(b-i)(-1)^{b-i}+(i-a)(-1)^{i-a}\right]\beta_i}{(a-b)(-1)^{a-b}+(b-c)(-1)^{b-c}+(c-a)(-1)^{c-a}}\,. \qquad \text{(C.26)}
\end{aligned}
$$

As with β_a and β_b, β_c can be simplified if fewer constraints are used. If $\beta_{\rm va}$ is set free,

$$
\begin{aligned}
\beta_c &= -\frac{a(-1)^a\beta_{\rm va} + (-1)^a\beta_{\rm sl}\frac{R_e}{2} - (a-b)(-1)^{a-b}\beta_\infty}{(a-b)(-1)^{a-b}+(c-a)(-1)^{c-a}} \\
&\quad +\sum_{i=0}^{N}\frac{\left[(a-b)(-1)^{a-b}+(i-a)(-1)^{i-a}\right]\beta_i}{(a-b)(-1)^{a-b}+(c-a)(-1)^{c-a}} \\
&= \frac{\beta_{\rm sl}\frac{R_e}{2} + b(-1)^b\beta_\infty - \sum_{i=0}^{N}\left[b(-1)^b - i(-1)^i\right]\beta_i}{b(-1)^b - c(-1)^c}\,, \qquad \text{(C.27)}
\end{aligned}
$$

which can be obtained from Eq. (C.26) if all terms that do *not* have the factor $(-1)^a$ were ignored, and by setting $a = 0$. Similarly, if $\beta_{\rm sl}$ was not constrained,

$$
\begin{aligned}
\beta_c &= -\frac{-(-1)^b\beta_{\rm va} + (-1)^{a-b}\beta_\infty + \sum_{i=0}^{N}\left[-(-1)^{a-b} + (-1)^{b-i}\right]\beta_i}{-(-1)^{a-b}+(-1)^{b-c}} \\
&= \frac{\beta_{\rm va} - (-1)^a\beta_\infty - \sum_{i=0}^{N}\left[(-1)^i - (-1)^a\right]\beta_i}{(-1)^c - (-1)^a}\,, \qquad \text{(C.28)}
\end{aligned}
$$

which occurs when $b^{-1} = 0$ in Eq. (C.26). Finally, by dropping any terms in Eq. (C.26) that do not contain the factor $(-1)^a$, and by setting a, $b^{-1} = 0$,

$$\beta_c = \beta_\infty - \sum_{i=0}^{N} \beta_i \ , \tag{C.29}$$

which is equivalent to using only the β_∞ constraint.

C.4 Partial Derivatives of Constrained Parameters

Since the constraints imposed on the potential depend on the other parameters in the function, the partial derivatives need to be modified to incorporate these changes.

Let us begin with changes to the partial derivatives with respect to the exponent parameters. We can easily determine the changes to the partial derivatives by invoking the chain rule, where the partial derivative with respect to β_m ($m \neq a$, $m \neq b$, and $m \neq c$) is

$$\begin{aligned} \frac{\partial V(R)}{\partial \beta_m} &= \left(\frac{\partial V(R)}{\partial \beta_m}\right)_{[\beta_a,\beta_b,\beta_c]} + \left(\frac{\partial V(R)}{\partial \beta_a}\right)\left(\frac{\partial \beta_a}{\partial \beta_m}\right) \\ &\quad + \left(\frac{\partial V(R)}{\partial \beta_b}\right)\left(\frac{\partial \beta_b}{\partial \beta_m}\right) + \left(\frac{\partial V(R)}{\partial \beta_c}\right)\left(\frac{\partial \beta_c}{\partial \beta_m}\right) \ . \end{aligned} \tag{C.30}$$

For the Morse family of oscillators

$$\left(\frac{\partial V(R)}{\partial \beta_m}\right)_{[\beta_{i\neq m}]} = 2\mathcal{D}_e^a f_a(R)\left[1 - f_a(R)\right]\left[\gamma_a(R)\zeta_a(R)^m - \delta_{n,0}\frac{1 - e^{\beta_a \gamma_a(R)}}{1 - e^{\beta_a^\infty}}\right] \tag{C.31}$$

and

$$\frac{\partial \beta_a}{\partial \beta_m} = -\frac{(m-b)(-1)^{m-b} + (b-c)(-1)^{b-c} + (c-m)(-1)^{c-m}}{(a-b)(-1)^{a-b} + (b-c)(-1)^{b-c} + (c-a)(-1)^{c-a}} \ , \tag{C.32}$$

$$\frac{\partial\beta_b}{\partial\beta_m} = -\frac{(a-m)(-1)^{a-m}+(m-c)(-1)^{m-c}+(c-a)(-1)^{c-a}}{(a-b)(-1)^{a-b}+(b-c)(-1)^{b-c}+(c-a)(-1)^{c-a}}\,, \tag{C.33}$$

$$\frac{\partial\beta_c}{\partial\beta_m} = -\frac{(a-b)(-1)^{a-b}+(b-m)(-1)^{b-m}+(m-a)(-1)^{m-a}}{(a-b)(-1)^{a-b}+(b-c)(-1)^{b-c}+(c-a)(-1)^{c-a}}\,. \tag{C.34}$$

The other partial derivatives affected in this way are calculated similarly.

Since constraining the C_n coefficient is usually very common for the MLJ, the appropriate partial derivatives are listed here:

$$\frac{\partial V_{\rm MLJ}}{\partial\beta_c}\frac{\partial\beta_c}{\partial\mathcal{D}_e} = 2z^{c+1}\left(\frac{R_e}{R}\right)^n e^{-\beta_{\rm MLJ}(R)\,z}\left[1-\left(\frac{R_e}{R}\right)^n e^{-\beta_{\rm MLJ}(R)\,z}\right]\,, \tag{C.35}$$

$$\begin{aligned}\frac{\partial V_{\rm MLJ}}{\partial\beta_c}\frac{\partial\beta_c}{\partial R_e} &= -2\mathcal{D}_e\left(\frac{R_e}{R}\right)^n e^{-\beta_{\rm MLJ}(R)\,z}\left[1-\left(\frac{R_e}{R}\right)^n e^{-\beta_{\rm MLJ}(R)\,z}\right]\\ &\quad\times\left[-\frac{n}{R_e}z^{c+1}+\frac{2R}{(R+R_e)^2}(c+1)\beta_c^{\rm MLJ}z^c\right]\,,\end{aligned} \tag{C.36}$$

$$\frac{\partial V_{\rm MLJ}}{\partial\beta_c}\frac{\partial\beta_c}{\partial\beta_m^{\rm MLJ}} = -2\mathcal{D}_e\left(\frac{R_e}{R}\right)^n e^{-\beta_{\rm MLJ}(R)\,z}\left[1-\left(\frac{R_e}{R}\right)^n e^{-\beta_{\rm MLJ}(R)\,z}\right]z^{c+1}\,, \tag{C.37}$$

where

$$\beta_{\rm MLJ}(R) = \sum_{i=0}^{N}\beta_i^{\rm MLJ}z^i+\beta_c z^c\,. \tag{C.38}$$

Appendix D

The SCE Function

The Self-Constraining Expansion (SCE) function has the form

$$\beta(R) \;=\; \beta_a + a(R)\left[(-1)^n\beta_a + \beta_b + \sum_{i=1}\beta_i\,[b(R)]^i\right]\;, \tag{D.1}$$

in which $a(R)$ and $b(R)$ are functions of the intermolecular separation R, and β_a, β_b, and n are constants. The partial derivatives of the SCE are

$$\frac{\partial\beta(R)}{\partial\beta_a} \;=\; 1+(-1)^n a(R)\;,\quad \frac{\partial\beta(R)}{\partial\beta_b} \;=\; a(R)\;,\quad \frac{\partial\beta(R)}{\partial\beta_i} \;=\; a(R)b^i(R)\;, \tag{D.2}$$

and

$$\frac{\partial\beta(R)}{\partial R_e} \;=\; \frac{\partial a(R)}{\partial R_e}\left[(-1)^n\beta_a+\beta_b+\sum_{i=1}b^i(R)\beta_i\right] + a(R)\frac{\partial b(R)}{\partial R_e}\sum_{i=1} i b^{i-1}(R)\beta_i\;. \tag{D.3}$$

For the Expanded Morse Oscillator potential we require that $a(R=0)=-1$, $a(R=\infty)=1$, $b(R=0)=0$, $b(R=\infty)=1$, and

$$a(R) \;=\; \frac{R-R_e}{R+R_e}\,,\quad b(R) \;=\; \frac{R}{R+R_e}\,,\quad \beta_a \;=\; \beta_0\,,\quad \beta_b \;=\; -\beta_{-1}\,,\quad \text{and}\quad n \;=\; 0\,. \tag{D.4}$$

The SCE for the EMO potential can then be expressed as

$$\beta(R) \;=\; \beta_0 + \frac{R-R_e}{R+R_e}\left[\beta_0 - \beta_{-1} + \sum_{i=1}\left(\frac{R}{R+R_e}\right)^i \beta_i\right] \;, \tag{D.5}$$

so that the partial derivatives are

$$\frac{\partial\beta}{\partial\beta_0} \;=\; \frac{2R}{R+R_e} \;, \quad \frac{\partial\beta}{\partial\beta_{-1}} \;=\; -\,\frac{R-R_e}{R+R_e} \;, \quad \frac{\partial\beta}{\partial\beta_i} \;=\; \frac{R-R_e}{R+R_e}\left(\frac{R}{R+R_e}\right)^i \;, \tag{D.6}$$

and

$$\frac{\partial\beta}{\partial R_e} \;=\; -\,\frac{2R}{(R+R_e)^2}\left[\beta_0 - \beta_{-1} + \sum_{i=1}\left(\frac{R}{R+R_e}\right)^i \beta_i\right] - \frac{R-R_e}{(R+R_e)^2}\sum_{i=1} i\left(\frac{R}{R+R_e}\right)^i \beta_i \;. \tag{D.7}$$

For the Modified Lennard-Jones potential, we have

$$a(R) \;=\; \frac{R-R_e}{R+R_e} \;, \quad b(R) \;=\; \frac{1}{R+R_e} \;, \quad \beta_a \;=\; \beta_0 \;, \quad \beta_b \;=\; \beta_\infty \;, \quad \text{and} \quad n \;=\; 1 \;, \tag{D.8}$$

so that the SCE becomes

$$\beta(R) \;=\; \beta_0 + \frac{R-R_e}{R+R_e}\left[-\beta_0 + \beta_\infty + \sum_{i=1}\frac{\beta_i}{(R+R_e)^i}\right] \tag{D.9}$$

and the partial derivatives of the $\beta(R)$ function are

$$\frac{\partial\beta(R)}{\partial\beta_0} \;=\; \frac{2R_e}{R+R_e} \;, \quad \frac{\partial\beta(R)}{\partial\beta_\infty} \;=\; \frac{R-R_e}{R+R_e} \;, \quad \frac{\partial\beta(R)}{\partial\beta_i} \;=\; \frac{R-R_e}{R+R_e}\left(\frac{1}{R+R_e}\right)^i \;, \tag{D.10}$$

and

$$\frac{\partial\beta(R)}{\partial R_e} \;=\; -\,\frac{2R}{(R+R_e)^2}\left[-\beta_0 + \beta_\infty + \sum_{i=1}\left(\frac{1}{R+R_e}\right)^i \beta_i\right] - \frac{R-R_e}{(R+R_e)^2}\sum_{i=1} i\left(\frac{1}{R+R_e}\right)^i \beta_i \;. \tag{D.11}$$

Bibliography

[1] *Webster's Online Dictionary - based on Webster's Seventh New Collegiate Dictionary*, (G. & C. Merriam Company, Springfield, 1972).

[2] J. A. Coxon, J. Mol. Spectrosc. **117**, 361 (1986).

[3] J. K. G. Watson, J. Mol. Spectrosc. **45**, 99 (1973).

[4] J. K. G. Watson, J. Mol. Spectrosc. **80**, 411 (1980).

[5] E. G. Lee, J. Y. Seto, T. Hirao, P. F. Bernath, and R. J. Le Roy, J. Mol. Spectrosc. **194**, 197 (1999).

[6] J. Y. Seto, Z. Morbi, F. Charron, S. K. Lee, P. F. Bernath, and R. J. Le Roy, J. Chem. Phys. **110**, 11756 (1999).

[7] J. Y. Seto, R. J. Le Roy, J. Vergès, and C. Amiot (unpublished).

[8] R. Rydberg, Z. Phys. **73**, 376 (1931).

[9] O. Klein, Z. Phys. **76**, 226 (1932).

[10] A. L. G. Rees, Proc. Roy. Soc. London **59**, 998 (1947).

[11] R. J. Le Roy and J. van Kranendonk, J. Chem. Phys. **61**, 4750 (1974).

[12] J. M. Hutson, J. Chem. Phys. **96**, 4237 (1992).

[13] J. M. Hutson, J. Chem. Phys. **96**, 6752 (1992).

[14] W. M. Kosman and J. Hinze, J. Mol. Spectrosc. **56**, 93 (1975).

[15] C. R. Vidal and H. Scheingraber, J. Mol. Spectrosc. **65**, 46 (1977).

[16] G. Gouedard and J. Vigue, Chem. Phys. Lett. **96**, 293 (1983).

[17] J. A. Coxon and P. G. Hajigeorgiou, J. Mol. Spectrosc. **142**, 254 (1990).

[18] J. A. Coxon and P. G. Hajigeorgiou, J. Mol. Spectrosc. **150**, 1 (1991).

[19] H. G. Hedderich, M. Dulick, and P. F. Bernath, J. Chem. Phys. **99**, 8363 (1993).

[20] P. G. Hajigeorgiou and R. J. Le Roy, J. Chem. Phys. **112**, 3949 (2000).

[21] J. B. White, M. Dulick, and P. F. Bernath, J. Chem. Phys. **99**, 8371 (1993).

[22] J. M. Campbell, M. Dulick, D. Klapstein, J. B. White, and P. F. Bernath, J. Chem. Phys. **99**, 8379 (1993).

[23] M. Born and J. R. Oppenheimer, Ann. Phys. **84**, 457 (1927).

[24] R. J. Le Roy, J. Mol. Spectrosc. **194**, 189 (1999).

[25] J. F. Ogilvie, J. Phys. B: At. Mol. Opt. Phys. **27**, 47 (1994).

[26] A. G. Maki, W. B. Olson, and G. Thompson, J. Mol. Spectrosc. **144**, 257 (1990).

[27] J. A. Coxon and J. F. Ogilvie, Can. J. Spec. **34**, 137 (1989).

[28] J. F. Ogilvie, J. Oddershede, and S. P. A. Sauer, Chem. Phys. Lett. **228**, 183 (1994).

[29] P. M. Morse, Phys. Rev. **54**, 57 (1929).

[30] P. J. Kuntz and A. C. Roach, J. Chem. Soc. Faraday Trans. II **68**, 259 (1972).

[31] R. J. Duchovic and W. L. Hase, Chem. Phys. Lett. **110**, 474 (1984).

[32] R. J. Le Roy, in *Molecular Spectroscopy* (Specialist Periodical Report of the Chemical Society of London, London, 1973), Vol. 1, Chap. 3.

[33] R. J. Le Roy, J. Mol. Spectrosc. **191**, 223 (1998).

[34] T. Karkanis, M. Dulick, Z. Morbi, J. B. White, and P. F. Bernath, Can. J. Phys. **72**, 1213 (1994).

[35] R. S. Ram, M. Dulick, B. Guo, K. -Q. Zhang, and P. F. Bernath, J. Mol. Spectrosc. **183**, 360 (1997).

[36] R. J. Le Roy, *LEVEL 7.0 A Computer Program Solving the Radial Schrödinger Equation for Bound and Quasibound Levels*, University of Waterloo Chemical Physics Research Report CP-642 (2000). The source code and manual for this program are distributed freely throught the www site *http://theochem.uwaterloo.ca/~leroy*.

[37] J. Cooley, Math Computations **15**, 363 (1961).

[38] J. Cashion, J. Chem. Phys. **39**, 1872 (1963).

[39] R. N. Zare and J. Cashion, University of California Lawrence Radiation Laboratory Report UCRL-10881, University of California (unpublished).

[40] R. N. Zare, University of California Lawrence Radiation Laboratory Report UCRL-10925, University of California (unpublished).

[41] R. N. Zare, J. Chem. Phys. **40**, 1934 (1964).

[42] H. Wang, T. -J. Whang, A. M. Lyyra, L. Li, and W. C. Stwalley, J. Chem. Phys. **94**, 4756 (1991).

[43] W. Kolos and L. Wolniewicz, J. Chem. Phys. **50**, 3228 (1969).

[44] H. Hellmann, *Einfuhring in die Quantemchemie* (F. Deuticke, Leipzig, 1937), p. 285.

[45] R. P. Feynman, Phys. Rev. **56**, 340 (1939).

[46] J. L. Dunham, Phys. Rev. **41**, 713 (1932).

[47] J. L. Dunham, Phys. Rev. **41**, 721 (1932).

[48] K. P. Huber and G. Herzberg, *Constants of Diatomic Molecules*, 4th ed. (Van Nostrand Reinhold Company, New York, 1979).

[49] G. Audi and A. Wapstra, Nuclear Physics **A565**, 1 (1993).

[50] B. Guo, M. Dulick, S. Yost, and P. Bernath, Mol. Phys. **91**, 459 (1997).

[51] Z. Morbi, Ph.D. thesis, University of Waterloo, 1998.

[52] S. Beaton and K. Evenson, J. Mol. Spectrosc. **142**, 336 (1990).

[53] T. Varberg and K. Evenson, J. Mol. Spectrosc. **164**, 531 (1994).

[54] T. Okabayashi and M. Tanimoto, Astrophys. J. **487**, 463 (1997).

[55] W. Fernando, L. O'Brien, and P. Bernath, J. Mol. Spectrosc. **139**, 461 (1990).

[56] U. Ringström, Ark. Phys. **32**, 211 (1966).

[57] C. E. Fellows, M. Rosberg, A. P. C. Camps, R. F. Gutteres, and C. Amiot , J. Mol. Spectrosc. **185**, 420 (1997).

[58] G. Simons, R. G. Parr, and J. M. Finlan, J. Chem. Phys. **59**, 3229 (1973).

[59] J. M. Finlan and G. Simons, J. Mol. Spectrosc. **57**, 1 (1975).

[60] C. C. Tsai, R. S. Freeland, J. M. Vogels, H. M. J. M. Boesten, B. J. Varhaar, and D. J. Heinzen, Phys. Rev. Lett. **79**, 1245 (1997).

[61] M. Marinescu, H. Sadeghpour, and A. Dalgarno, Physical Review A **49**, 982 (1994).

[62] Z. H. Zhu, F. H. Wang, B. Chen, M. L. Tan, and H. Y. Wang, Mol. Phys. **92**, 1061 (1997).

[63] A. Boutalib and F. Gadéa, J. Chem. Phys. **97**, 1144 (1992).

[64] J.-J. Chen, W.-T. Luh, and G.-H. Jong, J. Chem. Phys. **110**, 4402 (1999).

[65] C. R. Vidal and W. C. Stwalley, J. Chem. Phys. **77**, 883 (1982).

[66] G. Maitland and E. Smith, Chem. Phys. Lett. **22**, 443 (1973).

[67] P. F. Bernath and R. J. Le Roy, Private Communication.

[68] M. Gruebele, Mol. Phys. **69**, 475 (1990).